2013

ACENES AND ACENEQUINONES FOR OPTICS AND ORGANIC ELECTRONICS

Matthew Bruzek
University of Kentucky, mjbruzek@hotmail.com

STUDENT AGREEMENT:

I represent that my thesis or dissertation and abstract are my original work. Proper attribution has been given to all outside sources. I understand that I am solely responsible for obtaining any needed copyright permissions. I have obtained and attached hereto needed written permission statements(s) from the owner(s) of each third-party copyrighted matter to be included in my work, allowing electronic distribution (if such use is not permitted by the fair use doctrine).

I hereby grant to The University of Kentucky and its agents the non-exclusive license to archive and make accessible my work in whole or in part in all forms of media, now or hereafter known. I agree that the document mentioned above may be made available immediately for worldwide access unless a preapproved embargo applies.

I retain all other ownership rights to the copyright of my work. I also retain the right to use in future works (such as articles or books) all or part of my work. I understand that I am free to register the copyright to my work.

REVIEW, APPROVAL AND ACCEPTANCE

The document mentioned above has been reviewed and accepted by the student's advisor, on behalf of the advisory committee, and by the Director of Graduate Studies (DGS), on behalf of the program; we verify that this is the final, approved version of the student's dissertation including all changes required by the advisory committee. The undersigned agree to abide by the statements above.

Matthew Bruzek, Student

Dr. John E. Anthony, Major Professor

Dr. Dong-Sheng Yang, Director of Graduate Studies

ACENES AND ACENEQUINONES FOR OPTICS AND ORGANIC ELECTRONICS

DISSERTATION

A dissertation submitted in partial fulfillment of the
requirements for the Degree of Doctor of Philosophy in the
College of Arts and Sciences
at the University of Kentucky

By
Matthew J. Bruzek

Lexington, Kentucky

Director: Dr. John E. Anthony, Professor of Chemistry

Lexington, Kentucky

2013

ABSTRACT OF DISSERTATION

ACENES AND ACENEQUINONES FOR OPTICS AND ORGANIC ELECTRONICS

Acenes have been explored by a number of research groups in the field of organic electronics with a particular emphasis on transistor materials. This group has been actively studying acene-based organic semiconductors for more than a decade using a crystal engineering approach and has developed acene derivatives for applications in field-effect transistors, light-emitting diodes, and photovoltaics. In addition to organic electronics, crystal engineering has important applications in a number of other fields, quite notably in the design of metal-organic frameworks.

Chapters 2 and 3 of this dissertation focus on applying crystal engineering to the synthesis of acene derivatives for use as solid-state, long-wavelength fluorescent organic dyes in the field of biomedical imaging. More specifically, this work studied the synthesis and properties of dioxolane-functionalized pentacenes and hexacenes. One of these pentacene derivatives has already been demonstrated in biomedical imaging which may lead to improved treatment of tuberculosis. The dioxolane-functionalized hexacene is still under evaluation for bioimaging applications.

Chapters 4 and 5 focus on crystal engineering in relation to organic electronics. Chapter 4 deals with fine-tuning of crystal packing and demonstrated that small differences in molecular structure can result in significant changes to the solid-state structure which affects semiconductor properties. Finally, chapter 5 studies the use of singlet fission in photovoltaics and demonstrated that this process does occur in a solar cell incorporating a hexacene derivative. Pentadithiophenes were also synthesized for singlet fission photovoltaics, but they have yet to be studied further.

KEYWORDS: Crystal Engineering, Biomedical Imaging, Acenes, Singlet Fission, Organic Semiconductors

Matthew Bruzek

September 2, 2013

ACENES AND ACENEQUINONES FOR OPTICS AND ORGANIC ELECTRONICS

By

Matthew J. Bruzek

John E. Anthony

Director of Dissertation

Dong-Sheng Yang

Director of Graduate Studies

September 3, 2013

Date

ACKNOWLEDGEMENTS

The past 5 years have definitely been a journey. Having moved 850 miles from Minnesota to Lexington for graduate school, I had no family nearby and was basically on my own. Lexington seemed like a nice place, having spent the summer of 2007 working with acenes and fullerenes in John Anthony's lab as an REU student supported by the National Science Foundation. Thank you, NSF! Even though organic chemistry was nearly my worst chemistry sub-discipline when arriving in Lexington for graduate school, organic electronics piqued my interest, and I decided to join John Anthony's group and become an organic chemist. The first semester was absolutely brutal, and classes seemed to cover material at an impossible pace. I felt like a complete moron in attempting to master organic chemistry, one of my worst subjects. Eventually, I discovered the wisdom in Dr. Robert Grossman's little book on mechanisms and worked through it toward the end of my third semester. That book was largely responsible for me passing my cumulative exams (cumes). Thank you, Dr. Grossman!

Once cumes were over, life became much easier. There was now much more time to focus on my research and the practical aspects of organic chemistry. All of my lab mates contributed to my learning in their own way: Genay Jones, Zhong Li, Marcia Payne, Emilie Ripaud, Karl Thorley, Thilanga Liyanage, Balaji Purushothaman, Ying Shu, Marsha Grimminger, Kerri Shelton, Rawad Hallani, Jenny Washbourne, Devin Granger, and Pat Simmons. Thank you all! None of this would have been possible if not for my advisor, Dr. John Anthony, who guided me through the research process and kept me motivated when progress was slow. Thank you! Dr. Sean Parkin played a large role in providing me with almost all of the X-ray crystallography in this dissertation. Thank you! I would also like to thank my parents, Tom and Pam Bruzek, for their love and support over the years. I love you! My wife, Paula, also bears special mention. Thank you for supporting me all this time. I love you! I would also like to thank my high school chemistry teacher Mrs. Karen Hohenstein for being such a great teacher and giving me the solid general chemistry foundation on which I have built my knowledge over the

past nine years. In addition, I would like to thank the University of Kentucky RCTF for fellowship support for the past two years, as well as the National Science Foundation Division of Materials Research grant DMR-1035257 for additional support. Also, I would like to thank my other committee members Dr. Mark Watson, Dr. John (Jack) Selegue, and Dr. Bruce Hinds for the time they have given me over the years to help me become a better chemist. Thank you! Finally, I would like to thank Dr. Jay Brown at Southwest Minnesota State University for teaching me both theoretical and practical NMR spectroscopy. It has been and will continue to be very helpful. Thank you!

TABLE OF CONTENTS

LIST OF TABLES

LIST OF FIGURES

LIST OF SCHEMES

Chapter 1. Introduction

1.1 History of Fluorescence

Luminescent and incandescent phenomena have a certain intrinsic appeal among a wide range of people. As children, many of us were mesmerized by fireworks, glow sticks, glow-in-the-dark toys and fishing lures, and fireflies. Those familiar with hunting know the bright glow of blaze orange clothing, and those who have taken an introductory chemistry course may remember flame tests of various salts and observing their characteristic colors. Scientists have developed a deeper understanding of these phenomena over the past several centuries. Of these phenomena, the one most relevant to a significant portion of this work is fluorescence, and a very brief history is presented here.

One of the earliest accounts of fluorescence dates back to 1565 when a doctor reported that water exposed to a type of wood known as *lignum nephriticum* (Latin for "kidney wood") would glow in the sunlight[1]. This wood is also known as "narra." At the time, this somewhat magical-looking water was believed to cure kidney stones. Interestingly, it was not until 2009 that the fluorophore responsible for this glow was isolated from the wood and its structure determined[2]. The mineral fluorite (CaF_2) is known to fluoresce in many different colors due to inclusions of various impurities, and an early observation of fluorescence from this material was described by Edward Clarke in 1819[3]. In his experiments with the "green colour of the vegetable world" in 1834, Sir David Brewster reported seeing a brilliant red color coming from a green alcoholic chlorophyll solution when exposed to sunlight[4]. In 1845, Sir John Herschel described fluorescence in reference to a solution of quinine sulfate[5], a substance already known as a treatment for malaria. (This first known fluorophore is still often used in undergraduate chemistry courses to introduce students to fluorescence spectroscopy.) Only several years later in 1852 did Sir George Stokes actually coin the term "fluorescence," naming it after the "double colour" exhibited by some samples of fluorite. Additionally, he described what is now referred to as Stokes shift—the

tendency of molecules to emit light at longer wavelengths than those absorbed[6]. Following this, the list of names associated with fluorescence grows substantially, and it is not my intent to cover all of them. One individual who bears mentioning is Aleksander Jablonski (1898 – 1980), who greatly expanded our knowledge of fluorescence and is regarded as the father of fluorescence spectroscopy. The commonly used Jablonski energy level diagram bears his name and will be used several times in this dissertation.

An important property of fluorescence is that it can be detected with high sensitivity. This was first demonstrated in 1877 with the use of fluorescein, synthesized by Adolf Baeyer only 6 years prior. There was believed to be a subterranean connection between the Danube and Rhine rivers in Europe. As a test, 10 kg of fluorescein was dumped into the headwaters of the Danube, and its green fluorescence appeared 60 hours later in a river that led to the Rhine which established that the rivers were connected[1, 7]. While in this case fluorescence was detected merely by the eye, much more sophisticated instruments have been developed to measure fluorescence. During WWII, the U.S. Department of War was interested in antimalarial drugs, and researchers found they could quantify concentrations of these experimental drugs (including quinine, the first known fluorophore) in blood using simple fluorometers. This success sparked interest in commercializing more advanced spectrofluorometers, further extending the spectral range in which fluorescence could be observed and allowing the technology to be used by more people[8].

1.2 Bioimaging

Biomedical imaging, or bioimaging, is a very broad and general topic concerned with the imaging of biological matter. Taken in its broadest sense, this can include technologies such as radiography (X-ray imaging), ultrasound, magnetic resonance imaging, positron emission tomography, fluorescence imaging, microscopy, and other techniques[9]. As mentioned, an important feature of fluorescence is the extremely high sensitivity that can be obtained, and this has allowed fluorescence imaging to become a prevalent tool adopted in biomedical research to visualize biological molecules and

tissues. Since the initial discovery of fluorescence and the advent of fluorescence spectroscopy, thousands of probes have been developed and applied to bioimaging. These fluorophores can be broadly divided into two classes: intrinsic and extrinsic[10].

Intrinsic fluorophores are produced by the organism being studied and include certain amino acids (tryptophan, tyrosine, and phenylalanine), fluorescent proteins such as green fluorescent protein (GFP), enzyme cofactors such as reduced nicotinamide adenine dinucleotide (NADH), riboflavin, flavin mononucleotide (FMN), flavin adenine dinucleotide (FAD), as well as other fluorophores like porphyrins (hemoglobin) and those present in tissues like collagen. These intrinsic fluorophores have absorptions and emissions spanning from the ultraviolet to red at approximately 650 nm.

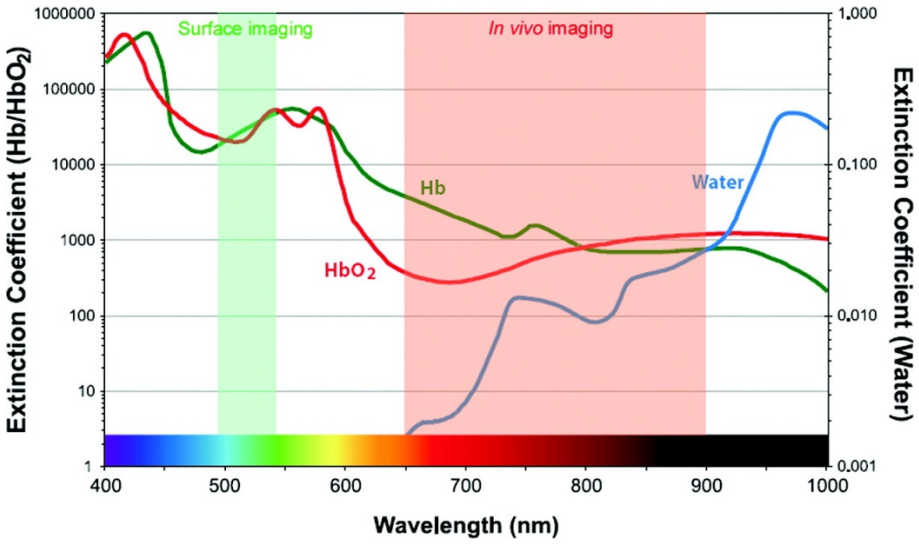

Figure 1-1. Bioimaging window. This encompasses the far-red to NIR wavelengths where tissues are more transparent and lack autofluorescence. Adapted with permission from the American Chemical Society, Copyright © 2010[9].

While a great deal of information can be learned using intrinsic fluorophores, they can cause two main problems, the first of which is autofluorescence. Autofluorescence refers to the background fluorescence from other intrinsic fluorophores that are not of interest. This background is essentially "noise," resulting in a smaller signal/noise ratio and therefore reduced sensitivity. The second problem caused by intrinsic fluorophores, in addition to other intrinsic non-emissive

chromophores, is the absorption of light. The high extinction coefficients of these chromophores result in most of the light being absorbed in a thin section of sample near the surface. Ultraviolet and visible wavelengths are unable to penetrate tissues and excite probes at greater depths which generally confines fluorescence imaging to only surfaces or shallow depths. These problems can be overcome using light wavelengths in the "bioimaging window." This window is between approximately 650 - 900 nm encompassing the far-red to near-infrared (NIR), a region where tissues do not strongly absorb light.

1.3 Extrinsic Fluorophores

Extrinsic fluorophores are artificial substances added to a system when useful fluorescence is not otherwise present. Traditionally, fluorescence imaging has relied on the intrinsic fluorophores mentioned earlier as well as the many commercially-available extrinsic probes. However, most of these classic materials are limited to the ultraviolet and visible regions of the electromagnetic spectrum and are thus limited to surface imaging because they do not absorb or fluoresce in the bioimaging window. There is a great deal of current interest in developing fluorescent probes whose excitation and/or emission wavelengths fall in this range[11]. Ideally, materials best suited for deep-tissue fluorescence imaging are capable of both absorbing *and* emitting in this range so the excitation wavelengths can easily penetrate tissue and the emission can effectively exit the tissue and be observed. Examples of materials having one or both of these properties are given here.

There are a number of different extrinsic fluorophores and overall processes encompassing both inorganic and organic materials which show potential in extending traditional fluorescence imaging into the bioimaging window. Inorganic materials include quantum dots and up-converting nanoparticles. Organic materials include organic dyes and two-photon absorption dyes. Additionally, hybrid inorganic/organic materials have been developed which utilize the process of sensitized triplet-triplet annihilation. While all of these materials exhibit fluorescence, three of them—up-

converting nanoparticles, two-photon absorption dyes, and sensitized triplet-triplet annihilation—involve up-conversion. Up-conversion is a nonlinear photophysical process in which long-wavelength (low energy) light is absorbed and short-wavelength (high energy) light is emitted, and is sometimes called anti-Stokes fluorescence. Quantum dots are unique in that fluorescence is generally obtained by excitation with shorter wavelengths; however, longer wavelengths can also be used in some cases due to a large two-photon action cross-section.

1.3.1 Quantum Dots

Quantum dots consist of nanometer-sized particles whose optical properties depend on the material composition, particle size, size distribution, and surface chemistry[12]. The nanoparticles range from 1 - 6 nm with larger nanoparticles being more red-shifted, and the emission profile therefore depends on the size distribution of the sample. There are several different elemental compositions including CdS, CdSe, CdTe, InP, PbS, and PbSe. Cadmium-containing nanoparticles emit in the range of 370-750 nm while InP, PbS, and PbSe emit at 620-720 nm, >900 nm, and >1000 nm, respectively. A series of quantum dots is shown in Figure 1-2. The fluorescence quantum yields of these nanoparticles are sensitive to the surface chemistry, and they are often protected with a very thin surface coating such as ZnS to maintain higher quantum yields[13]. Other important features of quantum dots are the very high molar absorption coefficients in the range of 25,000 - 250,000 $M^{-1}cm^{-1}$ and the high fluorescence quantum yields: 65-85% for CdSe, 60% for CdS, 10-40% for InP, 40-65% for CdTe, 30-70% for PbS, and 10-80% for PbSe[12]. The wide range of quantum yield values reported reflects the importance of the surface chemistry. Together, these features combine to give materials with very high brightness, a property which is very important to deep-tissue bioimaging. Additionally, CdSe quantum dots coated with ZnS (denoted CdSe-ZnS) have been shown to have a two-photon action cross-sections ($\delta\phi_F$) as high as 47,000 GM, much larger than most organic dyes[14]. (More detail on two-photon absorption and the GM unit is given in section 1.3.4.) The materials most often used for bioimaging studies consist of

CdSe or CdTe. One potential problem with quantum dots is that many of the materials are toxic, and this may limit their use as bioimaging probes. While acute toxicity in cell cultures exposed to quantum dots has been demonstrated, *in vivo* studies of a CdSe/CdS/ZnS quantum dot formulation in rhesus monkeys showed no acute toxicity over a 90-day period[15]. While nearly all of the cadmium remained in the monkeys, there was evidence that some of the cadmium had leached from the quantum dots suggesting chronic toxicity studies are needed to properly assess their safety.

Figure 1-2. Quantum dot fluorescence spanning the visible spectrum. Although not shown here, some formulations emit in the NIR bioimaging window. Adapted with permission from Elsevier, Copyright © 2009[16].

1.3.2 Up-Converting Nanoparticles

Up-converting nanoparticles (UCNPs) fall into the category of nonlinear optics. These nanoparticle crystals consist of a crystal host matrix material doped with various rare-earth lanthanides and have the unusual ability to absorb long-wavelength light and emit shorter wavelengths through a sequential multi-photon absorption process[17]. While a number of different types have been synthesized, by far the most efficient is $NaYF_4$ doped with Yb^{3+} and Er^{3+}, denoted as $NaYF_4$:Yb^{3+},Er^{3+}. Since these lanthanide ions have nearly the same ionic radius as Y^{3+}, substitution results in a crystal structure that is unchanged. Two crystalline phases of this material have been formed–the cubic α-phase and the hexagonal β-phase. The hexagonal β-phase is a much more efficient emitter, and considerable effort has resulted in methods of producing this phase nearly exclusively.

The up-conversion mechanism in $NaYF_4$:Yb^{3+},Er^{3+} is an energy transfer process. It has the ability to absorb light from roughly 900 to 1000 nm and emit at 540 nm (green)

and 660 nm (red). Light in this excitation wavelength range can be conveniently provided by lasers at 915 or 980 nm. The 980 nm excitation is most often quoted in the literature, but this wavelength is somewhat attenuated by water, which may result in excessive heating of tissues[18]. Although up-converting nanoparticles do not absorb the 915 nm laser quite as strongly, water has only 1/6 of the attenuation at this wavelength, so it may be used for practical reasons if necessary. This particular nanoparticle formulation operates by a sequential two-photon absorption process, although other materials undergo three- and four-photon absorption. This sort of absorption is made possible by a combination of specific electronic energy levels and the relatively long-lived excited states of these ions. The Er^{3+} functions as the light-emitting species, and the Yb^{3+} functions as a sensitizer. Er^{3+} ions in the crystals are very prone to radiationless deactivation when in close proximity to other lanthanides, and this limits their useful concentration to typically only 2%. Since this concentration only absorbs a very small fraction of the light, the highly absorbing Yb^{3+} ion is included in the crystal. Highest efficiency is realized with doping levels of approximately 20% Yb^{3+} and 2% Er^{3+}. In the crystal, a 915 or 980 nm photon is absorbed by Yb^{3+} which transfers its energy to Er^{3+}, having a very similar energy level, as shown in Figure 1-3. When a second photon is absorbed by Yb^{3+} and the energy transfer repeats, the already-excited electron of Er^{3+} is promoted to an even higher electronic energy level with nearly double the energy of the excitation photons. From this point, various non-radiative energy transfer and multiphonon relaxation processes occur to bring the electron to lower energy levels where it finally undergoes radiative decay, releasing a green or red photon. Since the sequential photon absorption mechanism involved in these materials is much different from the simultaneous two-photon absorption operative in quantum dots and some dyes, it is not surprising that UCNPs are much more efficient in terms of up-conversion. A comparison of up-conversion in CdSe-ZnS quantum dots and $NaYF_4$:Yb^{3+},Er^{3+} showed the UCNPs were 7-10 orders of magnitude brighter[19]. The up-conversion quantum yield (QY) has only been measured for the green (≈550 nm) band, and results show it varies dramatically based on particle size[20]. In the saturation regime, the smallest crystals of 8-

10 nm have a QY of only 0.005% while 100 nm crystals have a QY of 0.3%. A powdered bulk sample with crystal sizes >>100 nm showed a QY of 3%. This size dependence is explained by the surface area/volume ratio. Smaller crystals have a larger ratio, so proportionally more Er^{3+} ions are close to the surface and susceptible to nonradiative decay. It was also shown that a shell of undoped $NaYF_4$ tripled the QY of 30 nm crystals, demonstrating the need to carefully modify the surface chemistry of these materials to achieve the highest possible QY.

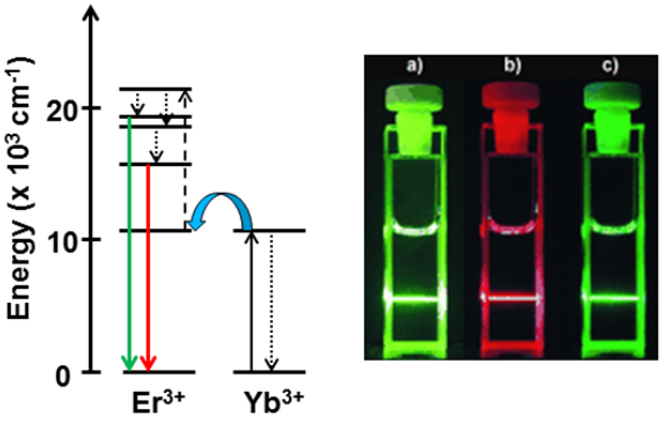

Figure 1-3. UCNP energy level schematic and emission. This illustrates relevant energy levels and absorption/relaxation processes. The blue arrow represents energy transfer from Yb^{3+} to Er^{3+}. To the right is shown a) raw emission, b) filtered red emission, and c) filtered green emission. Adapted with permission from John Wiley & Sons, Copyright © 2004[19].

1.3.3 Fluorescent Organic Dyes

Fluorescent organic dyes are one of the oldest and most established categories of probes used in bioimaging. The versatility of organic synthesis is demonstrated by the large number of classes of organic dyes useful for fluorescence imaging. Characteristic fluorescent organic compounds are rigid, highly conjugated, and often aromatic molecules with low-energy $\pi \rightarrow \pi^*$ transitions[21]. Many of the most popular and established dyes are derivatives of rhodamine, fluorescein, coumarin, cyanine, and BODIPY[10]. Unfortunately, most classic organic dyes cannot be used in the bioimaging window. Nevertheless, there are dyes which are useful in this wavelength range.

One class of dyes includes BODIPY (boron dipyrromethene) derivatives which were first synthesized in 1968[22]. The majority of these dyes are only useful outside the imaging window, but several long-wavelength derivatives have been synthesized[23]. The Suzuki group recently developed the Keio Fluor dye series with seven derivatives having absorptions and emissions ranging from 652 to 723– and 661 to 738 nm, respectively[24]. These dyes feature a BODIPY core fused with two furan moieties and additional aryl substituents and show excellent molar absorptivity, quantum yield, and photostability. O'Shea *et. al.* synthesized several tetraaryl-substituted aza-BODIPY derivatives[25]. These have absorptions and emissions ranging from 681 to 702 nm and 711 to 735 nm, respectively. However, both the molar absorption coefficients and quantum yields are significantly lower than those reported by Suzuki, resulting in lower brightness of the probes.

Cyanines are another class of materials whose photophysical properties have been extended into the imaging window. The closed-chain cyanines consist of two nitrogen-containing aromatic groups linked by a polymethine chain. In general, quantum yields are somewhat low, and stability usually decreases as the polymethine chain length increases. This becomes problematic because the dyes which absorb and emit at longer wavelengths have longer polymethine chains. Indocyanine green (ICG) is one of only two fluorophores that are approved by the FDA for clinical use, and the only one of which is useful in the bioimaging window. While it absorbs at 775 nm and emits at 831 nm, ICG suffers from low photostability as well as a quantum yield of only 1.3%. Cy5, Cy5.5, and Cy7 are other commercially available cyanine dyes which absorb from 648-745 nm and fluoresce from 666-775 nm with quantum yields of approximately 20-30%. Additionally, they have large extinction coefficients on the order of 250,000 $M^{-1}cm^{-1}$.

Squaraines have also been developed for use in the bioimaging window. These materials are derivatives of squaric acid, a small, square-shaped organic compound, and are sometimes considered a sub-class of cyanines. Yagi *et. al.* have developed bis-squaraines incorporating thiophene and pyrene units[26]. These dyes have absorptions

between 724 and 807 nm, although quantum yields are very low. Das *et. al.* synthesized some interesting anthracene-squaraine hybrids, one of which absorbed and emitted at 782 and 805 nm, respectively, with a quantum yield of 24%[27]. In addition to BODIPY dyes mentioned, the Suzuki group has also worked with squaraines[28]. They synthesized dihydropyrimidine derivatives with quantum yields up to 56% at 751 nm in low polarity solvents. Water-soluble versions were later synthesized giving a quantum yield of 8% at 812 nm. Würthner *et. al.* discovered an unusual halogen effect in two series of dicyanovinyl squaraines[29]. Increased polarizability of larger halogens such as iodine increased both the molar absorptivity and the quantum yields of both series. This is contrary to the heavy atom effect which typically decreases fluorescence due to spin-orbit coupling. The most outstanding dye absorbed out to 900 nm with a quantum yield of 17% at 922 nm.

Several other long-wavelength dyes can be classified as rhodamine-inspired dyes in that their structures resemble this classic fluorophore[30]. Nagano *et. al.* replaced the oxygen of the rhodamine core with a dimethylsilyl group and obtained highly photostable dyes absorbing and emitting in the far-red with quantum yields near 30%[31]. Extending the conjugation of this core further shifted the optical properties into the NIR and was shown to be useful for tumor imaging in mice[32]. Yuan *et. al.* recently developed a series of rhodamine-cyanine hybrids known as Changsha fluorophores which exhibited appropriate NIR dye photophysics[33]. These take advantage of spirocyclic lactone and lactam formation to switch between fluorescent and nonfluorescent states under different conditions, opening the possibility of use as biological analyte sensors. Of all the structures shown in Figure 1-4, it is worth noting they are all quite polar molecules, and many are formally charged. This is a common feature of most fluorescent dyes and often makes them quite water-soluble.

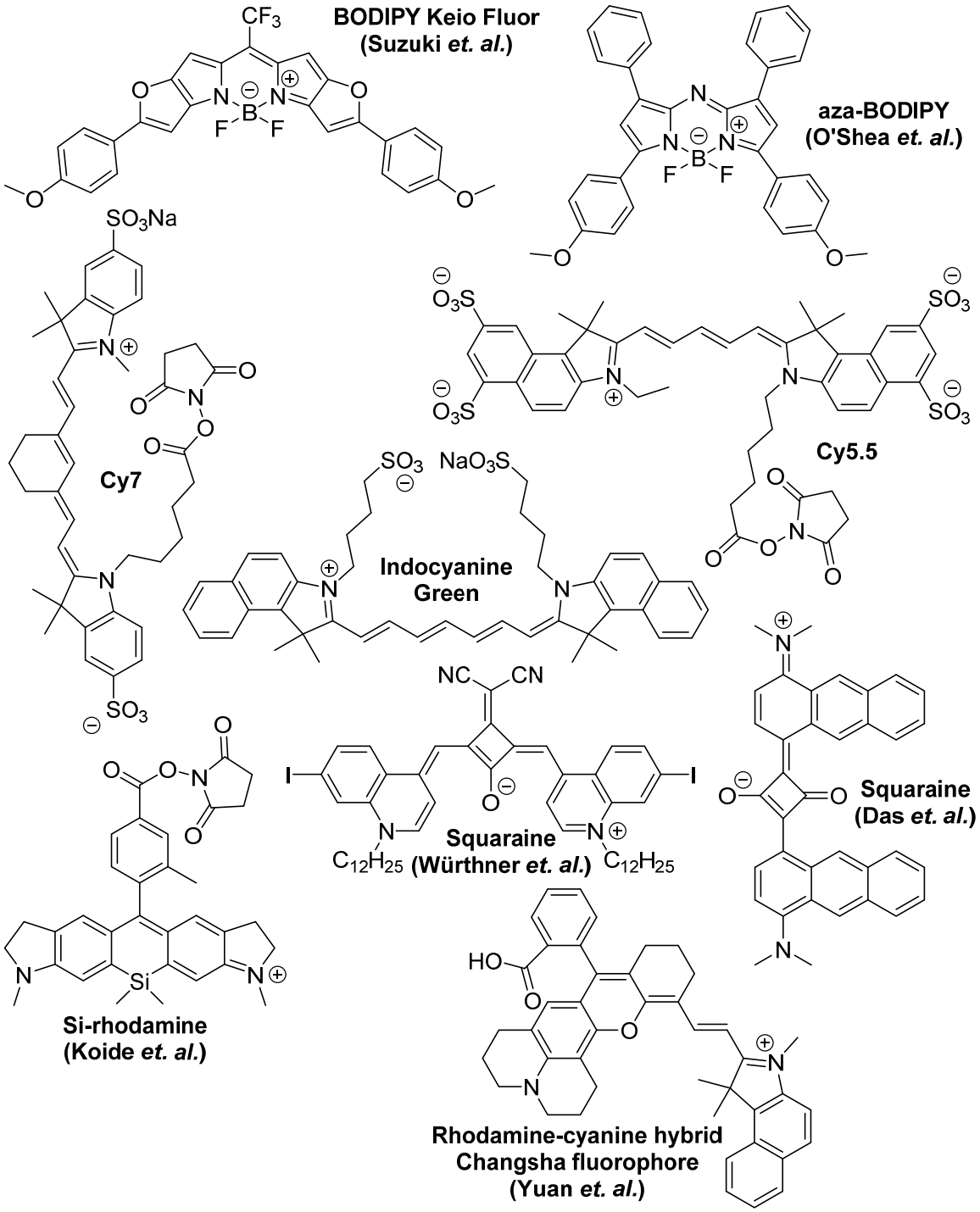

Figure 1-4. Fluorescent dye molecular structures. This includes several long-wavelength organic fluorophores including BODIPYs, cyanines, squaraines, and rhodamine-inspired dyes.

1.3.4 Two-Photon Absorption Dyes

Two-photon absorption (2PA) dyes are also classified as nonlinear optical materials[34]. These include many organic compounds in addition to a number of metal porphyrins. Similar to the UCNPs already discussed, these operate by absorbing two long-wavelength photons to populate upper electronic excited states. The theory of 2PA was first developed by Maria Göppert-Mayer in the 1930s. Whereas UCNPs undergo *sequential* absorption of photons allowed by relatively long-lived excited states, 2PA dyes operate by *nearly simultaneous* absorption of photons due to transient "virtual states" to access excited electronic states[35]. This "virtual state" only exists for about 5 fs and a transition to this state from the ground state has a very low probability (small transition dipole). Under light intensities in a typical spectrophotometer, the transition is too weak to be noticed and the photon density is too low for a second absorption. Because very intense light is required to observe this phenomenon, it was first demonstrated in 1961 after the discovery of the laser[36]. The process is depicted in Figure 1-5. Under intense laser light, a molecule can absorb a long-wavelength photon ($h\nu_1$) and be excited from the ground state (g) to a "virtual state" (i). Since the photon density from a laser is very high, there is a much higher probability for a second photon ($h\nu_2$) to be absorbed within the 5 fs lifetime, inducing a second transition to a real excited state (f).

Two-photon absorption occurs in many different materials to varying extents, and there is still much to learn about what molecular design parameters increase its efficiency. One relevant parameter to characterize these materials is the molecular two-photon absorption cross-section δ which is reported in Göppert-Mayer (GM) units where 1 GM = 10^{-50} $cm^4 \cdot s \cdot photon^{-1} \cdot molecule^{-1}$. A sense of scale relating to this unit can be developed by knowing the some of the highest 2PA cross sections recorded are on the order of 10^5 GM. In the case of dyes used in 2PA fluorescence microscopy, a second important parameter is obviously the fluorescence quantum yield ϕ_F. For 2PA in fluorescence microscopy imaging, the most relevant parameter is the product of these

two individual parameters $\delta\phi_F$ which defines the combined efficiency of excitation and emission. This is sometimes called the two-photon action cross section. To complicate matters further, deep-tissue imaging imposes additional requirements on the excitation and emission wavelengths.

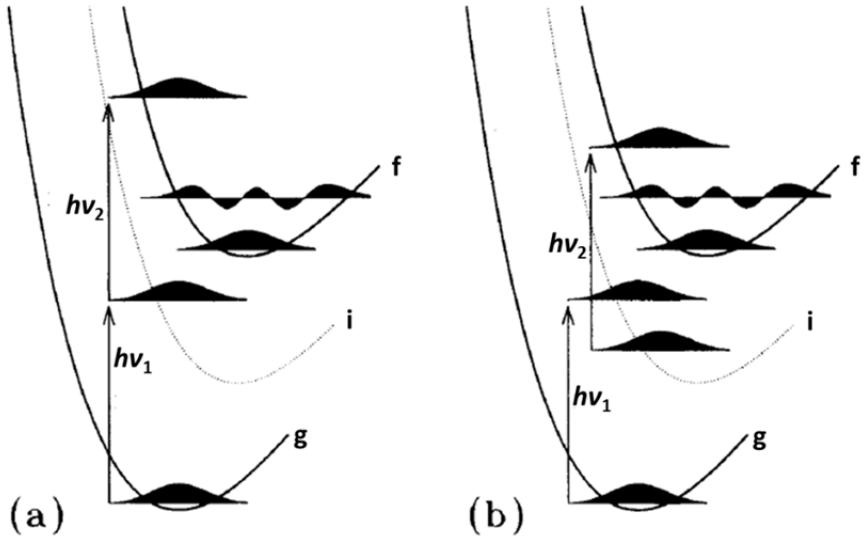

Figure 1-5. Photon absorption in two-photon absorption dyes. The letters "g", "i", and "f" designate ground, intermediate (or "virtual"), and final electronic states, respectively. Diagram (a) depicts simultaneous absorption in which there is no time for energetic relaxation. Diagram (b) depicts nearly simultaneous absorption in which slight relaxation has occurred in less than a few fs. Adapted with permission from John Wiley & Sons, Copyright © 1986[35].

Marder and Brédas published some of the first theoretical design rules for enhancing 2PA showing asymmetric donor-acceptor (push-pull) chromophores in addition to symmetric push-push or pull-pull structures were good targets[37]. Since then, additional promising molecular features have gradually emerged such as long, coplanar, π-conjugated chains. It has also been found that centrosymmetric molecules of the form D-π-A-π-D (D = donor, π = π-conjugated linker, A = acceptor) are often the most efficient 2PA dyes[36]. Avoiding *meta*-substitution in aromatic linker units also seems beneficial[38].

The vast majority of these materials do not have sufficient emission wavelengths for use in the bioimaging window, and only those with emissions beyond 600 nm are discussed here. The structures of these 2PA dyes and relevant photophysical parameters

are given in Figure 1-6. Albota *et. al.* developed an A-π-D-π-A structure incorporating thiobarbituric acid moieties as electron acceptors to achieve a 2PA cross section (δ) of 1750 GM and emitting at 641 nm[39]. Lee *et. al.* incorporated anthracene into a D-π-A-π-D system to yield a dye with a δ value of 5530 GM with 650 nm emission[40]. Huang *et. al.* used the increased electron-rich character of pyrene (relative to benzene or naphthalene) to make a material having a δ value of 1180 GM and 645 nm emission[41]. Cho *et. al.* developed a dendrimer with a δ value of 2480 GM and 614 nm emission[42]. Ahn *et. al.* recently synthesized a squaraine dye with a much higher δ value of 20,000 GM and emission at 719 nm[43]. It should be noted that all of these materials are centrosymmetric, and this is consistent with empirical observations as well as theory.

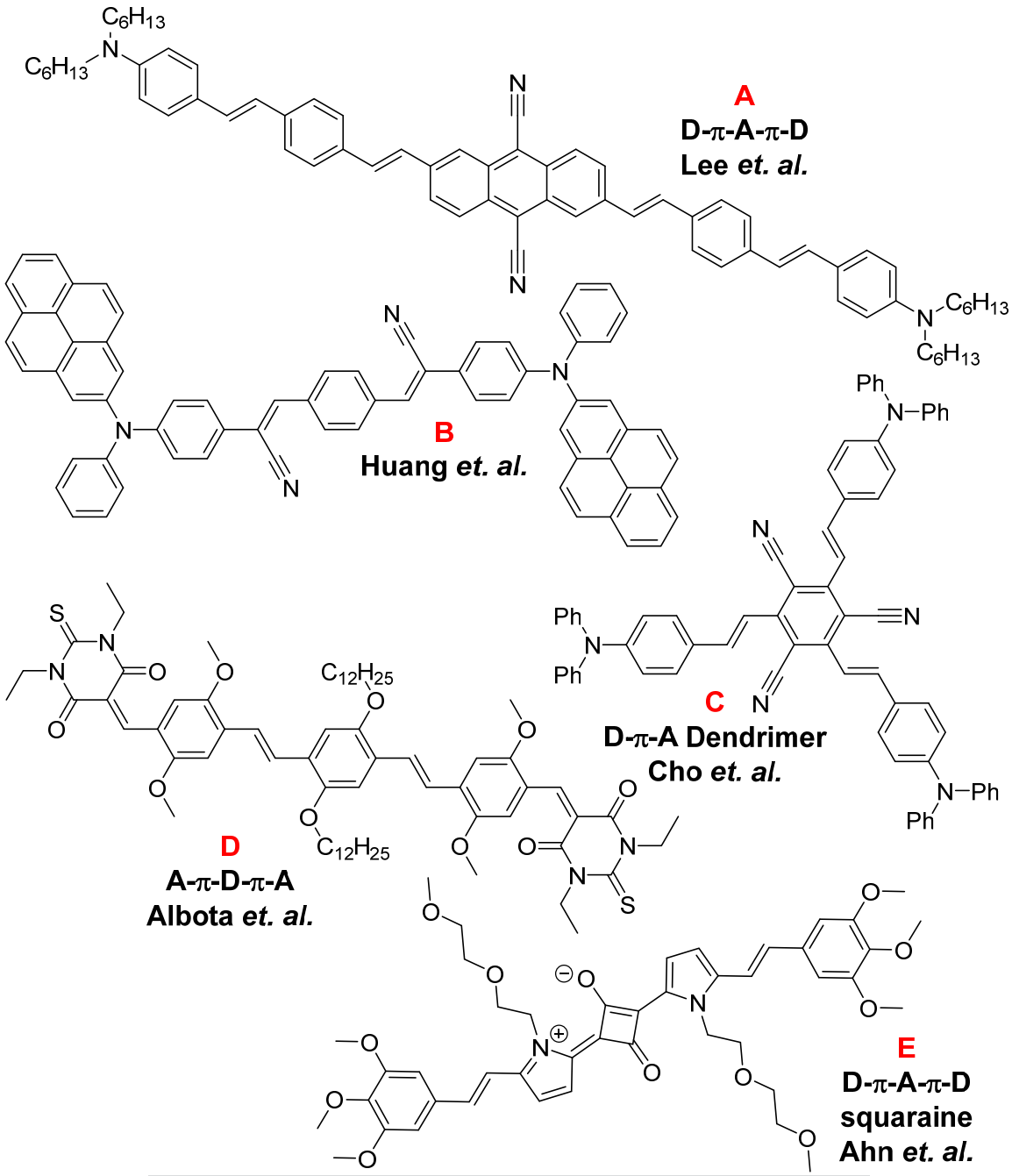

Compound	Excitation (nm)	Emission (nm)	δ (GM)	ϕ_F
A	980	650	5530	13%
B	800	645	1180	5%
C	990	614	2480	25%
D	970	641	1750	6%
E	800	719	20000	11%

Figure 1-6. Structures and photophysical properties of several 2PA dyes.

1.3.5 Sensitized Triplet-Triplet Annihilation

The photophysical phenomenon of sensitized triplet-triplet annihilation (TTA) also has potential in bioimaging and was first introduced in the early 1960's[44]. It is another type of nonlinear up-conversion process illustrated in Figure 1-7 and combines a sensitizer with an acceptor/emitter[45]. In this process, a sensitizer absorbs light and then populates the excited triplet state through efficient intersystem crossing (ISC). This triplet sensitizer then undergoes triplet-triplet energy transfer (TTET) to yield the triplet acceptor. As this process repeats, the population of the triplet acceptor increases and makes collisions more probable. When two acceptor triplet molecules collide, they annihilate to produce one excited-state singlet and one ground-state singlet. Finally, the excited singlet acceptor relaxes to the S_1 through internal conversion (IC) and fluoresces at a shorter wavelength than the original excitation photon.

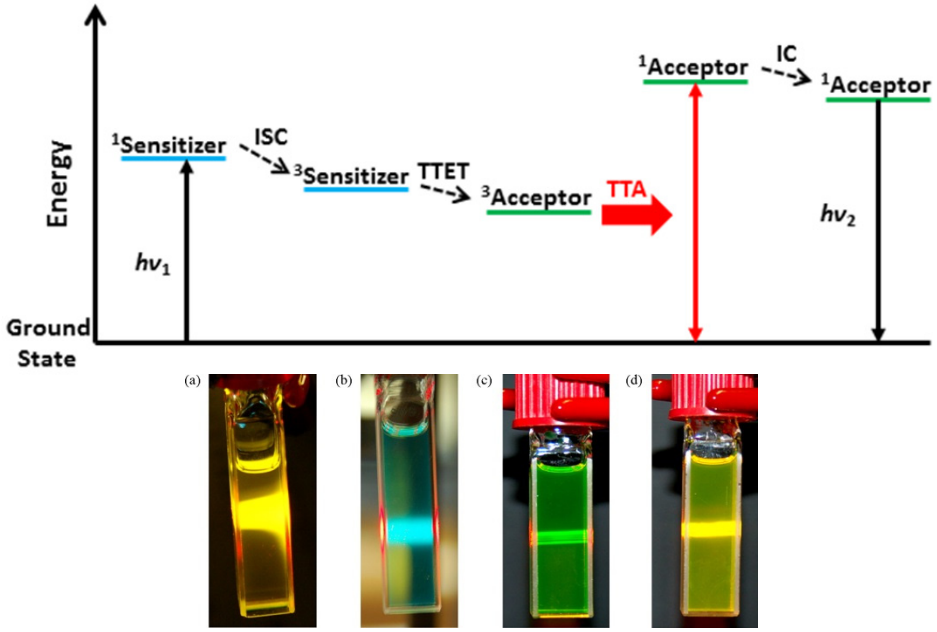

Figure 1-7. Sensitized triplet-triplet annihilation. Top: Jablonski diagram illustrating sensitized TTA where low-energy photons absorbed by the sensitizer result in high-energy photons emitted by the acceptor. Bottom: Solutions demonstrating sensitized triplet-triplet annihilation being excited by 725 or 635 nm light. Bottom images adapted with permission from Elsevier, Copyright © 2010[45a].

This type of up-conversion scheme requires carefully matched triplet energy levels between sensitizer and acceptor with the acceptor being slightly lower in energy. An additional constraint on the acceptor is the excited triplet energy level (T_1) must be ≥ half the excited singlet energy level (S_1) for annihilation to occur. The sensitizer is a type of material designed for efficient intersystem crossing (ISC) into the triplet state, which is generally accomplished by utilizing the heavy-atom effect of metal-centered complexes. Examples include ruthenium polyimines[46], platinum porphyrins[47], palladium porphyrins[48], platinum acetylides[49], and iridium complexes[50]. Ruthenium polyimines generally have shorter excited-state lifetimes and lower absorption coefficients than platinum porphyrins. Platinum acetylide complexes seem to have the advantage of easily tunable absorption and emission wavelengths by altering the acetylide ligands. Acceptors have largely been limited to small hydrocarbons which fit these requirements such as derivatives of anthracene, tetracene, and pyrene, as well as some BODIPY dyes. Essentially all of these materials are commercially available. Basically, no research has been reported on the design of new materials with the discussed energy level requirements. As a result, this up-conversion strategy has only been shown to emit visible and ultraviolet wavelengths which are outside the window needed for deep-tissue imaging. However, there have been reports of this system used in bioimaging.

Liu *et. al.* very recently demonstrated two examples of imaging in mice[51]. The first report utilized a green-to-blue (532-to-433 nm) up-conversion using a palladium porphyrin sensitizer and diphenylanthracene acceptor embedded in a water-soluble silica nanoparticle. The second report outlined red-to-green (635-to-528 nm) and red-to-yellow (635-to-546 nm) up-conversion in a soybean oil nanocapsule containing a platinum porphyrin sensitizer with different BODIPY dyes as acceptors. These systems were used *in vivo* to image lymph nodes of mice with laser powers of 8.5 - 12.5 mW/cm^2. Good results were obtained in that autofluorescence was largely avoided; however, the visible wavelengths used restricted the techniques to rather shallow depths. NIR-to-visible up-conversion has been demonstrated[46, 52], but this has not yet been applied to bioimaging. This would allow for less attenuation of the excitation

wavelengths and slightly deeper imaging, but would still be limited by visible emission wavelengths.

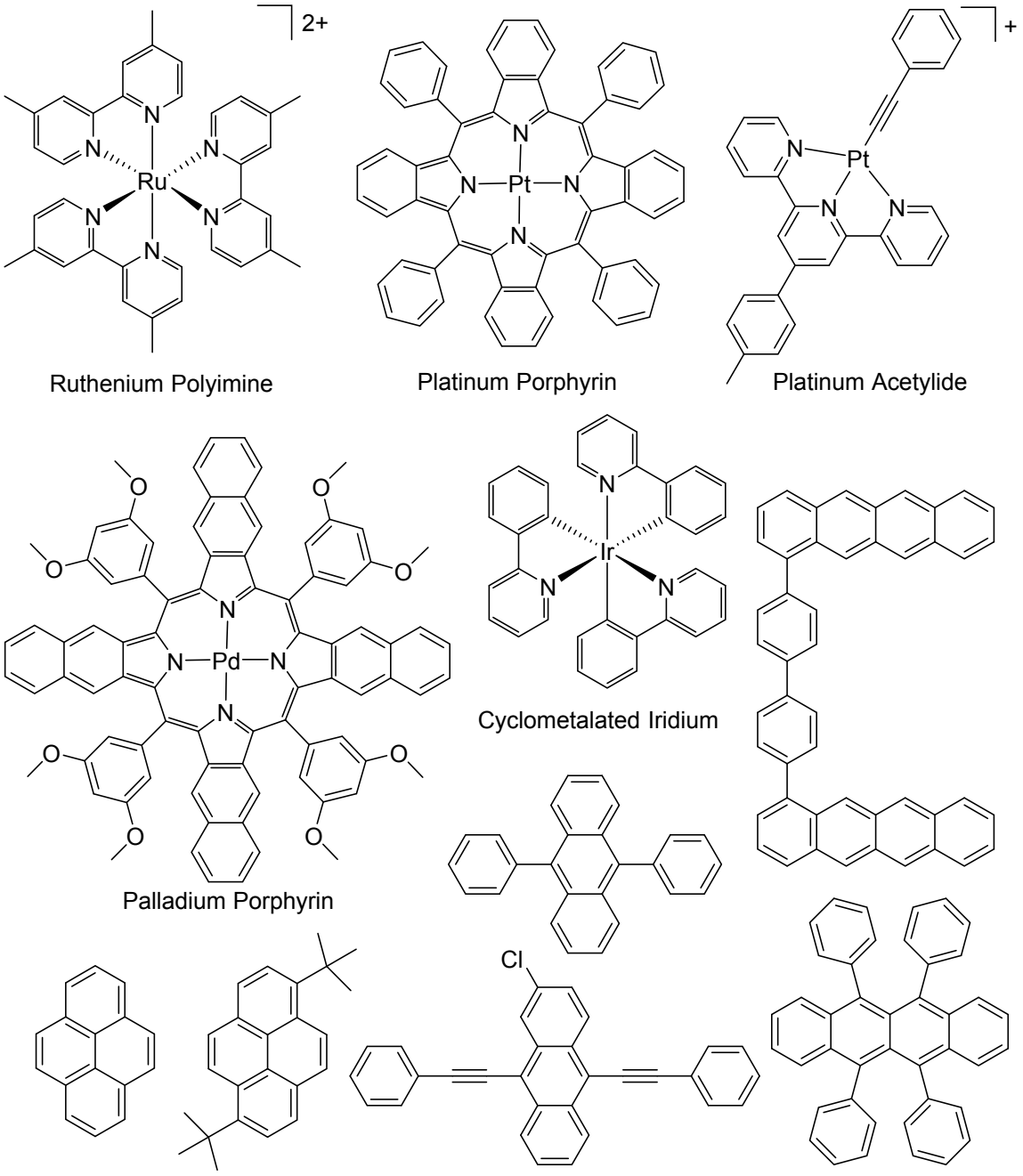

Figure 1-8. Sensitized triplet-triplet annihilation materials. These include metal-complex sensitizers and common acceptors such as anthracene, tetracene, and pyrene derivatives.

1.4 Bioimaging Project Outline

The major focus of the bioimaging work in this dissertation is the design of a deep-tissue optical imaging probe for the non-invasive detection of tumors in mice. In collaboration with the group of Robert Prud'homme at Princeton University, we are working toward a solution. His group has developed a process called flash nanoprecipitation which produces nanoparticles of narrow size distribution depending on variables such as concentration and mixing time, and is shown in Figure 1-9.[53]. In this process, a core material such as an organic drug or dye and an amphiphilic block copolymer are dissolved in a water-miscible organic solvent. This solution is then combined rapidly with water in a confined impinging jets mixer over a period of milliseconds, almost instantly creating a supersaturated solution where nanoparticles spontaneously form. These nanoparticles are composed of an inner core (drug, dye, etc.) surrounded by water-solubilizing polymer chains in a solid micelle structure. This technique has been used to encapsulate up-converting nanoparticles with organic dye sensitizers for application in photodynamic therapy[54]. By replacing organic dye sensitizers with fluorescent organic dyes, this technique could be expanded to make imaging probes. The size of the particles formed by flash nanoprecipitation is also an important property. It has been shown that particles in the range of 10 - 500 nm circulating in the bloodstream can localize in tumor tissue through the enhanced permeation and retention (EPR) effect[55], and particles produced through flash nanoprecipitation fall nicely within this range.

For this type of deep-tissue bioimaging application, the fluorescent organic dye has a number of requirements. First, it must be hydrophobic so it is not dissolved into blood. Many of the current organic dyes mentioned previously are water soluble and cannot be used in this application. Second, because of the core particle density associated with this method, it needs solid-state fluorescence with high brightness. None of the dyes available have this very important property since they aggregate and quench significantly. Third, the dye must emit in the NIR region to take advantage of the

optical imaging window. Finally, the dye must absorb light at the emission wavelengths of up-converting nanoparticles (540 and 660 nm) in order for the Förster resonant energy transfer (FRET) mechanism to operate.

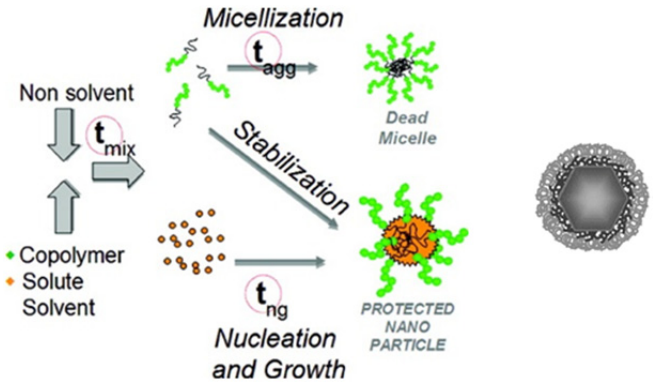

Figure 1-9. Flash nanoprecipitation. Left: Schematic of flash nanoprecipitation process including block copolymer and dye producing water-soluble nanoparticles. Right: Solubilized UCNP/dye core nanoparticle formulation. Adapted with permission from John Wiley & Sons, Copyright © 2011[54b] and from the American Chemical Society, Copyright © 2012[11].

Solid-state fluorescence is an unusual property among organic dyes in general since most fluorescent dyes are quenched at high concentrations. Additionally, the goal is to create a dye with NIR emission. Of all the materials synthesized in the Anthony group, the dioxolane-functionalized pentacene chromophore is one with potential in achieving this goal[56]. Driven by the desire for materials useful in organic light-emitting diodes, this material was synthetically modified with ethyl substituents positioned orthogonal to the acene face in a solid-state molecular engineering strategy designed to inhibit π-stacking and therefore reduce quenching[57]. Increasing the interchromophore distance has been shown to result in solid-state fluorescence in other crystals as well[58]. Crystal structures are shown in Figure 1-10. This strategy resulted in a material which maintained bright red fluorescence in the solid state and was useful for red light-emitting diodes. For pentacenes, this chromophore showed an unusually high fluorescence quantum yield of 72% in toluene, and crystals of this pentacene are fluorescent to the naked eye. The main problem with this chromophore for deep-tissue imaging is its emission wavelength which is centered near 630 nm, just outside the

imaging window. A major focus of this dissertation is modifying the emission characteristics of this material using a synthetic chemistry/crystal engineering approach, and this research is presented in chapters 2 and 3.

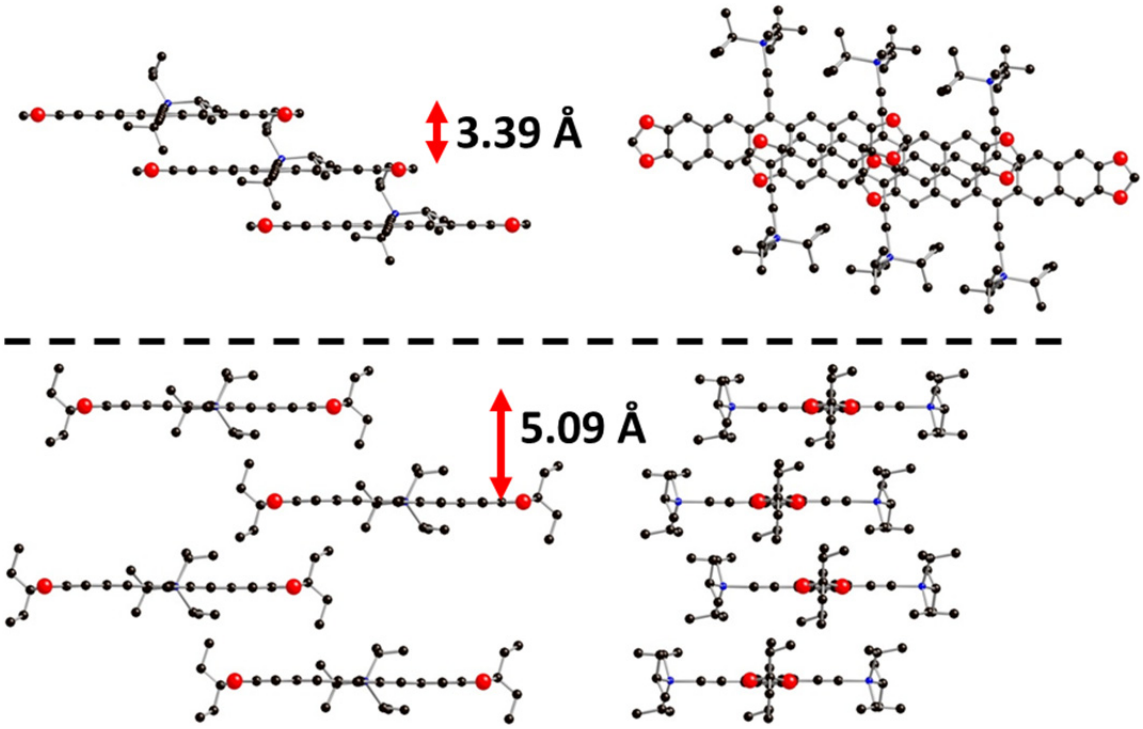

Figure 1-10. Crystal packing of dioxolane pentacene derivatives. Crystal packing of TIPS dioxolane pentacene (top) and ethyl-TIPS dioxolane pentacene (bottom) are shown with respective interchromophore distances. π-Stacking is evident in the top structure and absent in the bottom structure, resulting in solid-state fluorescence. TIPS groups were removed for clarity where necessary.

1.5 Crystal Engineering

While bioimaging and organic electronics are seemingly dissimilar topics, the use of crystal engineering binds this work together. E. J. Corey formalized retrosynthetic analysis in organic chemistry, and Desiraju extended this idea into designing crystals[59]. Crystal engineering can be described as supramolecular synthesis, making it apparent it lies within the discipline of chemistry rather than classical engineering, and can be defined as "the understanding of intermolecular interactions in the context of crystal packing and the utilization of such understanding in the design of new solids with desired physical and chemical properties[60]." It includes many different operations such

as growing crystals, analysis of crystal structures, determination of new crystal structures, and the use of this information to design crystals with desired properties and specific functions. The process can be divided into three main stages: "(i) Understanding intermolecular interactions in the context of crystal packing; (ii) Developing a strategic plan by which these interactions can lead to a certain desired packing; (iii) Fine-tuning of crystal properties to achieve a pre-determined goal[60]." As will be seen, the projects presented in this dissertation lie in these different stages of development.

One area that has enjoyed considerable success from crystal engineering is the development of coordination polymers called metal-organic frameworks. These structures vary widely based on different metals and organic ligand units. Overall properties can be tuned for gas storage of hydrogen, methane, and acetylene[61], separation of light gases and liquids[62], catalysis[63], "crystal-free" X-ray crystallography[64], and a host of other applications. Key aspects of the success of metal-organic framework design are the strength of the bonding interactions involved and the metal center directional coordination. These supramolecular assemblies are formed from metal-ligand bonds with energies ranging from roughly 40 to 120 kcal/mol. The coordination number and bond directionality provided by the metal center simplifies structural prediction.

Work in the Anthony group has focused on molecular and crystal engineering of acene organic semiconductors for more than a decade, spurred by the success of TIPS pentacene in thin-film transistors[65]. This work is in contrast to metal-organic frameworks in that these organic crystals are held together only by much weaker *intermolecular* interactions such as Van der Waals forces and π-stacking. Utilizing these much smaller energies makes predicting crystal packing more difficult, but significant progress has been made. The silylethynyl-functionalization approach increases molecular solubility and alters crystal packing; it has become a trademark of this group's work. Whereas unsubstituted acenes as large as hexacene[66] pack in a herringbone motif, silylethynyl-functionalization at the middle acene ring often results in a face-to-

face interaction which is further tuned by the size of the silylethynyl substituent with several examples shown Figure 1-11. The 1-D slip-stacked and 2-D slip-stacked (brickwork) π-stacking motifs are commonly observed, whereas the sandwich herringbone motif, which is itself a special case of 1-D π-stacking, is less frequent. Over the years, this functionalization strategy has been used to extend the length of crystalline acenes and heteroacenes to include tetra- and pentadithiophenes[67], hexacenes[68], heptacenes[68a], and nonacenes[69] which exhibit the desired face-to-face π-stacking interaction.

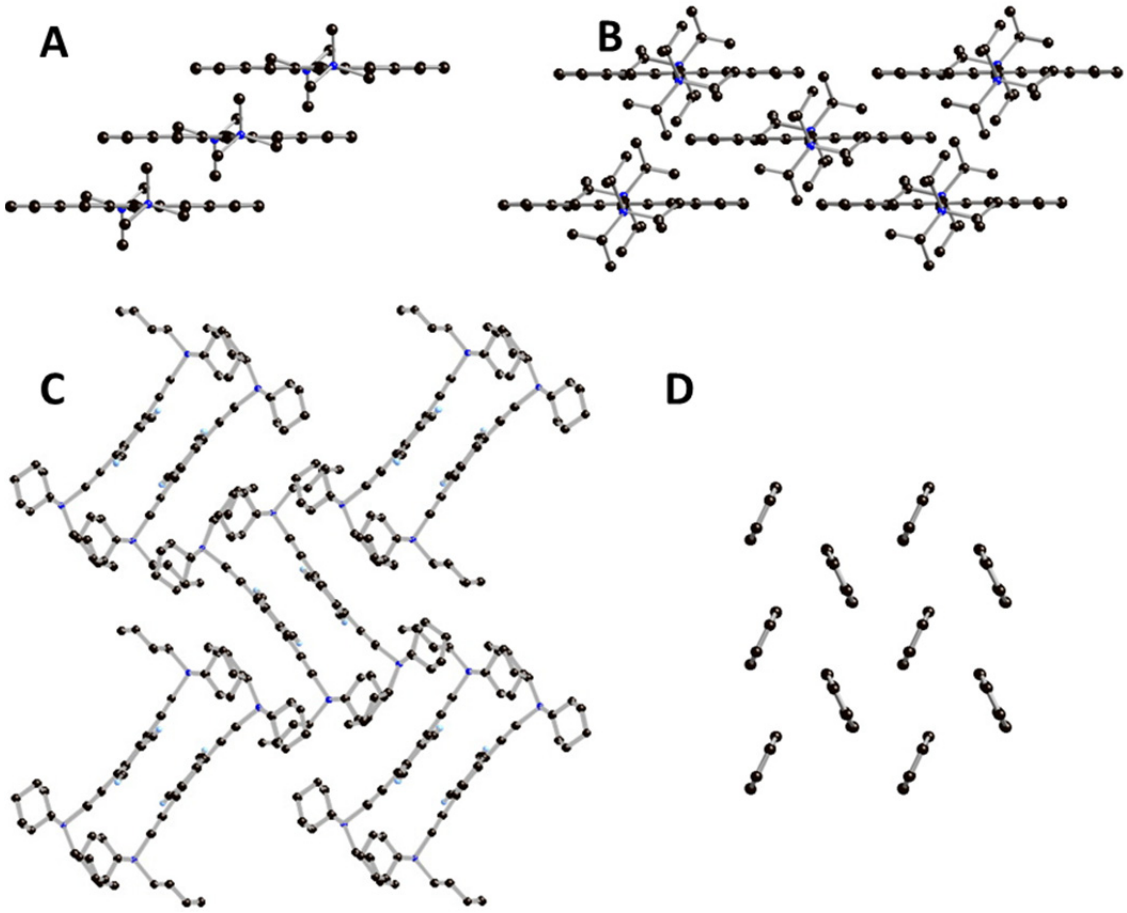

Figure 1-11. Several crystal packing motifs observed in acenes. Diagrams A - C utilize the silylethynyl-functionalization approach. Examples shown are (A) 1-D slip-stacked, (B) 2-D slip-stacked, (C) sandwich herringbone, and (D) herringbone.

Functionalization at other positions of the acene and heteroacene cores affects the molecular properties and crystal packing in other ways. The dioxolane pentacenes are an example of this and were discussed earlier. Halogenation has also been explored and shown to be useful. Fluorination can reduce the distance between acene faces in crystals and improve electronic properties[70]. Bromination and iodination can also be used as synthetic handles to introduce other substituents using palladium catalysts, with cyano-functionalized pentacenes synthesized in this fashion.

It has been demonstrated that different packing motifs work best with specific organic electronic applications such as transistors and solar cells. The 2-D π-stacking motif has consistently produced the best transistor materials as shown with TIPS pentacene[65b], TES-ADT[71], F-TES-ADT[70b], and F-TSBS-PDT[67b]. Bulk-heterojunction solar cells consist of mixtures of compounds rather than a pure, crystalline material, and this makes relating device performance to crystal packing more ambiguous. However, some work suggests 1-D π-stacking produces more efficient solar cells as demonstrated by ethyl-TES-ADT[72] and several cyano-, trifluoromethyl-, and chloro-substituted pentacenes[73]. There have been two cyano-functionalized pentacenes synthesized in this lab which exhibit 2-D π-stacking, those being TIPS- and TIBS-2,3-dicyanopentacene. In terms of a crystal engineering strategy, it was reasoned that replacing the nitrile substituents with similarly sized substituents might also result in molecules which also adopt the desired 2-D π-stacking motif and make useful transistor materials. This is presented in chapter 4, along with other crystal engineering work.

1.6 Singlet Fission

Singlet fission is a rapid photophysical process observed in only a few classes of molecules and can be viewed as a special case of intersystem crossing. Among the best molecules studied are small-molecule crystals including oligophenyls, tetracyano-*p*-quinodimethane charge-transfer complexes, diphenylisobenzofuran, and acenes[74]. It operates by the following simplified mechanism:

$$S_0 + S_1 \leftrightarrow {}^1(TT) \leftrightarrow T_1 + T_1$$

where S_0 and S_1 are two chromophores in their ground and first excited singlet states, respectively, ^{1}(TT) is a correlated triplet pair, and T_1 is a chromophore in the first excited triplet state. In principle, the process is reversible, with the reverse process being triplet-triplet annihilation. Some computational work also suggests an additional optically dark state may be involved prior to formation of the correlated triplet pair[75]. The ^{1}(TT) is a rather vaguely-defined pair-state consisting of two coupled triplets with an overall combined spin of a singlet, making singlet fission a spin-allowed process[76]. Singlet fission is observed when the triplet energy is approximately ½ the energy (or less) of the S_1 state, or $E(S_1) \approx 2E(T_1)$. This process has been well-studied in tetracene and pentacene and was found to be slightly endergonic in tetracene by ≈0.2 eV and exergonic in pentacene by 0.11 eV[77]. In the case of tetracene, thermal activation is required. As with chemical equilibria, the equation can be biased toward singlet fission if $E(S_1) > 2E(T_1)$, and a Jablonski energy level diagram is shown in Figure 1-12.

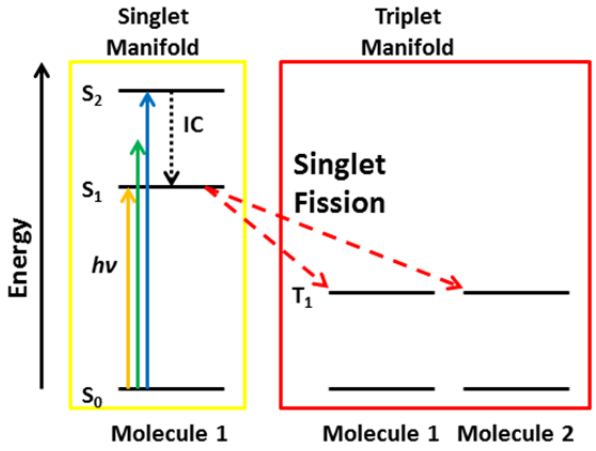

Figure 1-12. Jablonski energy level diagram outlining singlet fission. Molecule 1 absorbs light of various frequencies and relaxes to the S_1 state by internal conversion (IC). It then transfers some of its energy to neighboring Molecule 2 through singlet fission (dashed red arrows) and both arrive in the T_1 state.

Singlet fission is of interest due to its potential to enhance the efficiency of organic solar cells consisting of a donor and acceptor active layer. Shockley and Queisser demonstrated that a single p-n junction solar cell has a maximum efficiency of ≈30% due to unavoidable energy losses[78]. Singlet fission can reduce energy losses due to incomplete absorption and thermalization of photon energy in excess of $E(S_1)$, thereby

increasing the maximum efficiency to 41.9% for single bandgap photovoltaic cells and slightly higher for tandem cells[79]. Since *two* excitons can be produced from a single absorbed photon, the quantum efficiency can be as high as 200%. A schematic of this process is shown in Figure 1-13.

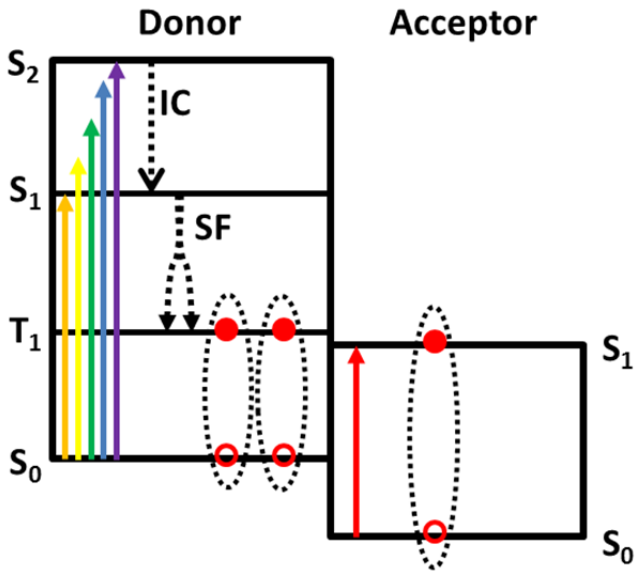

Figure 1-13. Active layer of a photovoltaic cell utilizing singlet fission. The donor layer absorbs high-energy light frequencies and creates two triplet excitons from one photon through singlet fission (SF). The acceptor is a standard material which absorbs lower-energy frequencies and generates one exciton per absorbed photon.

Fullerene derivatives are often used in solar cells as acceptors due to their fast electron-transfer characteristics[80]. As such, they are typically used as electron acceptors in singlet fission photovoltaics to help study the fission process[77a, 81]. In a practical photovoltaic, this is problematic because fullerenes generally absorb only high-energy photons[82]. Therefore, this would not give any overall efficiency increase and simply result in halving the voltage produced. Baldo *et. al.* demonstrated this problem can be addressed by using a third component in the active layer which gave a 71% singlet fission efficiency[83]. Alternatively, this problem can be solved by using a tandem photovoltaic device in which a second cell absorbs the remaining light frequencies. This second cell can be of a standard design in which each photon absorbed produces one

exciton, or it can also utilize singlet fission. A schematic of the absorption enhancement of a singlet fission tandem cell is shown in Figure 1-14. Photons with energies of at least twice the triplet energy result in a 200% quantum yield, as denoted by the step function.

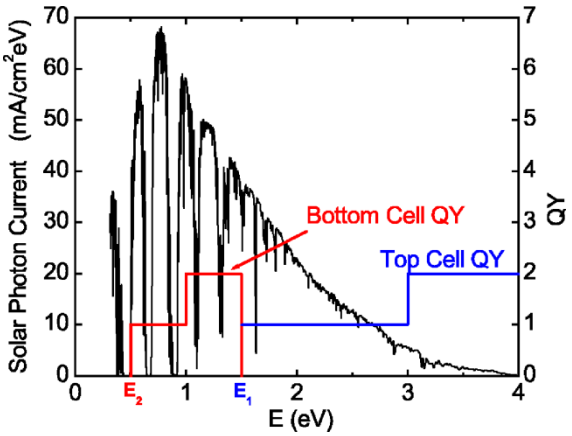

Figure 1-14. Absorption enhancement of a tandem photovoltaic in which both cells utilize singlet fission. The maximum theoretical efficiency of such a cell is 45.7%. Adapted with permission from the American Institute of Physics, Copyright © 2006[79].

As a whole, singlet fission is a poorly understood process. While the energy requirements are understood, molecular orientation is another major component to overall efficiency. As posed by Smith and Michl, "How should neighboring chromophores be coupled into pairs or higher aggregates[74]?" Singlet fission is not a well understood process in terms of crystal requirements. The molecules need to be oriented in a very balanced manner in that they couple strongly enough to ensure singlet fission occurs quickly, yet weakly enough for the two triplets to independently undergo charge separation. A model of orbital overlap between tetracene molecules suggests they should be slip-stacked with the slip in the direction of the short molecular axis[84]. Efficient singlet fission has recently been reported in crystalline TIPS pentacene which is slip-stacked in this manner, but it is also slip-stacked along the long molecular axis and has face-to-face π-stacking interactions rather than being tilted in the herringbone packing motif[85]. The situation is complicated further by 5,12-diphenyltetracene in which largely amorphous films were shown to exhibit singlet fission. Even in a macroscopically disordered state, it is likely tiny crystallites formed with sufficient intermolecular

coupling. From a crystal engineering standpoint, this research is in stage (i): understanding intermolecular interactions in the context of crystal packing. As mentioned by Johnson *et. al.*, a larger library of photostable materials demonstrating singlet fission with a low-cost and scalable method of self-assembling the correct intermolecular coupling is needed if singlet fission is to have any real impact on practical solar harvesting systems[86]. With this in mind, chapter 5 will discuss efforts in synthesizing new crystalline heteroacenes for singlet fission, as well as evaluating the utility of existing acenes for this process.

Chapter 2. Crystal Engineering & Bioimaging of Dioxolane Pentacenes

2.1 Crystal Engineering Approach & Synthesis

As described in chapter 1, the dioxolane pentacene chromophore gives a high fluorescence quantum yield in solution, but forms close face-to-face π-stacking aggregates in the solid state in which fluorescence is mostly quenched. A solid-state/crystal engineering strategy focused on adding ethyl substituents to the dioxolane rings to prevent close π-stacking and yielded a solid-state fluorescent material. Since solid-state fluorescence is a necessary property of the bioimaging probe outlined in chapter 1, this project began with substituting the dioxolane ring with other groups which might also prevent close chromophore π-stacking. This was thought to be a conceptually simple extension of the crystal engineering strategy which might allow for more synthetic flexibility when the focus of this project eventually shifted to altering the absorption and fluorescence wavelengths necessary for the bioimaging window.

Synthesis of three new derivatives incorporating different bulky dioxolane ring substituents were synthesized in a similar manner as outlined in Scheme 2-1. Synthesis began with enolization of 2,3-butanedione (**2-1**) and trapping as the trimethylsilyl ether (**2-2**). This diene then underwent a Diels-Alder reaction with dimethyl acetylenedicarboxylate followed by oxidation with bromine to give dimethyl-4,5-dihydroxyphthalate(**2-3**)[87]. From this point synthesis proceeded following a modified procedure previously reported in the literature[88]. Acid-catalyzed condensation with an appropriate ketone led to acetals as mixtures of anhydrides and dimethyl esters (**2-4**). The first and third derivatives were produced by condensation with isovalerone and benzophenone, providing isobutyl and phenyl substituents, respectively. A bulky methylenecyclohexyl substituent was desired for the second derivative, but the corresponding ketone was not commercially available. It was synthesized by Grignard formation with (bromomethyl)cyclohexane (**2-9**) and reaction with ethyl formate to give alcohol (**2-10**), followed by Swern oxidation to ketone (**2-11**) as outlined in Scheme 2-2. Following condensation, the mixtures were reduced with lithium aluminum hydride to

dimethanols (**2-5**) and then oxidized under Swern conditions to give phthalaldehydes (**2-6**). These were combined with 1,4-cyclohexanedione in a 4-fold aldol condensation[89] to give pentacenequinones (**2-7**). Finally, addition of lithiated TIPS acetylene followed by deoxygenation with $SnCl_2$/HCl gave the final dioxolane pentacene derivatives(**2-8**)[90].

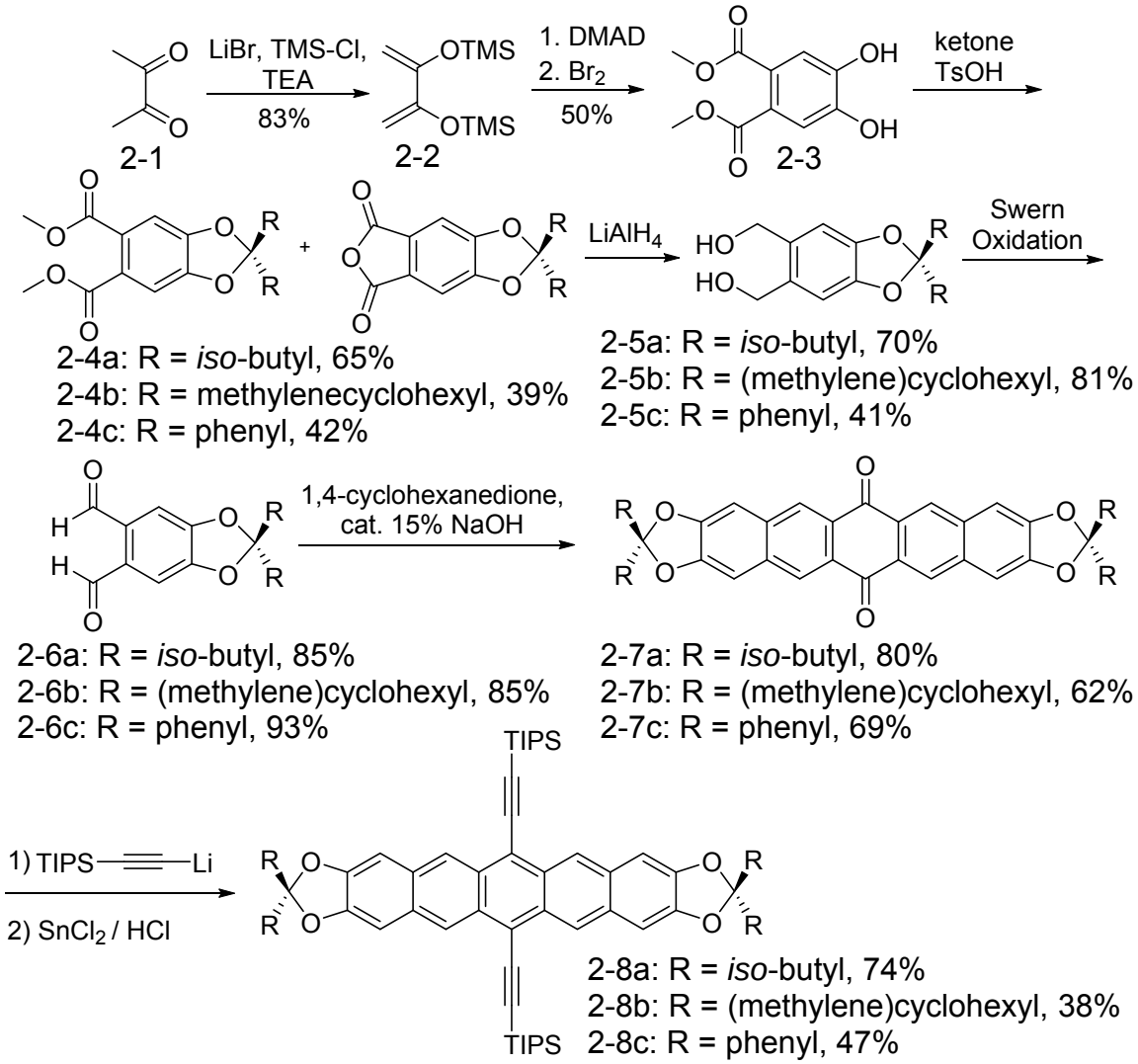

Scheme 2-1. Synthetic outline of dioxolane pentacene derivatives.

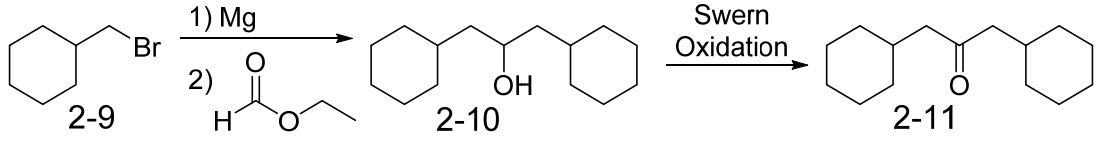

Scheme 2-2. Synthesis of ketone (**2-11**).

2.2 X-ray Crystallography

Crystals of these three pentacenes were suitable for X-ray crystallography and produced refined models as shown in Figures 2-1 through 2-3. Isobutyl derivative (**2-8a**) shows a large interchromophore stacking distance of 6.99 Å. The methylenecyclohexyl derivative (**2-8b**) shows some rotational disorder of the cyclohexane rings, but also has a large interchromophore spacing of 6.63 Å. Phenyl derivative (**2-8c**) crystallized with disordered solvent molecules, but also exhibits large interchromophore spacings of 6.30 and 6.72 Å.

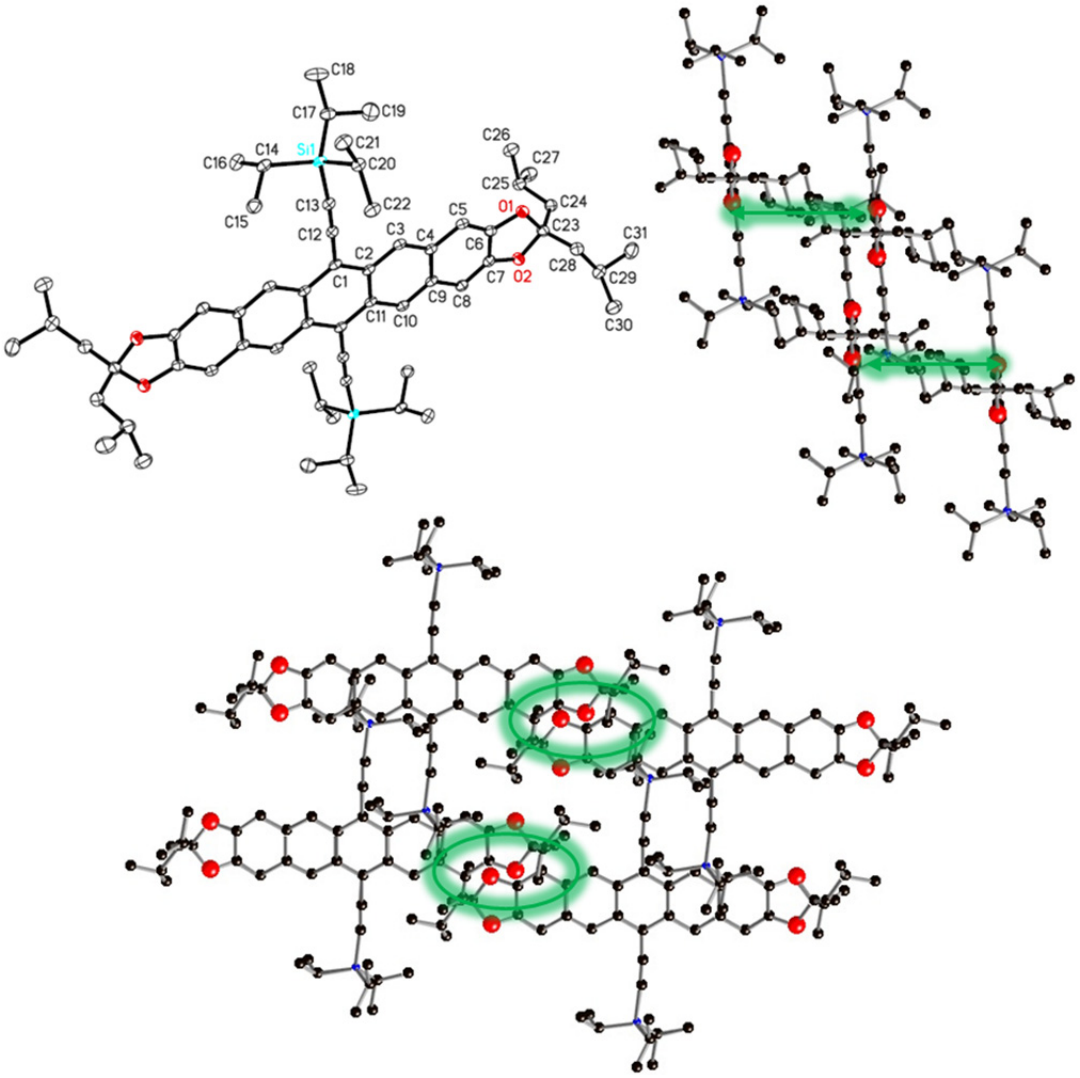

Figure 2-1. X-ray crystal structure of dioxolane pentacene (**2-8a**). The distant interchromophore spacing of 6.99 Å is highlighted in green.

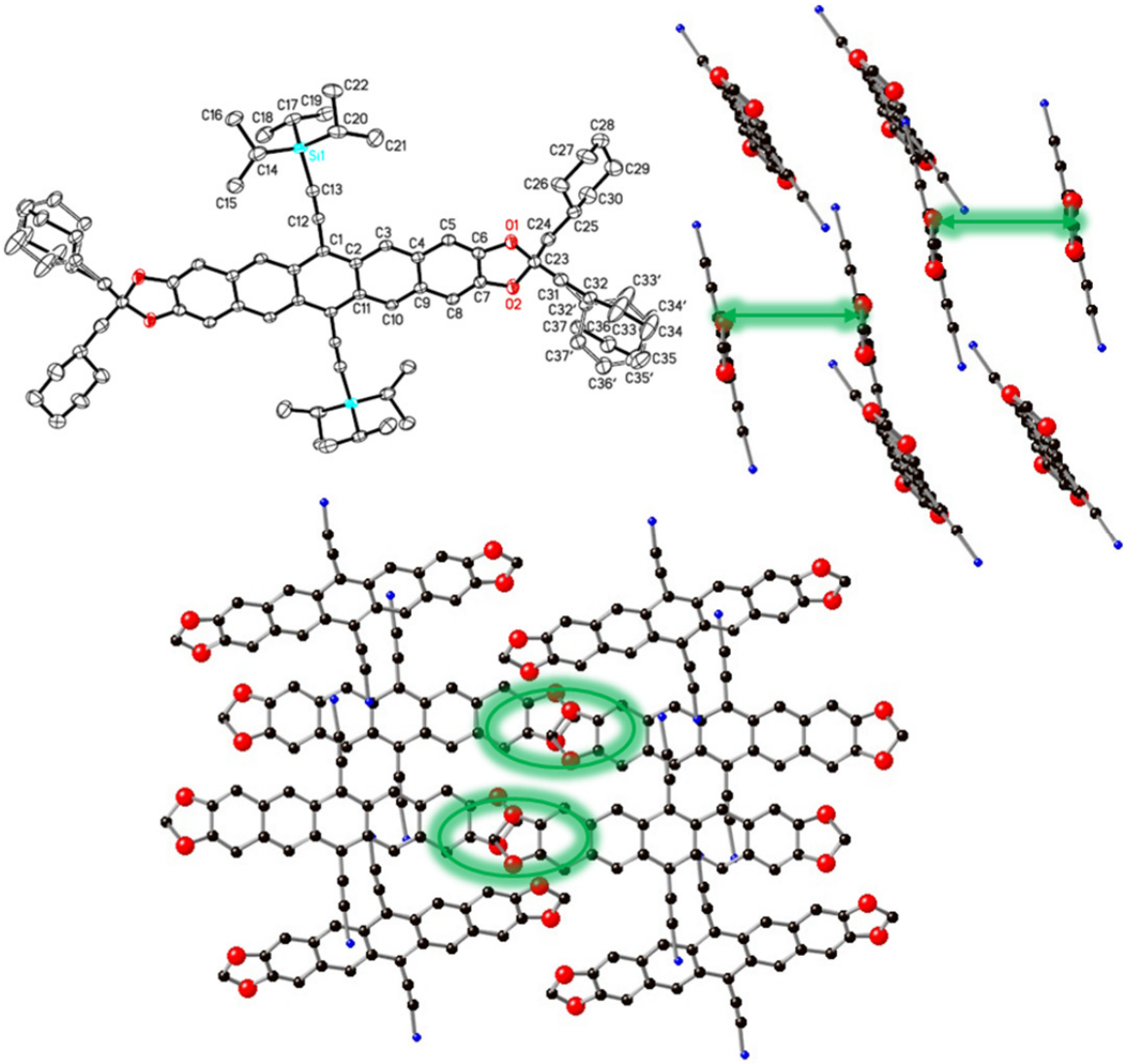

Figure 2-2. X-ray crystal structure of dioxolane pentacene (**2-8b**). Rotational disorder of the cyclohexyl moieties is evident in the thermal ellipsoid plot. The distant interchromophore spacing of 6.63 Å is highlighted in green. All alkyl substituents were removed for clarity.

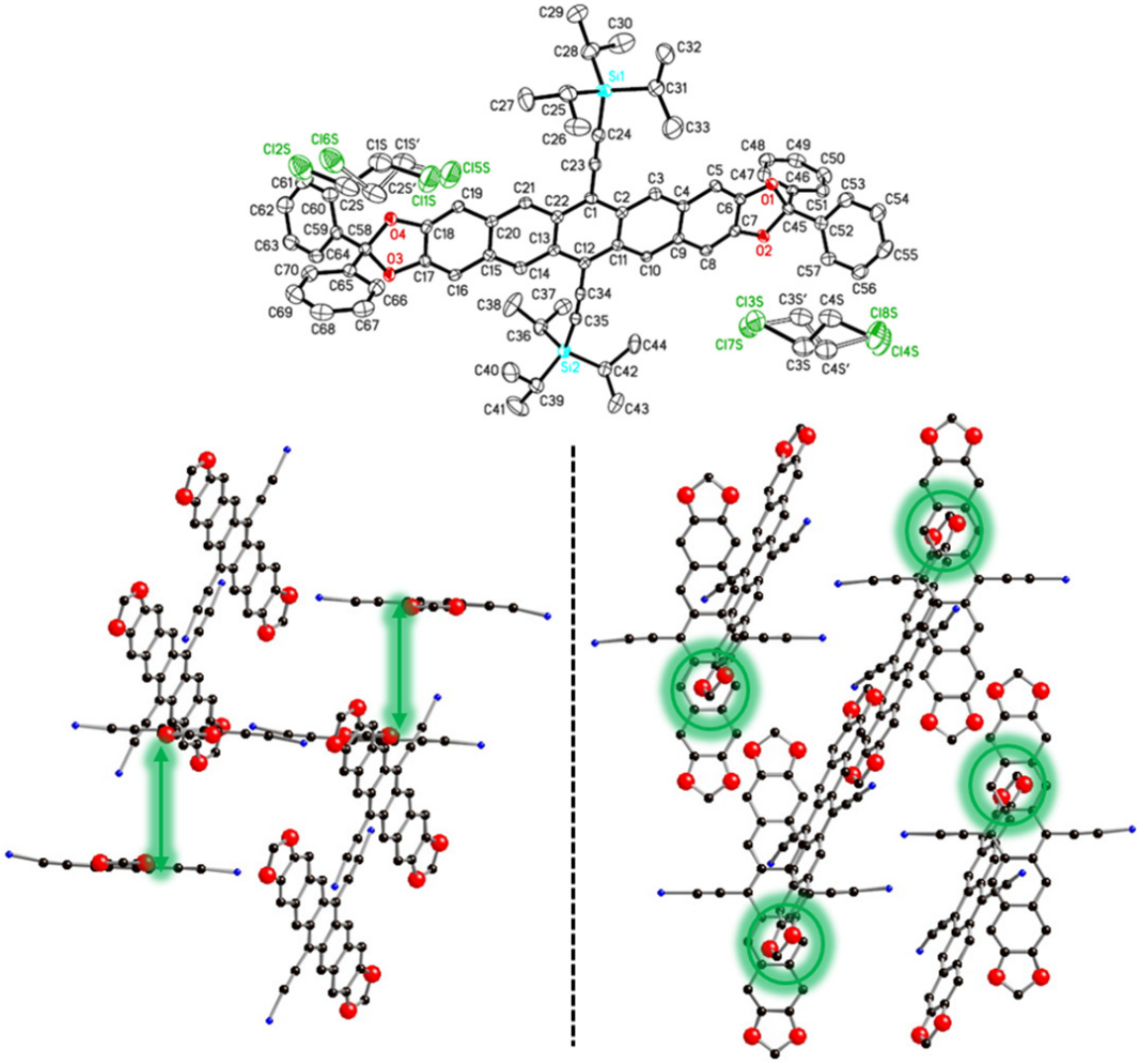

Figure 2-3. X-ray crystal structure of dioxolane pentacene (**2-8c**). The thermal ellipsoid plot shows disordered 1,2-dichloroethane (solvent) in the structure. Two different interchromophore spacings are highlighted in green as lines (6.72 Å) and circles (6.30 Å). Solvent, alkyl, and phenyl moieties were removed for clarity.

2.3 Solid-State Fluorescence

Since all three of these new derivatives show the absence of π-stacking, this crystal engineering strategy was successful. Importantly, all three pentacenes showed visible solid-state fluorescence, and images of each derivative are shown in Figure 2-4. The fluorescence varies substantially among these derivatives. Isobutyl derivative (**2-8a**) appears very bright whereas methylenecyclohexyl derivative (**2-8b**) has only a faint

glow. This may be a consequence of different crystal habits. The methylenecyclohexyl derivative forms mostly small, blocky crystals whereas the isobutyl derivative forms somewhat thinner plates. Phenyl derivative (**2-8c**) formed very tiny, powderlike crystals. Strong UV attenuation by molecules nearer the crystal surface would result in diminished intensity near the center of the crystal, so less emission would be observed. Since the isobutyl derivative crystallizes as thinner plates, both excitation and emission would be attenuated less.

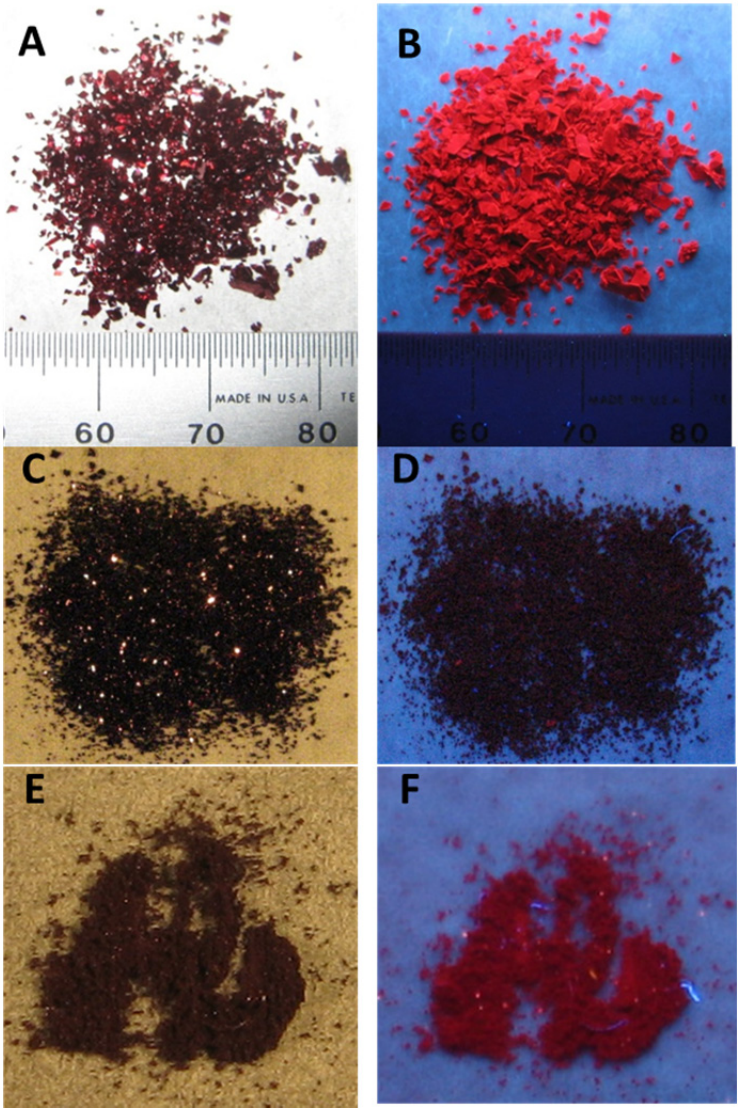

Figure 2-4. Images of crystalline dioxolane pentacenes. These were taken under bright light (left) and long-wavelength UV lamp illumination (right). Images A & B are isobutyl derivative (**2-8a**), C & D are methylenecyclohexyl derivative (**2-8b**), and E & F are phenyl derivative (**2-8c**).

2.4 Bathochromic Shift

As mentioned, the overall goal of this bioimaging research is developing a fluorescent probe which can be used in the bioimaging window. The purpose of synthesizing dioxolane pentacenes (**2-8a**), (**2-8b**), and (**2-8c**) was to identify additional dioxolane substituents ("tools") which could effectively disrupt π-stacking and result in a solid-state fluorescent dye, a requirement for this particular bioimaging probe. These three derivatives add to the list of "tools" already available, including ethyl, butyl, and spirocyclohexyl. With six of these "tools" now identified, the focus of this research shifted to address the absorption and emission properties of the dioxolane pentacene fluorophore. Representative solution absorbance and fluorescence spectra of dioxolane pentacene (**2-8a**) are shown in Figure 2-5. Based on the spectra, it is clear these wavelengths need to be bathochromically shifted at least 30 nm for use in the bioimaging window. Synthetic changes needed to induce this shift will be combined with the above "tools" to yield a material with solid-state fluorescence in the bioimaging window.

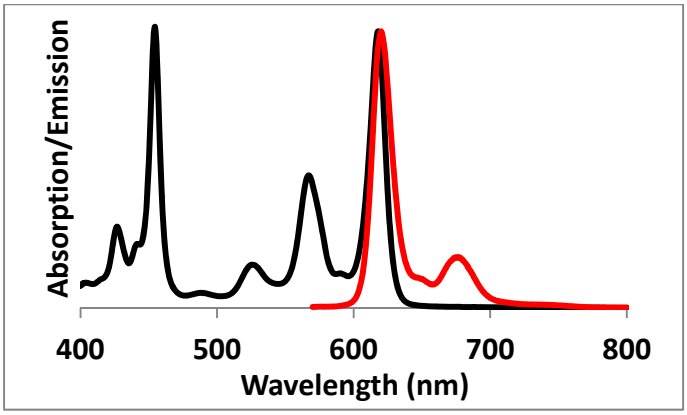

Figure 2-5. Absorption and emission spectra of dioxolane pentacene (**2-8a**). The compound features a long-wavelength absorption maximum of 618 nm and mirror-image fluorescence with a maximum at 620 nm in hexanes.

A general way of inducing large shifts in absorption is by increasing the polarization of a chromophore. Tykwinski *et. al.* demonstrated this in a series of pentacenes which were polarized by asymmetric phenylacetylene substitution,

enhancing the pentacene transition dipole[91]. This work resulted in pentacenes absorbing out to 664 nm with emission at 679 nm. Based on this, a similar strategy was attempted for dioxolane pentacenes. In the first case, two different phenylacetylene substituents were chosen, dimethylaminophenylacetylene and 4-ethynylbenzonitrile, to give asymmetric dioxolane pentacene (**2-12**). Characterization by UV-Vis and fluorescence spectroscopies, although questionable due to fluorescent impurities, indicated a long-wavelength absorption maximum at 672 nm with a fluorescence maximum at 712 nm. Unfortunately, this material could only be synthesized in milligram yields and was very difficult to purify. Tykwinski's results indicated materials of this type were unlikely to be stable, and this was supported by the very poor yields in this case. In the second case, identical 4-ethynylbenzonitrile substituents were added to produce symmetric dioxolane pentacene (**2-13**), which showed a long-wavelength absorption maximum at 665 nm with a fluorescence maximum at 695 nm. Molecular structures and spectra are shown in Figure 2-6. While optical characterization showed pentacene (**2-13**) was much more pure than pentacene (**2-12**), there were still impurities present and it also suffered from very difficult purification and low synthetic yields. Given these poor results, it was concluded that a new strategy was needed to give materials with higher stabilities which could be produced on larger scales. This work will be presented in chapter 3.

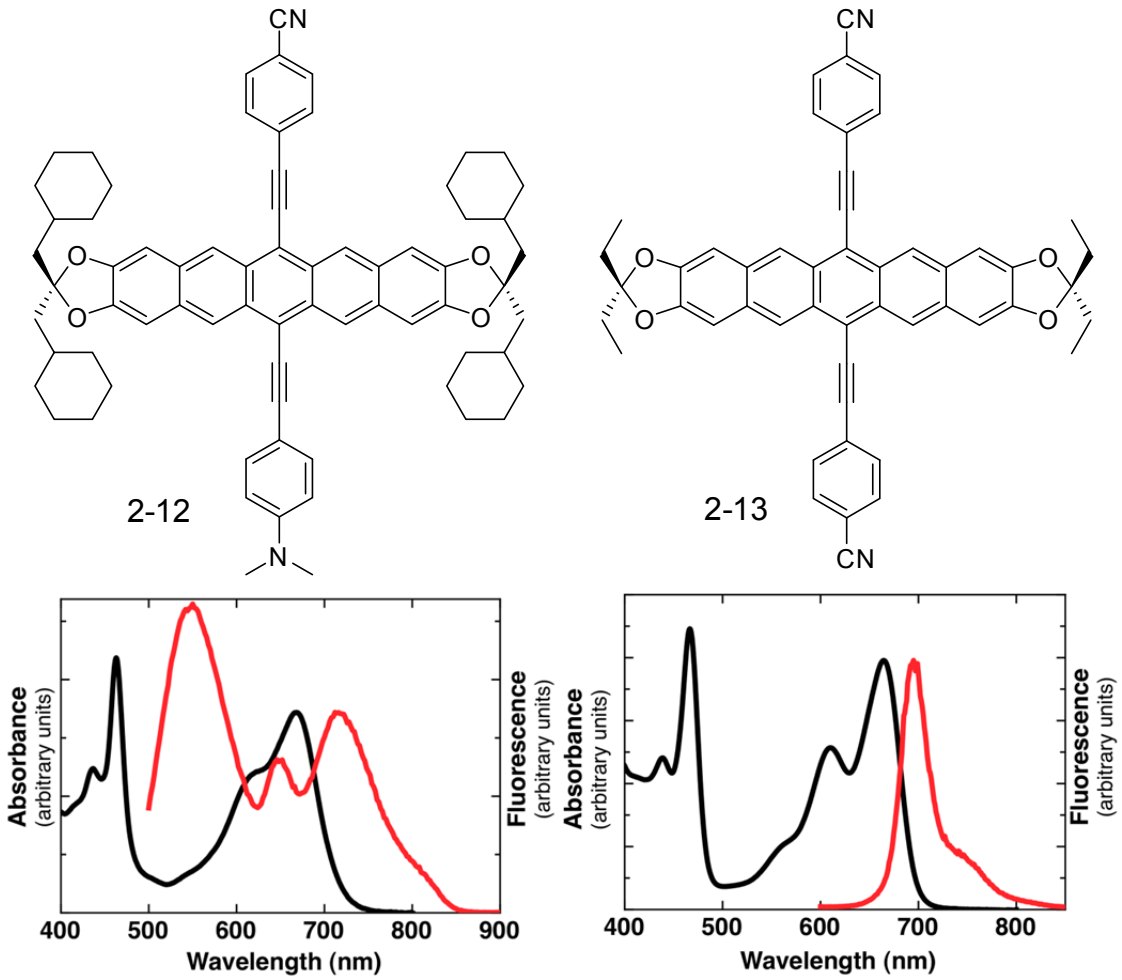

Figure 2-6. Bathochromically shifted pentacenes. Top: Molecular structures of asymmetric pentacene (**2-12**) and symmetric pentacene (**2-13**). Bottom left: UV-Vis and fluorescence spectra of asymmetric pentacene (**2-12**) with maxima at 672 and 712 nm. There is clear evidence of one or more fluorescent impurities. Bottom right: Symmetric pentacene (**2-13**) with maxima at 665 and 695 nm, respectively.

2.5 Dioxolane Pentacene Imaging

While not useful for deep-tissue imaging, the properties of the dioxolane pentacene fluorophore are still sufficient for use as general fluorescent probes since they mostly avoid tissue autofluorescence. As mentioned, this bioimaging project was done in collaboration with the group of Robert Prud'homme at Princeton University. The flash nanoprecipitation process discussed in chapter 1 has been demonstrated with dioxolane pentacene (**2-14**) and used as a fluorescent probe. In one example, these nanoparticles were used to quantify the total concentration of nanoparticles within a

microparticle[92]. This helped demonstrate a glass microcapillary microfluidic device in which microparticles formed could contain nanoparticle loadings as high as 67%, making them potentially useful for drug delivery.

A second study emphasized the utility of imaging nanoparticles in which the core is fluorescent, a result of the inherent volume available (manuscript submitted: Pansare, Bruzek, *et. al.*). While a nanoparticle may have a volume in which ≈ 10^5 fluorophores could pack, there may be only ≈ 10^2-10^3 surface sites at which a fluorophore could be usefully conjugated. Because of this, there is potential for core-fluorescent nanoparticles to be orders of magnitude brighter than similar surface-fluorescent probes. In addition, removing fluorophores from a probe's surface could reduce interference with surface modifications designed for specific receptor targeting. Based on this, nanoparticles formed by flash nanoprecipitation gave an optimized per-fluorophore fluorescent maximum at 2.3 wt%, limited essentially only by Förster resonance energy transfer. A third study based on this work developed nanoparticle formulations designed to target immune cell macrophages for tuberculosis treatment[93]. Tuberculosis bacteria have a surface protein coating capped by the sugar mannose, and this is recognized by the mannose receptors on immune cell macrophages. The bacteria are consumed through phagocytosis but are not killed by the macrophage. Instead, the normal enzymatic digestion is arrested, and the tuberculosis bacteria are free to replicate within the macrophage host cell. Treatment of tuberculosis is difficult because drugs can be limited by toxicity, poor solubility, side-effects, or degradation. As a proof-of-concept, this study used flash nanoprecipitation to produce fluorescent nanoparticles (containing pentacene (**2-14**)) with mannose functionalities designed to specifically target the mannose receptors of macrophage cells. As shown in Figure 2-7, these targeted nanoparticles were taken up by the macrophage cells. As a follow-up study, the fluorescent dye could be replaced by a drug which would allow for higher drug concentrations within the macrophage cells where the bacteria thrive and reproduce. This could help mitigate problems associated with low drug solubility and reduced side-effects since targeting allows for smaller doses.

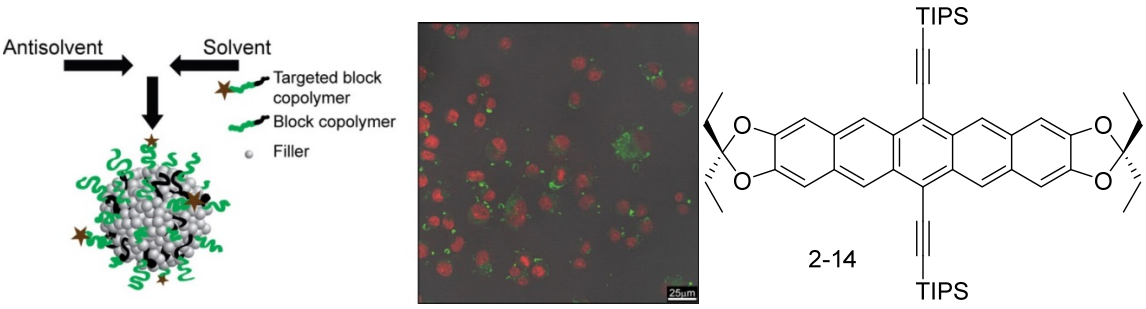

Figure 2-7. Targeted cell imaging. Left: Formation of targeted nanoparticles through flash nanoprecipitation. Middle: Immune macrophage cells containing ingested targeted fluorescent nanoparticles. Cell nuclei are shown in red and fluorescent nanoparticles are shown in green. Right: Structure of dioxolane pentacene (**2-14**). Adapted with permission from Elsevier, Copyright © 2013[93].

To reiterate, the dioxolane pentacene core does not possess sufficient optical properties for use in the deep-tissue bioimaging window. This is seen most clearly in Figure 2-8 which shows a mouse with nanoparticles containing pentacene (**2-14**) injected into the lungs. No fluorescence from the lung region can be seen in the intact mouse. The dye clearly must be modified so its absorption and emission wavelengths are contained in the deep-tissue bioimaging window. As mentioned, this work will be presented in the next chapter.

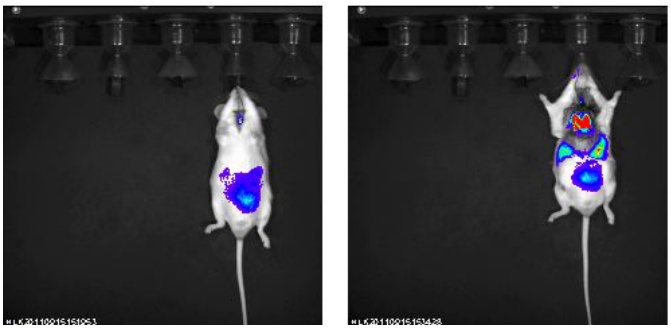

Figure 2-8. Mouse imaging. Fluorescence images of a mouse with nanoparticles containing pentacene (**2-14**) injected into the lungs. Left: No fluorescence is visible from the lung region since absorption and emission are outside the deep-tissue bioimaging window. Right: With the lung cavity exposed, the fluorescent nanoparticles are easily visible.

2.6 Experimental

General methods for entire dissertation:

All solvents were purchased from Pharmco Aaper, Fisher Scientific, Alfa Aesar, and Sigma-Aldrich. *n*-Butyllithium was purchased from Sigma-Aldrich. Chromatography was performed on silica gel (60 Å, 40-63 μm) purchased from SiliCycle. Several different spectrophotometers were used in this dissertation which included a Hewlett-Packard model HP 8453, a Thermo-Fisher Scientific Evolution 60, an Agilent Cary 60 model G6860A, and a Shimadzu model UV-2501PC. Fluorescence measurements were recorded on a Horiba Fluorolog-3 spectrophotometer. Crystalline emission was recorded by spreading a powdered sample of crystalline material onto a piece of clear, double-sided tape mounted on a glass slide and positioned at a 45° angle with respect to both the excitation source and detector. NMR spectra were recorded on a Varian Inova 400 MHz spectrometer. Routine GC-MS was done with either an Agilent instrument equipped with a model 6890N gas chromatograph (helium) and model 5793N mass spectrometer or a Bruker Scion SQ instrument. High-resolution mass spectra of were recorded in MALDI mode on a Bruker Daltonics Autoflex MALDI-TOFMS or in EI mode in a JOEL JMS-700T MStation. Combustion analyses were done by Midwest Microlab (Indianapolis, IN). Melting points of precursory compounds were measured with a standard capillary melting point apparatus. Melting points of some larger compounds were additionally determined by differential scanning calorimetry using a Thermo-Fisher Scientific DSCQ100 with a heating rate of 10°C / minute under nitrogen. DSC melting points are given as the endotherm peak onset. Electrochemistry was performed with a BASi Epsilon model E2 potentiostat. Measurements were taken in a 0.1 M NBu_4PF_6 solution of dichloromethane (degassed with N_2) with a Pt button working electrode and silver wire reference electrode. Ferrocene was subsequently added as an internal standard. Single-crystal X-ray data was acquired on either a Nonius KappaCCD sealed-tube MoKα diffractometer or a Bruker-Nonius X8 Proteum CuKα diffractometer.

2,2,7,7-Tetramethyl-4,5-dimethylene-3,6-dioxa-2,7-disilaoctane **(2-2)**

In a 500 mL RB flask equipped with a Dean-Stark trap and reflux condenser was added LiBr (34.7 g, 400 mmol) and benzene. The mixture was dried azeotropically overnight. Benzene was then evaporated and the flask was cooled under N_2 in an ice bath. While stirring, 120 mL anhydrous THF was added followed by slow addition of chlorotrimethylsilane (38.1 mL, 300 mmol), 2,3-butanedione (**2-1**) (8.60 g, 8.80 mL, 100 mmol), and triethylamine (41.8 mL, 300 mmol). The reaction was then removed from the ice bath and heated at 45 ^{o}C for 2 days. GC-MS analysis revealed the reaction was complete. The flask was cooled in an ice bath and poured in a separatory funnel where pentane, saturated $NaHCO_3$, NaCl brine, and ice were added. The product was extracted 3x with pentane. Organic layers were combined, washed with brine, dried with $MgSO_4$, filtered, and the solvent was removed by rotary evaporation with low heat. The resulting liquid was distilled under vacuum to give clear, colorless, foul-smelling liquid (19.26 g, 83%). *Product should be used in a timely manner as it does not store well*. ^{1}H NMR (400 MHz, $CDCl_3$) δ 4.83 (s, 2H), 4.34 (s, 2H), 0.23 (s, 18H). ^{13}C NMR (100 MHz, $CDCl_3$) δ 153.1, 93.1, 0.2. MS (EI 70 eV) *m/z* 230 (M^+, 70%), 147 (M^+ - 83, 65%), 73 (M^+ - 157, 100%).

Dimethyl-4,5-dihydroxyphthalate **(2-3)**

In a 100 mL sealed tube was added 30 mL benzene and degassed for 10 min. To this was added DMAD (18.24 mL, 148.4 mmol) and 2,2,7,7-tetramethyl-4,5-dimethylene-3,6-dioxa-2,7-disilaoctane **(2-2)** (31.10 g, 135.0 mmol). The solution was degassed an additional 5 minutes before the tube was sealed and heated at 90 ^{o}C for 2 days. GC-MS analysis revealed the reaction was complete. The solution was poured into a 500 mL RB flask and the benzene evaporated to give a light yellow liquid. The solution was cooled in an ice bath while a ~5% solution of bromine (6.92 mL, 135 mmol) in 1,2-dichloroethane (300 mL) was added dropwise with stirring. The resulting dark brown solution was then heated at 60^{o}C for 2 hours with a reflux condenser. Following this, the reaction was cooled in an ice bath for 1-2 hours to complete precipitation. The reaction

was then filtered and rinsed with cold 1,2-dichloroethane to give a gray-white powder (15.15 g, 50%). ^{1}H NMR (400 MHz, $(CD_3)_2CO$) δ 7.18 (s, 2H), 3.78 (s, 6H). ^{13}C NMR (100 MHz, $(CD_3)_2CO$) δ 168.3, 148.3, 125.6, 116.9, 52.6.

Dimethyl 2,2-diisobutylbenzo[*d*][1,3]dioxole-5,6-dicarboxylate & 2,2-Diisobutylisobenzofuro[5,6-*d*][1,3]dioxole-5,7-dione mixture **(2-4a)**

In a 100 mL RB flask was added dimethyl-4,5-dihydroxyphthalate **(2-3)** (5.00 g, 22.1 mmol), diisobutyl ketone (10.0 mL, 8.08 g, 56.8 mmol), 1 g *p*-toluenesulfonic acid catalyst, and 22 mL benzene. The reaction was refluxed with a Dean-Stark trap and condenser for 21 days. Reaction was filtered and solvent was evaporated. The crude liquid was dissolved in dichloromethane and washed twice with cold water, dried with $MgSO_4$, filtered, and the solvent was removed by rotary evaporation. The remaining ketone was removed by distillation under high vacuum (and can be reused), leaving behind a dark brown material shown to be a mixture of anhydride and diester by GC-MS analysis (4.72 g, ~65% yield). The reaction was carried on to the next step in this impure form. Diester MS (EI 70 eV) *m/z* 350 (M^+, 8%), 293 (M^+ - 57, 100%) and anhydride MS (EI 70 eV) *m/z* 304 (M^+, 4%), 247 (M^+ - 57, 100%).

(2,2-Diisobutylbenzo[*d*][1,3]dioxole-5,6-diyl)dimethanol **(2-5a)**

To a flame-dried 250 mL RB flask was added the mixture of anhydride and diester **(2-4a)** (4.72 g, ~13.5 mmol) and dissolved in 10 mL anhydrous THF. The reaction was cooled in an ice bath and 1M $LiAlH_4$ in THF (17 mmol) was slowly added. After addition, the solution was stirred 4 hours and then refluxed overnight. TLC revealed the reaction was complete and the reaction was diluted with THF and cooled in an ice bath before being quenched with 0.65 ml water, 0.65 ml 15% NaOH, and 1.9 ml water. The reaction was filtered and the aluminum salts were boiled in ethyl acetate for 3-5 minutes. The salts were filtered and the process repeated once more. Organic layers were combined, dried with $MgSO_4$, filtered, and the solvent was removed. The material was purified on a silica gel plug with 2 dichloromethane: 1 ether yielding pure product, 2.76 g, 70%. ^{1}H NMR (400 MHz, $CDCl_3$) δ 6.74 (s, 2H), 4.59 (s, 4H), 3.27 (br, 2H), 1.85 (m, 2H), 1.79 (d, J = 6.0

Hz, 4H), 0.93 (d, J = 6.4 Hz, 12H). ^{13}C NMR (100 MHz, $CDCl_3$) δ 147.8, 132.6, 122.1, 109.8, 64.0, 46.4, 24.0, 23.5. MS (EI 70 eV) *m/z* 276 (M^+ - 18, 10%), 219 (M^+ - 75, 100%).

2,2-Diisobutylbenzo[*d*][1,3]dioxole-5,6-dicarbaldehyde **(2-6a)**

To a 250 mL flame-dried RB flask was added 35 mL dichloromethane and 2.44 mL (28.1 mmol, 3.00 eq.) oxalyl chloride. The mixture was cooled to -78^{o}C and maintained at this temperature throughout the reaction. DMSO (4.0 mL, 56 mmol, 6.0 eq.) was dissolved in 10 mL dichloromethane and added dropwise to the flask with a dry addition funnel. After addition, the solution was stirred for 5 minutes. (2,2-Diisobutylbenzo[*d*][1,3]dioxole-5,6-diyl)dimethanol **(2-5a)** (2.76 g, 9.37 mmol, 1.00 eq.) was dissolved in DMSO and diluted with dichloromethane up to ~6 mL. This solution was added dropwise to the flask with an addition funnel over about 30 minutes. The mixture was allowed to stir an additional 30 minutes, and then triethylamine (22.0 mL, 160 mmol, 17.0 eq.) was slowly added. The reaction was then removed from the dry ice/acetone bath and allowed to warm to room temperature. Once warmed, 75 mL ice water was added and the product extracted with dichloromethane three times. The organic layers were combined, washed with brine, dried with $MgSO_4$, filtered, and solvent was removed by rotary evaporation. The resulting orange/brown liquid was dissolved in dichloromethane and purified with a silica gel plug with dichloromethane as eluent. Solvent was evaporated to give thick yellow to colorless liquid which crystallized if left undisturbed for a few days. *The material slowly turns black over a few weeks and should therefore be used quickly.* (2.31 g, 85%). ^{1}H NMR (400 MHz, $CDCl_3$) δ 10.47 (s, 2H), 7.31 (s, 2H), 1.84 (m, 6H), 0.95 (d, J = 6.4 Hz, 12H). ^{13}C NMR (100 MHz, $CDCl_3$) δ 190.1, 152.8, 133.2, 125.4, 109.1, 46.6, 24.1, 23.6. MS (EI 70 eV) *m/z* 290 (M^+, 45%), 233 (M^+ - 57, 100%).

2,2,10,10-Tetraisobutyl-1,3,9,11-tetraoxa-dicyclopenta[*b,m*]pentacene-6,14-dione **(2-7a)**

In a small vial was combined 2,2-Diisobutylbenzo[*d*][1,3]dioxole-5,6-dicarbaldehyde **(2-6a)** (0.5554 g, 1.913 mmol) with 1,4-cyclohexanedione (0.1072 g, 0.9563 mmol) and 4

mL ethanol. The solution was heated until solids dissolved. Two drops of 15% NaOH were quickly added and yellow precipitates formed immediately. The reaction was stirred vigorously for about 1 minute and then diluted with ~20 mL MeOH and stirred an additional 5 minutes. The suspension was filtered and rinsed with MeOH followed by a small amount of ether giving the characteristic yellow quinone (0.4752 g, 80%). ^{1}H NMR (400 MHz, $CDCl_3$) δ 8.63 (s, 4H), 7.24 (s, 4H), 1.91 (m, 12H), 0.99 (d, J = 6.4 Hz, 24H). ^{13}C NMR (100 MHz, $CDCl_3$) δ 183.2, 151.3, 133.3, 129.3, 127.6, 123.5, 104.8, 46.6, 24.0, 23.5. X-ray crystal data (1.54178 Å Cu K_α): $C_{40}H_{44}O_6$, *M* = 620.75, monoclinic, *a* = 11.8834(4), *b* = 8.6466(3), *c* = 16.1286(5), α = 90.00°, β = 93.421(2)°, γ = 90.00°, *V* = 1654.28(10) Å^3, T = 90.0(2) K, space group $P2_1/c$, *Z* = 2, 20,244 reflections collected, 2982 unique (thermal ellipsoid plot shown below).

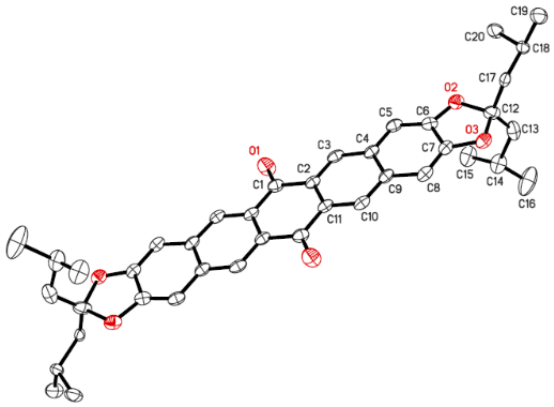

2,2,10,10-Tetraisobutyl-6,14-bis-(triisopropylsilylethynyl)-1,3,9,11-tetraoxa-dicyclopenta[*b,m*]pentacene **(2-8a)**

To a flame-dried 250 mL RB flask in an ice bath was added hexanes (50 mL) followed by TIPS acetylene (1.8 mL, 8.0 mmol), and 2.5 M n-BuLi (2.9 mL, 7.3 mmol). The mixture was stirred for 30 minutes at room temperature. THF (10 mL) and 50 mL hexanes were added, followed by pentacenequinone **(2-7a)** (1.00 g, 1.62 mmol) was added and the solution stirred overnight. TLC followed by $SnCl_2$/HCl treatment revealed the reaction was complete. It was quenched with 1 mL of saturated ammonium chloride and then 100 mL of THF, 4 scoops (excess) $SnCl_2$, and enough 10% HCl to dissolve the $SnCl_2$ were added. The reaction was stirred for 20 minutes and poured in a separatory funnel. The

aqueous layer was separated and the organic layer was diluted with hexanes, washed 4x with water, and dried with $MgSO_4$. This solution was poured on a silica gel plug and eluted first with hexanes to remove excess acetylene and then with a 5 hexanes: 1 dichloromethane mixture to elute the fluorescent red product. The solvent was removed and solids were recrystallized from ~200 mL acetone + 30 mL hexanes (for solubility) to yield 1.14 g, 74% of dark blue/red crystals with strong red solid-state fluorescence. ^{1}H NMR (400 MHz, $CDCl_3$) δ 8.96 (s, 4H), 7.06 (s, 4H), 1.93 (m, 12H), 1.35 (s, 42H), 1.00 (d, J = 6.4 Hz, 24H). ^{13}C NMR (100 MHz, $CDCl_3$) δ149.6, 130.9, 130.0, 123.9, 122.2, 116.4, 105.5, 105.2, 101.4, 47.1, 24.2, 23.7, 19.2, 11.9.

1,3-Dicyclohexyl-2-propanol **(2-10)**

In a flame-dried 250 mL RB flask was added 50 mL dry ether and magnesium turnings (2.007 g, 82.55 mmol). (Bromomethyl)cyclohexane (**2-9**)(13.26 g, 74.88 mmol) was dissolved in 100 mL dry ether and placed in a dry addition funnel. A catalytic amount of iodine was added to the flask and stirred rapidly. Small portions (1-2 mL) of (bromomethyl)cyclohexane solution was added about every 2 minutes until the reaction turned cloudy, at which point the solution was added at a rate sufficient to maintain a gentle reflux. When addition was complete, the reaction was stirred for 1 hour. The flask was then cooled in an ice bath and ethyl formate (1.81 ml, 22.5 mmol) was added dropwise and the solution stirred for 3 days. The reaction was quenched with 30 mL 10% sulfuric acid solution and the aqueous layer extracted twice with ether. All organic layers were combined, dried with $MgSO_4$, filtered and the solvent was removed by rotary evaporation. The liquid crystallized into a slurry. GC-MS analysis revealed it to be a mixture of the alcohol as well as Wurtz coupled product. The slurry was then vacuum filtered giving the desired alcohol (4.43 g, 88% based on ethyl formate). ^{1}H NMR (400 MHz, $CDCl_3$) δ 3.82 (m, 1H), 1.79 (d, J = 12.8 Hz, 1H), 1.67 (m, 8H), 1.43 (m, 2H), 1.24 (m, 12H), 0.90 (m, 4H). ^{13}C NMR (100 MHz, $CDCl_3$) δ 66.9, 46.3, 34.44, 34.35, 33.2, 26.8, 26.6, 26.4.

1,3-Dicyclohexyl-2-propanone **(2-11)**

To a 500 mL flame-dried RB flask was added 40 mL dichloromethane and 2.54 mL (29.6 mmol, 1.50 eq.) oxalyl chloride. The mixture was cooled to -78^{o}C and maintained at this temperature throughout the reaction. DMSO (4.2 mL, 59 mmol, 3.0 eq.) was dissolved in 8 mL DCM and added dropwise to the flask with a dry addition funnel. After addition, the solution was stirred for 5 minutes. 1,3-Dicyclohexyl-2-propanol **(2-10)** (4.43 g, 19.74 mmol, 1 eq.) was dissolved in DMSO and diluted with DCM up to ~5 ml. This solution was added dropwise to the flask with an addition funnel over about 30 minutes. The mixture was allowed to stir an additional 30 minutes, and then triethylamine (22 mL, 160 mmol, 17 eq.) was slowly added. The reaction was then removed from the dry ice/acetone bath and allowed to warm to room temperature. Once warmed, 80 mL ice water was added and the product was extracted 3x with dichloromethane. The organic layers were combined, washed with brine, dried with $MgSO_4$, filtered and the solvent was removed. The resulting orange/brown liquid was purified by silica gel chromatography with 2 hexanes: 1 dichloromethane as eluent. Solvent was evaporated to yield white/yellow crystals (4.12 g, 94%). ^{1}H NMR (400 MHz, $CDCl_3$) δ 2.23 (d, J = 6.8 Hz, 4H), 1.81 (m, 2H), 1.65 (m, 8H), 1.19 (m, 8H), 0.90 (m, 4H). ^{13}C NMR (100 MHz, $CDCl_3$) δ 211.2, 51.4, 34.1, 33.5, 26.4, 26.3. MS (EI 70 eV) *m/z* 222 (M^+, 5%), 141 (M^+ - 81, 25%), 97 (M^+ - 125, 45%), 55 (M^+ - 167, 100%).

Dimethyl 2,2-di(methylenecyclohexyl)benzo[*d*][1,3]dioxole-5,6-dicarboxylate & 2,2-Di(methylenecyclohexyl)isobenzofuro[5,6-*d*][1,3]dioxole-5,7-dione mixture **(2-4b)**

In a 100 ml RB flask was combined dimethyl-4,5-dihydroxyphthalate **(2-3)** (4.61 g, 21.38 mmol), 1,3-dicyclohexyl-2-propanone **(2-11)** (4.12 g, 18.5 mmol), 0.9 g *p*-toluenesulfonic acid catalyst, and 20 mL toluene. The reaction was refluxed at 250 ^{o}C with a Dean-Stark trap and reflux condenser for 11 days. Reaction was then filtered and solvent was evaporated. The crude liquid was dissolved in dichloromethane and washed twice with cold water, dried with $MgSO_4$, filtered, and the solvent was removed. The remaining ketone was mostly removed by distillation under high vacuum (and can be

reused), leaving behind a dark brown material shown to be a mixture of anhydride, diester, and a small amount of ketone by GC-MS analysis (3.49 g, ~39%). The reaction was carried on to the next step in this impure form. MS (EI 70 eV) *m/z* 430 (M^+, weak), 333 (M^+ - 97, 100%) and MS (EI 70 eV) *m/z* 384 (M^+, very weak), 287 (M^+ - 97, 100%).

(2,2-Di(methylenecyclohexyl)benzo[*d*][1,3]dioxole-5,6-diyl)dimethanol **(2-5b)**

In a flame-dried 50 mL RB flask was added the mixture of anhydride and diester mixture **(2-4b)** (3.49 g, ~9.08 mmol) and dissolved in 7 mL anhydrous THF. The reaction was cooled in an ice bath and 1M $LiAlH_4$ in THF (15 mmol) was slowly added. After addition, the solution was stirred 4 hours and then refluxed overnight. TLC revealed the reaction was complete and it was diluted with THF and cooled in an ice bath before being quenched with 0.57 mL water, 0.57 mL 15% NaOH, and 1.7 mL water. The reaction was filtered and the salts boiled in ethyl acetate for a few minutes. The salts were filtered and the process repeated once more. Organic layers were combined, dried with $MgSO_4$, filtered, and the solvent was removed by rotary evaporation. The material was purified on a silica gel plug with 2 dichloromethane: 1 ether yielding 2.74 g, 81% pure product. ^{1}H NMR (400 MHz, $CDCl_3$) δ 6.72 (s, 2H), 4.57 (s, 4H), 3.35 (br, 2H), 1.76 (d, J = 6.0 Hz, 4H), 1.57 (m, 10H), 1.15 (m, 8H), 0.94 (m, 4H). ^{13}C NMR (100 MHz, $CDCl_3$) δ 147.9, 132.8, 122.5, 110.1, 64.2, 45.0, 34.6, 33.0, 26.4.

2,2-Di(methylenecyclohexyl)benzo[*d*][1,3]dioxole-5,6-dicarbaldehyde **(2-6b)**

To a 250 mL flame-dried RB flask was added 30 mL dichloromethane and 1.91 mL (22.0 mmol, 3.00 eq.) oxalyl chloride. The mixture was cooled to -78^{o}C and maintained at this temperature throughout the reaction. DMSO (3.15 mL, 43.9 mmol, 6.00 eq.) was dissolved in 6 mL dichloromethane and added dropwise to the flask with a dry addition funnel. After addition, the solution was stirred for 5 minutes. (2,2-Di(methylcyclohexyl)benzo[*d*][1,3]dioxole-5,6-diyl)dimethanol **(2-5b)** (2.74 g, 7.32 mmol, 1 eq.) was dissolved in DMSO and diluted with dichloromethane up to ~6 mL. This solution was added dropwise to the flask with an addition funnel over about 30 minutes. The mixture was allowed to stir an additional 30 minutes, and then

triethylamine (17.0 mL, 125 mmol, 17.0 eq.) was slowly added. The reaction was removed from the dry ice/acetone bath and allowed to warm to room temperature. Once warmed, 75 mL ice water was added and the product extracted 3x with dichloromethane. The organic layers were combined, washed with brine, dried with $MgSO_4$, filtered, and the solvent was removed by rotary evaporation. The resulting orange/brown liquid was dissolved in dichloromethane and purified with a silica gel plug with dichloromethane as eluent. Solvent was evaporated to yield the product (2.30 g, 85%). ^{1}H NMR (400 MHz, $CDCl_3$) δ 10.47 (s, 2H), 7.30 (s, 2H), 1.84 (d, J = 6.4 Hz, 4H), 1.68 (m, 8H), 1.49 (m, 2H), 1.14 (m, 8H), 0.98 (m, 4H). ^{13}C NMR (100 MHz, $CDCl_3$) δ 190.2, 152.8, 133.2, 125.6, 109.1, 45.4, 34.5, 33.0, 26.34, 26.25.

2,2,10,10-Tetra(methylenecyclohexyl)-1,3,9,11-tetraoxa-dicyclopenta[*b,m*]pentacene-6,14-dione **(2-7b)**

In a small vial was combined 2,2-Di(methylenecyclohexyl)benzo[*d*][1,3]dioxole-5,6-dicarbaldehyde **(2-6b)** (0.5136 g, 1.386 mmol) with 1,4-cyclohexanedione (0.0777 g, 0.6931 mmol) and 2.5 mL ethanol. The solution was heated until solids dissolved. Two drops of 15% NaOH were quickly added and yellow precipitates formed immediately. The reaction was stirred vigorously for about 1 minute, diluted with ~20 mL MeOH, and stirred an additional 5 minutes. The suspension was filtered and rinsed with MeOH followed by ether giving the characteristic yellow quinone (0.3362 g, 62%). ^{1}H NMR (400 MHz, $CDCl_3$) δ 8.64 (s, 4H), 7.23 (s, 4H), 1.89 (d, J = 6.0 Hz, 8H), 1.74 (m, 16H), 1.57 (m, 4H), 1.15 (m, 16H), 1.01 (m, 8H). ^{13}C NMR (100 MHz, $CDCl_3$) δ 183.5, 151.5, 133.6, 129.5, 127.8, 123.9, 105.0, 45.6, 34.6, 33.0, 26.4, 26.3.

2,2,10,10-Tetra(methylenecyclohexyl)-6,14-bis-(triisopropylsilylethynyl)-1,3,9,11-tetraoxa-dicyclopenta[*b,m*]pentacene **(2-8b)**

To a flame-dried 250 ml RB flask in an ice bath was added hexanes (40 mL) followed by TIPS acetylene (0.71 ml, 3.2 mmol), and 2.5 M n-BuLi (1.15 ml, 2.88 mmol). The mixture was stirred for 30 minutes at room temperature and then diluted to 80 mL with hexanes. Quinone **(2-7b)** (0.4958 g, 0.6348 mmol) was added and the solution stirred

overnight. TLC followed by $SnCl_2$/HCl treatment revealed the reaction was complete. It was quenched with 10 drops of saturated ammonium chloride and then 40 mL of THF, 2 scoops (excess) $SnCl_2$, and 25 mL 10% HCl were added. The resulting fluorescent red mixture was stirred for 20 minutes and poured in a separatory funnel. The aqueous layer was separated and the organic layer was diluted with hexanes, washed 4x with water, and dried with $MgSO_4$. This solution was poured on a silica gel plug and eluted first with hexanes to remove excess acetylene and then with a 5 hexanes: 1 dichloromethane mixture to elute the fluorescent red product. The solvent was removed and solids were recrystallized in ethyl acetate/toluene to yield 271.0 mg, 38% of dark blue/black crystals with solid-state fluorescence. ^{1}H NMR (400 MHz, $CDCl_3$) δ 8.97 (s, 4H), 7.06 (s, 4H), 1.89 (d, J = 6.0 Hz, 8H), 1.77 (m, 16H), 1.60 (m, 4H), 1.35 (s, 42H), 1.20 (m, 16H), 1.04 (m, 8H). ^{13}C NMR (100 MHz, $CDCl_3$) δ 149.6, 131.0, 130.0, 123.9, 122.4, 116.4, 105.6, 105.2, 101.4, 45.7, 34.6, 33.0, 26.5, 26.4, 19.2, 11.9.

Dimethyl 2,2-diphenylbenzo[*d*][1,3]dioxole-5,6-dicarboxylate & 2,2-Diphenylisobenzofuro[5,6-*d*][1,3]dioxole-5,7-dione mixture **(2-4c)**

In a 100 mL RB flask was combined dimethyl-4,5-dihydroxyphthalate **(2-3)** (4.75 g, 21.0 mmol), benzophenone (11.5 g, 63.0 mmol), 0.9 g *p*-toluenesulfonic acid catalyst, and 21 mL toluene. The reaction was refluxed at 250 ^{o}C with a Dean-Stark trap and reflux condenser for 7 days. Solvent was evaporated. The crude liquid was dissolved in dichloromethane, washed twice with cold water, dried with $MgSO_4$, filtered, and the solvent was removed by rotary evaporation. Excess benzophenone was removed by distillation under high vacuum (and can be reused), leaving behind a dark brown material shown to be a mixture of anhydride, diester, and residual benzophenone by GC-MS analysis (3.04 g, ~42%). The reaction was carried on to the next step in this impure form. Diester MS (EI 70 eV) *m/z* 390 (M^+, 25%), 359 (M^+ - 31, 15%), 313 (M^+ - 77, 100%) and anhydride *m/z* 344 (M^+, 15%), 267 (M^+ - 77, 100%).

(2,2-Diphenylbenzo[*d*][1,3]dioxole-5,6-diyl)dimethanol **(2-5c)**

To a flame-dried 50 mL RB flask was added the mixture of anhydride and diester mixture **(2-4c)** (3.04 g, ~8.8 mmol) and dissolved in 10 mL dry THF. The reaction was cooled in an ice bath and 1M $LiAlH_4$ in THF (19 mmol) was slowly added. After addition, the solution was stirred 4 hours and then refluxed overnight. TLC with ≈8 dichloromethane: 1 MeOH revealed the reaction was complete and the reaction was diluted with THF and cooled in an ice bath before being quenched with 0.73 mL water, 0.73 mL 15% NaOH, and 2.2 mL water. The reaction was filtered and the salts boiled in ethyl acetate. The salts were filtered and the process repeated once more. Organic layers were combined, dried with $MgSO_4$, filtered, and the solvent was removed. GC-MS analysis revealed it to be a mixture of diphenylmethanol and desired product. The material was purified on a silica gel plug with 2 dichloromethane : 1 ether yielding white solid (1.21 g, 41%). ^{1}H NMR (400 MHz, $CDCl_3$) δ 7.56 (m, 4H), 7.34 (m, 6H), 6.87 (s, 2H), 4.55 (s, 4H), 3.00 (s, 2H). ^{13}C NMR (100 MHz, $CDCl_3$) δ 146.9, 140.0, 133.5, 129.2, 128.3, 126.3, 117.2, 110.4, 63.9.

2,2-Diphenylbenzo[*d*][1,3]dioxole-5,6-dicarbaldehyde **(2-6c)**

To a 100 mL flame-dried RB flask was added 14 mL DCM and 0.947 mL (10.9 mmol, 3.00 eq.) oxalyl chloride. The mixture was cooled to -78^{o}C and maintained at this temperature throughout the reaction. DMSO (1.55 mL, 21.7 mmol, 6.00 eq.) was dissolved in 5 mL DCM and added dropwise to the flask with a dry addition funnel. After addition, the solution was stirred for 5 minutes. (2,2-Diphenylbenzo[*d*][1,3]dioxole-5,6-diyl)dimethanol **(2-5c)** (2.74 g, 7.32 mmol, 1 eq.) was dissolved in DMSO and diluted with dichloromethane up to ~5 mL. This solution was added dropwise to the flask with an addition funnel over about 20 minutes. The mixture was allowed to stir an additional 30 minutes, and then triethylamine (8.0 mL, 62 mmol, 17 eq.) was slowly added. The reaction was then removed from the dry ice/acetone bath and allowed to warm to room temperature. Once warmed, 50 mL ice water was added and the product extracted 3x with dichloromethane. The organic layers were combined, washed with brine, dried with $MgSO_4$, filtered, and the solvent was removed by rotary evaporation. The resulting orange/brown liquid was dissolved in dichloromethane and purified with a silica gel plug

with dichloromethane as eluent. Solvent was evaporated to give yield (1.11 g, 93%). ^{1}H NMR (400 MHz, $CDCl_3$) δ 10.48 (s, 2H), 7.55 (m, 4H), 7.49 (s, 2H), 7.41 (m, 6H). ^{13}C NMR (100 MHz, $CDCl_3$) δ 189.8, 151.6, 138.7, 133.4, 129.8, 128.5, 126.1, 120.0, 109.9.

2,2,10,10-Tetraphenyl-1,3,9,11-tetraoxa-dicyclopenta[*b,m*]pentacene-6,14-dione **(2-7c)**

In a small vial was combined 2,2-diphenylbenzo[*d*][1,3]dioxole-5,6-dicarbaldehyde **(2-6c)** (0.3358 g, 1.017 mmol) with 1,4-cyclohexanedione (0.0570 g, 0.5083 mmol) and 2.5 mL ethanol. The solution was heated until solids dissolved, and slightly more ethanol added if necessary. Two drops of 15% NaOH were quickly added and yellow precipitates formed immediately. The reaction was stirred vigorously for about 30 seconds and then diluted with ~20 mL MeOH and stirred an additional 5 minutes. The suspension was filtered and rinsed with MeOH followed by ether giving the characteristic yellow/orange quinone (0.2452 g, 69%). ^{1}H NMR (400 MHz, $CDCl_3$) δ 8.66 (s, 4H), 7.61 (m, 8H), 7.41 (m, 12H), 7.40 (s, 4H). ^{13}C NMR (100 MHz, $CDCl_3$) δ 183.1, 150.3, 139.3, 133.4, 129.6, 129.5, 128.5, 127.9, 126.3, 118.5, 105.8.

2,2,10,10-Tetraphenyl-6,14-bis-(triisopropylsilylethynyl)-1,3,9,11-tetraoxa-dicyclopenta[*b,m*]pentacene **(2-8c)**

To a flame-dried 250 mL RB flask in an ice bath was added hexanes (10 mL) followed by TIPS acetylene (0.29 mL, 1.3 mmol), and 2.5 M n-BuLi (0.49 ml, 1.2 mmol). The mixture was stirred for 30 minutes at room temperature and then diluted to 30 mL with hexanes. Quinone **(2-7c)** (0.1830 g, 0.2611 mmol) was added and the solution stirred overnight. Not all quinone had dissolved. An additional 0.29 mL of TIPS acetylene was lithiated in a separate container by the same procedure and added to the flask, followed by 20 mL dry THF. The solution was allowed to stir again overnight. TLC with dichloromethane followed by $SnCl_2$/HCl treatment revealed the reaction was complete. It was quenched with a 6 drops of saturated ammonium chloride followed by 2 scoops (excess) $SnCl_2$ and 15 mL 10% HCl were added. The reaction was stirred for 20 minutes and poured in a separatory funnel. The aqueous layer was separated and the organic layer was diluted with 30 mL hexanes, washed 4x with water, and dried with $MgSO_4$.

This solution was poured on a silica gel plug and eluted first with hexanes to remove excess acetylene and then with a 5 hexanes: 1 dichloromethane mixture to elute the fluorescent red product. The solvent was removed and solids were recrystallized in 1,2-dichloroethane to yield 125.5 mg, 47% of dark blue/black crystals with red solid-state fluorescence. ^{1}H NMR (400 MHz, $CDCl_3$) δ 9.00 (s, 4H), 7.64 (m, 8H), 7.43 (m, 12H), 7.24 (s, 4H), 1.34 (s, 42H). ^{13}C NMR (100 MHz, $CDCl_3$) δ 148.5, 139.7, 130.6, 129.8, 129.4, 128.4, 126.3, 124.3, 117.2, 116.5, 105.7, 104.8, 102.4, 19.0, 11.7.

Chapter 3. Dioxolane Hexacenes & Heptacenes

3.1 Hexacene Mixture

Since all attempts at synthesizing stable dioxolane pentacenes with long-wavelength absorption and emission were unsuccessful, a new strategy was needed. The next logical synthetic target was the analogous dioxolane *hexacene*. Silylethynyl-functionalized pentacenes were shown to have a long-wavelength absorption maximum at 643 nm, whereas analogous hexacenes had a corresponding absorption at 738 nm—a bathochromic shift of 95 nm[65b, 68a]. Silylethynyl-functionalized dioxolane pentacenes such as (**2-8a**) are somewhat blue-shifted[88] and have a long-wavelength absorption maximum at 618 nm. Applying the same 95 nm bathochromic shift, one would predict a long-wavelength absorption maximum for dioxolane hexacene at roughly 713 nm. It was hoped that the dioxolane functionality would enhance fluorescence in hexacene as it did in pentacene and give a high fluorescence quantum yield. Additionally, it seemed reasonable that the "tools" developed in chapter 2 resulting in solid-state fluorescence would be amenable to dioxolane hexacene.

The silylethynyl-functionalized dioxolane hexacene chromophore is in the C_{2v} point group, having lost one plane of symmetry and the inversion center of the analogous D_{2h} pentacene. Since there is no central "benzene" ring in hexacene, the two silylethynyl substituents must necessarily be offset from the center. A consequence of the reduced symmetry of this target molecule requires that the synthesis be asymmetric. The initial retrosynthetic outline is shown in Scheme 3-1. The target functionalized dioxolane hexacene ("Target Chromophore") is naturally derived from hexacenequinone **A** through nucleophilic alkyne addition followed by deoxygenation with $SnCl_2$. Hexacenequinone **A** can be dissected further via a 4-fold aldol condensation into 1,4-cyclohexanedione and dialdehydes **B** and **C**. Dialdehydes of type **B** were previously synthesized in chapter 2 to make dioxolane pentacenes, and this simplifies the synthetic target to dialdehydes of type **C**. It was understood that the aldol condensation producing hexacenequinone **A** would also produce analogous pentacene-

and heptacenequinones; simplicity dictated this was an acceptable consequence, and it was thought the final acene mixture would be separable.

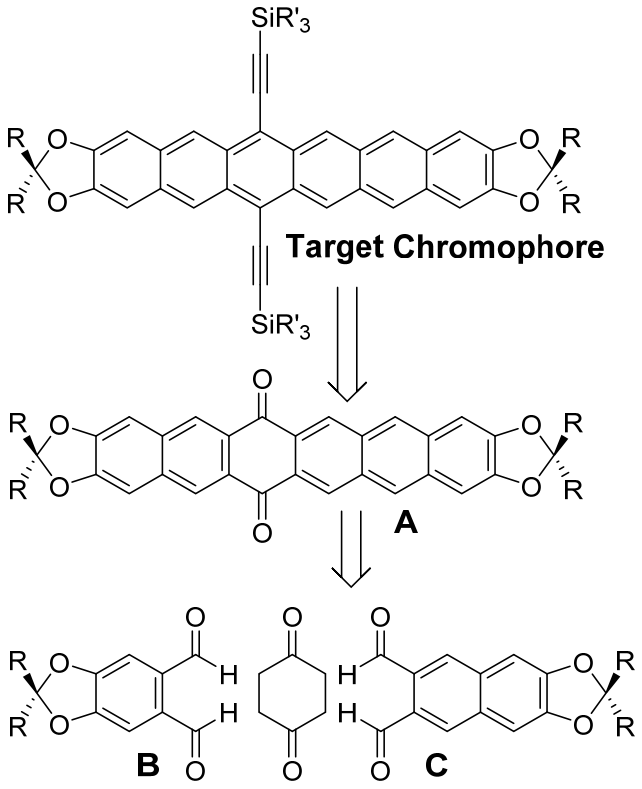

Scheme 3-1. Partial retrosynthetic outline for the dioxolane hexacene target.

With the problem simplified, the first task was synthesis of dialdehyde **C** and deciding what R-substituents to use of the several choices available. A choice was made after some practical synthetic considerations. First of all, the methylenecyclohexyl substituent came from a ketone which was not commercially available, resulting in additional synthesis steps. The phenyl substituent resulted in a dioxolane pentacene with low solubility, and it is likely the analogous hexacene would be even less soluble. Of the remaining options, isobutyl was chosen as a first attempt because of the enhanced solubility it could provide to the product.

After several failed synthetic routes, a successful synthesis of the target dialdehyde was devised as shown in Scheme 3-2. Synthesis began with 6,7-dibromo-2,3-dihydroxynaphthalene (**3-1**) which was synthesized from 2,3-dihydroxynaphthalene in

two steps according to the literature[94]. This was condensed with 2,6-dimethyl-4-heptanone to produce acetal (**3-2a**) followed by Rosenmund-von Braun cyanation to yield nitrile (**3-3a**). It should be noted that once the acetal was formed, acidic conditions were avoided in subsequent reactions to prevent deprotection. Hydrolysis gave the expected dicarboxylic acid (**3-4a**), but drying the material at high temperature (≈ 120°C) for use in the next step resulted in partial to nearly complete conversion to anhydride (**3-5a**). This mixture was then reduced with lithium aluminum hydride to dimethanol (**3-6a**) followed by Swern oxidation to yield dialdehyde (**3-7a**).

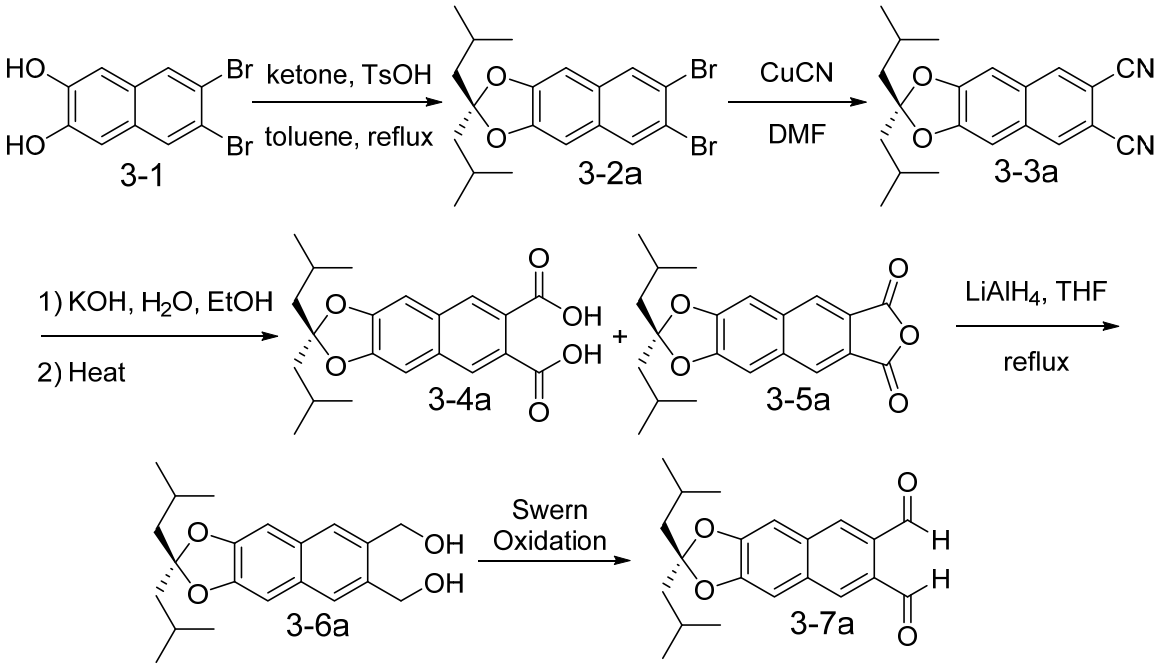

Scheme 3-2. First successful synthesis of dialdehyde (**3-7a**).

Newly synthesized dialdehyde (**3-7a**) was combined with previously synthesized dialdehyde (**2-6a**) and 1,4-cyclohexanedione in an aldol condensation giving the expected inseparable mixture of pentacenequinone, hexacenequinone, and heptacenequinone. This material was carried on to the final acene mixture. It was apparent the heptacene decomposed fairly rapidly, leaving pentacene and hexacene to be separated. The difference in retention factors was very small, and the hexacene still contained a trace of pentacene even after several silica gel columns. Recrystallization gave crystals, but these were found to still contain a slight impurity. Characterization by

UV-Vis and fluorescence spectroscopy also showed a long-wavelength absorption maximum at 720 nm and a fluorescence maximum at 723 nm—well within the deep-tissue bioimaging window. Also, the lengthy purification of this hexacene demonstrated it had sufficient solution stability—a general problem of larger acenes—and was therefore a worthy target. Given these promising results, it was important to measure the fluorescence quantum yield. Since this needs to be done with pure material, a new route was needed in which the hexacene would be produced as the sole product, avoiding the need for what proved to be an essentially impossible purification.

3.2 Asymmetric Synthesis

Scheme 3-1 outlined a retrosynthesis in which three organic components combined to form hexacenequinone **A** as a statistical mixture among three products. A new strategy was now developed to produce pure hexacenequinone **A** as outlined in Scheme 3-3. The aldol condensation was again envisioned as the best way to form the hexacenequinone, but an asymmetric synthesis was necessary in which only two organic components were combined. This simplified the synthesis to dialdehyde **C** (which had already been synthesized) and hydroquinone **D**.

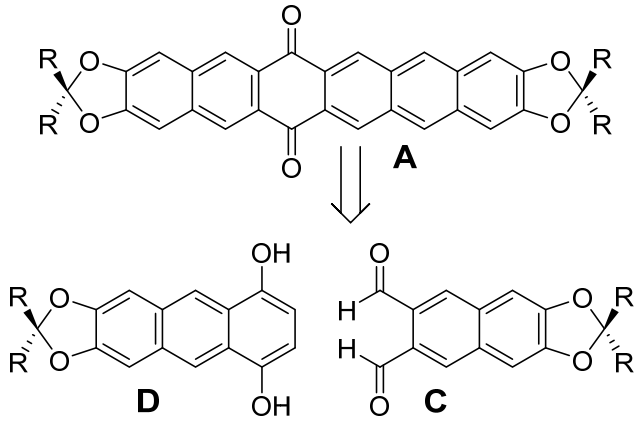

Scheme 3-3. New asymmetric retrosynthesis strategy for pure hexacenequinone **A**.

Hydroquinone **D** proved a conceptually very difficult compound to synthesize. In the end, this was solved, and efforts culminated in the successful asymmetric synthesis of hexacenequinone **A** after nine months of work. The full reaction sequence is outlined

in Scheme 3-4, although many of the reactions were already described from Scheme 3-2. The entire sequence was initially carried out on the isobutyl derivatives and subsequently repeated with the ethyl derivatives. Nitrile (**3-3b**) was initially synthesized by the Rosenmund von-Braun reaction with CuCN, as was done with nitrile (**3-3a**). It was later discovered the yield could be substantially improved to 90% using a palladium-catalyzed procedure with $Zn(CN)_2$, similar to that developed by Hanack[95]. Hydroquinones of type **D** were synthesized beginning with acetals (**3-2a**) and (**3-2b**). These acetals were treated with *n*-BuLi and the resulting arynes underwent Diels-Alder cyclization with furan to produce endoxides (**3-8a**) and (**3-8b**)[96]. Endoxides are generally ring-opened using aqueous acid, but this was expected to be a problem because of acetal functionality. The Lewis acid $Cu(OTf)_2$ has also been used for this transformation, and it was found to work well in this case to yield phenols (**3-9a**) and (**3-9b**)[97]. The hypervalent iodine reagent [bis(trifluoroacetoxy)iodo]benzene (BTI) was able to oxidize these phenols to *p*-quinones (**3-10a**) and (**3-10b**)[98]. A simple reduction with sodium dithionite finally produced the target hydroquinones (**3-11a**) and (**3-11b**). Hydroquinones are generally depicted in their enol forms as shown for compound **D** in Scheme 3-3. In this case, NMR data suggested theses hydroquinones were isolated as their keto tautomers. ^{1}H NMR for each compound showed a resonance at $\delta \approx 3.08$ ppm integrating to 4 hydrogens, consistent with the diketone structure. The corresponding enol tautomer is aromatic and this resonance would be expected farther downfield near 7 ppm with an integration of only 2 hydrogens. ^{13}C NMR shows resonances in the alkyl region for each of these compounds at $\delta \approx 38$ ppm, which does not correspond to ethyl and isobutyl alkyl substituents on the dioxolane ring. The enol tautomer would have this resonance in the aromatic region near 120 ppm. Following this, dialdehydes (**3-7a**) and (**3-7b**) were combined with hydroquinones (**3-11a**) and (**3-11b**) in an aldol condensation giving the expected hexacenequinones (**3-12a**) and (**3-12b**).

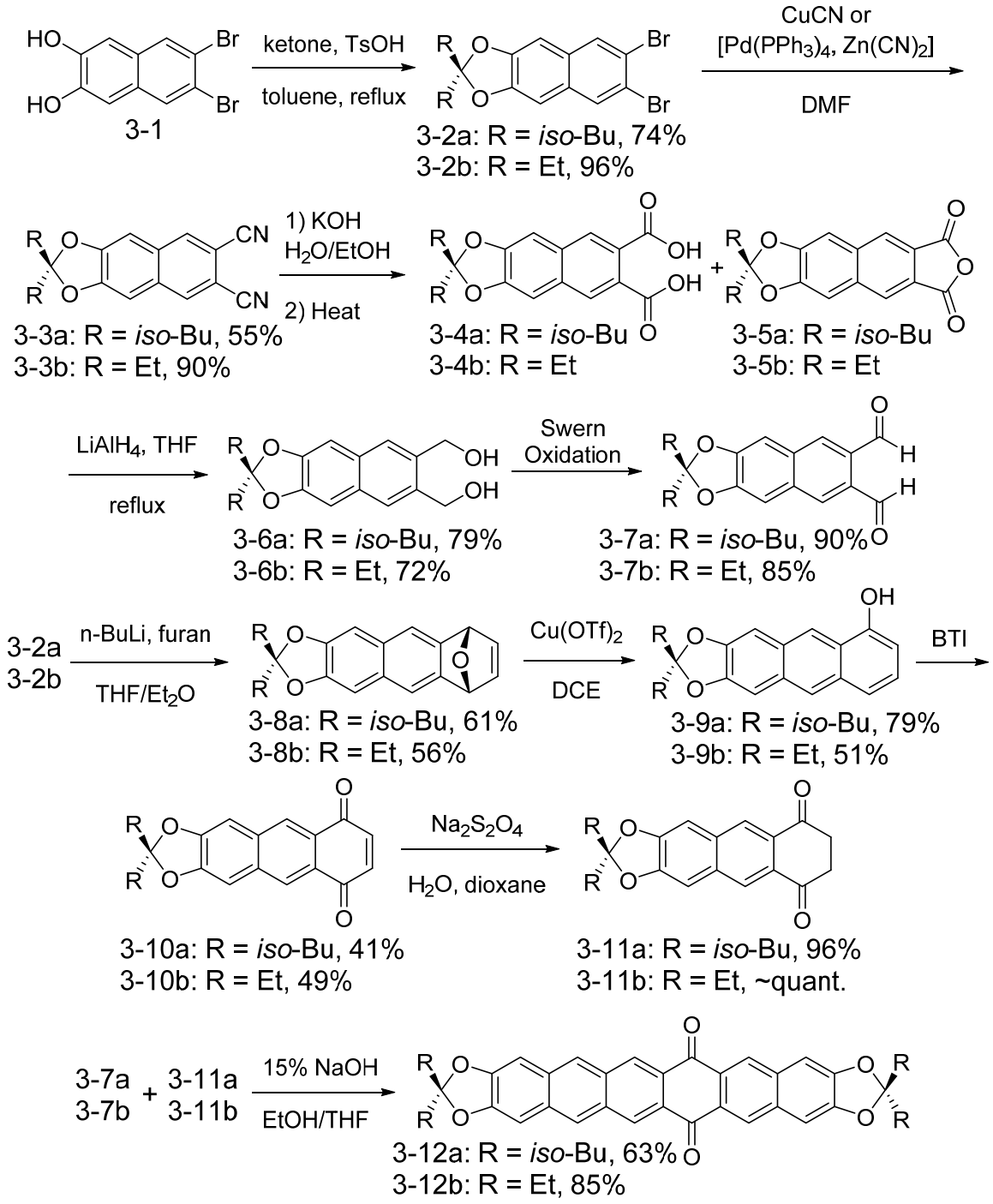

Scheme 3-4. Asymmetric synthesis of hexacenequinones (**3-12a**) and (**3-12b**).

In addition, both of these hexacenequinones were characterized by X-ray crystallography and produced refined models, confirming their structures. Crystals of both compounds were grown from toluene, and each incorporated solvent in their crystal structures, although toluene was too disordered in (**3-12b**) to sufficiently model.

Asymmetry about the molecular short axis is a result of only the two carbonyl oxygens, giving each molecule C_{2v} symmetry. However, each of these quinones crystallize with inversion symmetry, resulting in the observed disorder of carbonyl oxygens seen in the crystal structures in Figure 3-1. Images of bulk crystals are also shown.

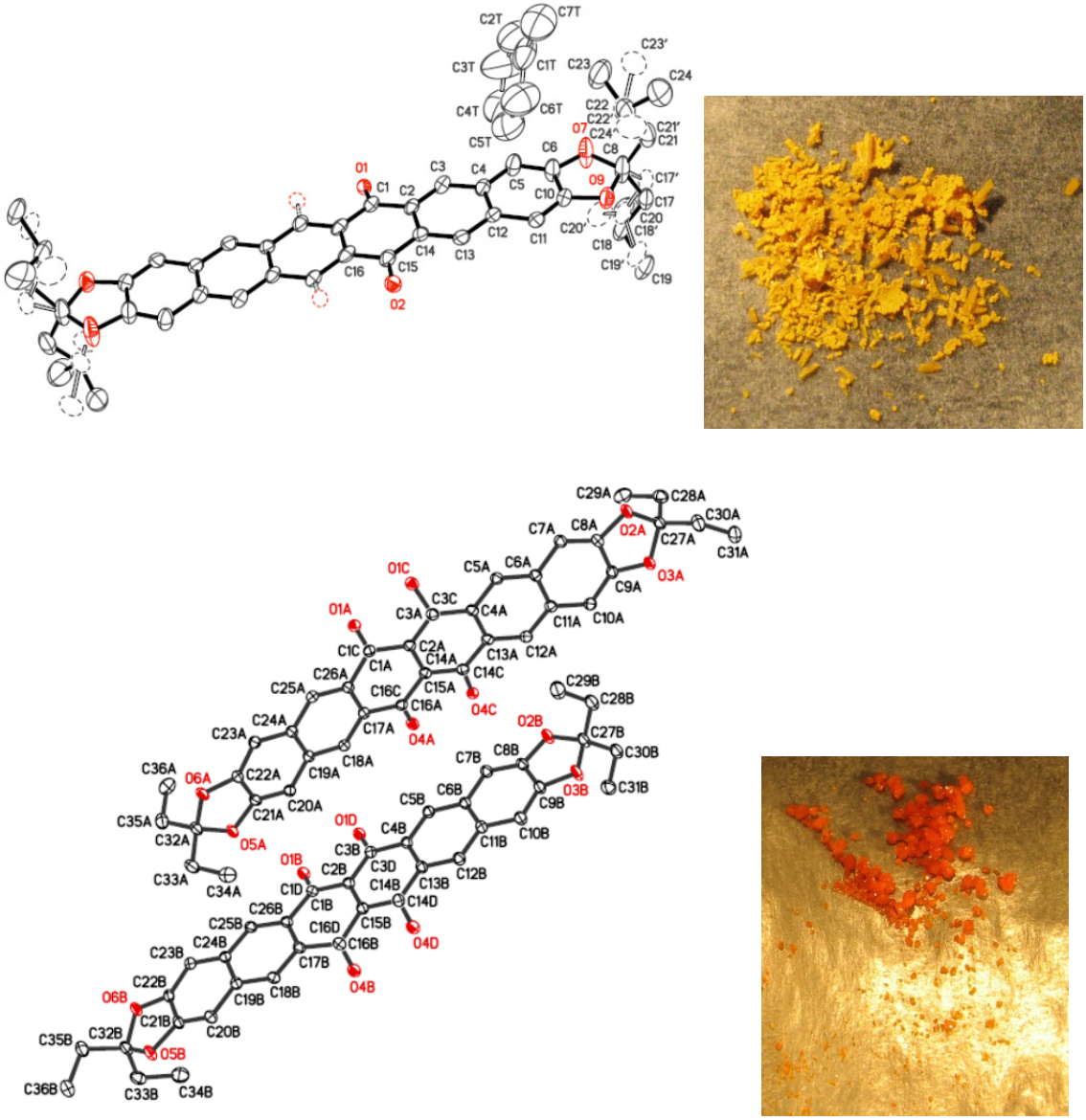

Figure 3-1. Hexacenequinone crystals. Thermal ellipsoid plots and crystal images of hexacenequinones (**3-12a**)—top and (**3-12b**)—bottom.

The pure hexacenequinones were then carried on to the final hexacenes by the standard method shown in Scheme 3-5. Structures of each hexacene are given in Figure 3-2. The three trialkylsilylacetylenes chosen were isobutyl, cyclopentyl, and *sec*-butyl. Combined steric protection from both the trialkylsilylethynyl and dioxolane substituents provided varying degrees of stability to the hexacenes. Only impure hexacenes (**3-13**) and (**3-14**) were isolated with triisobutylsilylethynyl substitution, regardless of the dioxolane substituents. In this case, increased flexibility of the isobutyl groups did not provide the necessary steric protection against dimerization via Diels-Alder reactions. Tricyclopentylsilylethynyl substituents gave adequate stability to hexacene (**3-16**), although samples of (**3-15**) also contained decomposition products despite forming large crystals. Finally, tri*sec*-butylsilylethynyl substitution resulted in hexacenes (**3-17**) and (**3-18**) which could be isolated as pure compounds. Hexacene (**3-17**) was found to decompose significantly faster than (**3-18**) by NMR. Additionally, (**3-18**) withstood recrystallization from boiling acetone whereas (**3-17**) significantly decomposed in solution with heating. These results provide evidence that the larger isobutyl groups situated on the acetal functional group provided greater steric hindrance to dimerization and resulted in increased stability[68b]. Of these six hexacenes synthesized, the purity, stability and higher yield of (**3-18**) dictated this material was the best candidate for further characterization of the dioxolane hexacene chromophore. Images of crystalline derivatives (**3-15**) and (**3-18**) are shown in Figure 3-3.

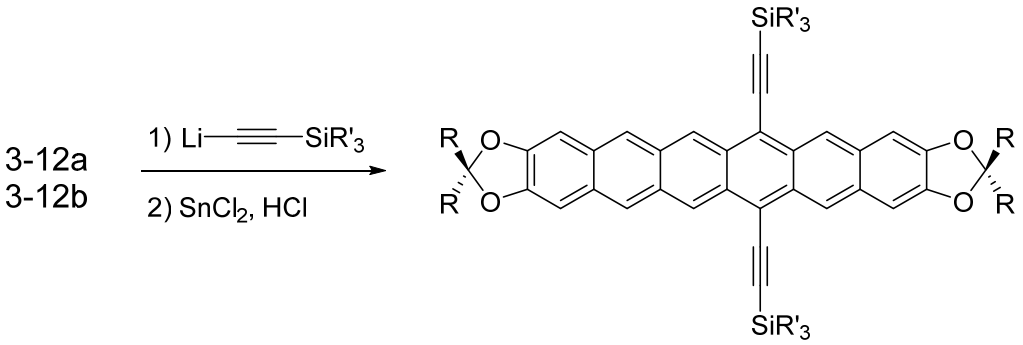

Scheme 3-5. General synthesis of dioxolane hexacene derivatives.

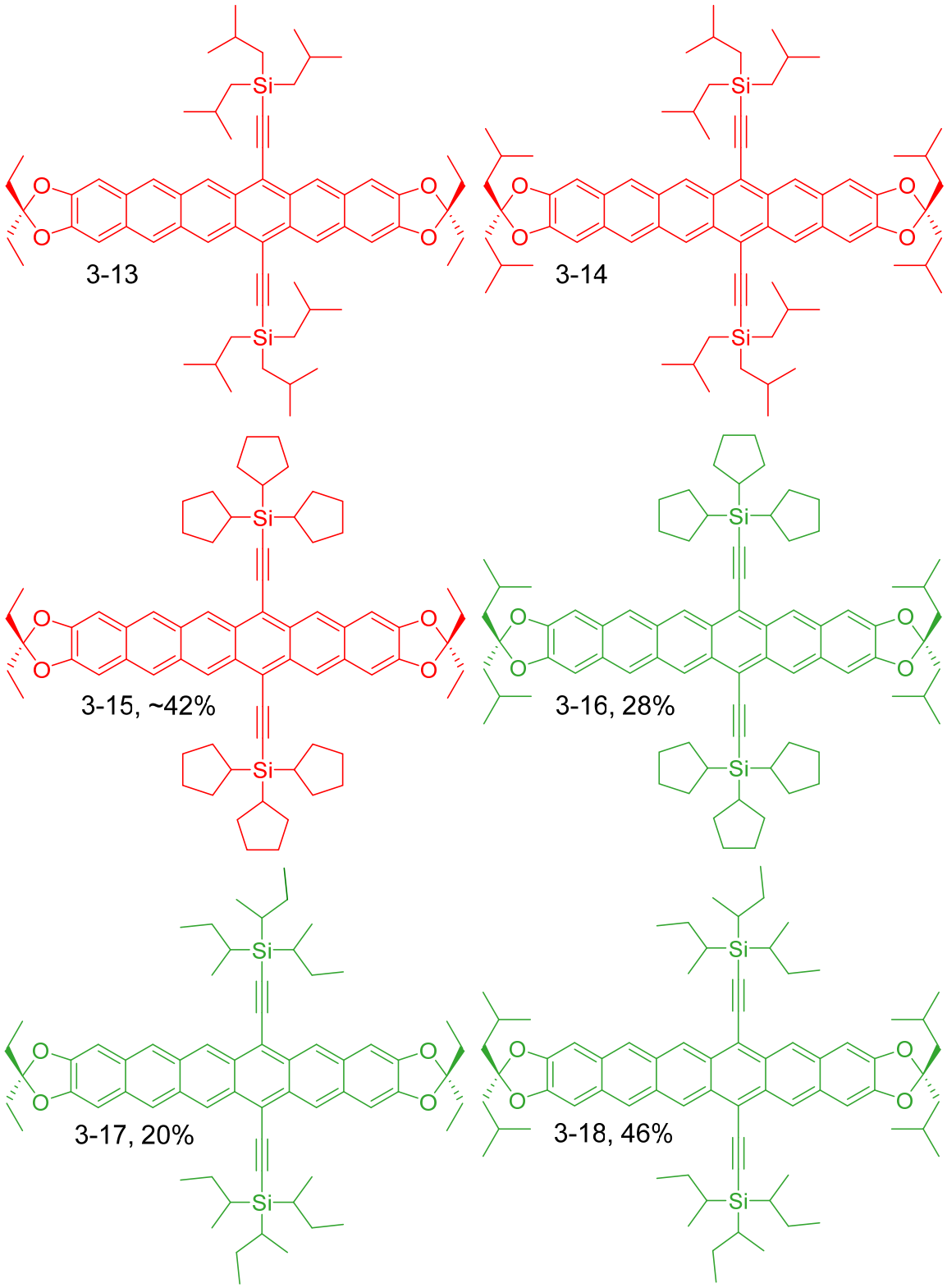

Figure 3-2. Structures of dioxolane hexacenes. Those shown in red were not isolated as pure compounds due to instability. Those shown in green were sufficiently purified but showed varying degrees of stability.

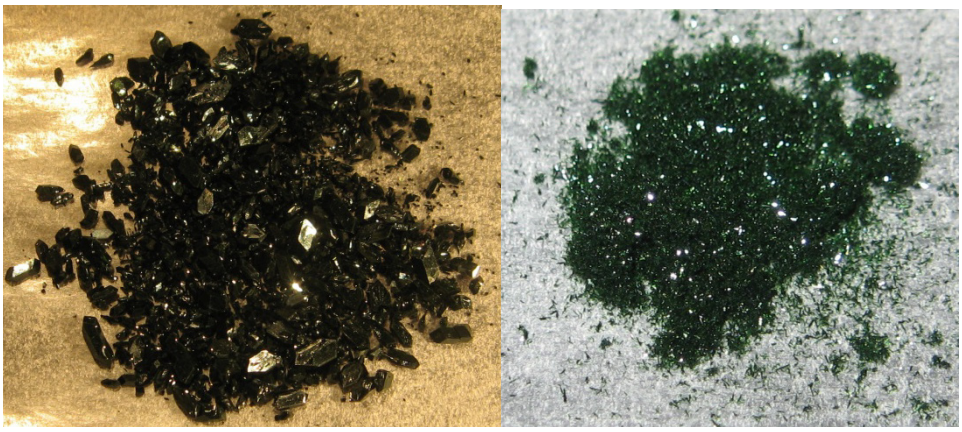

Figure 3-3. Hexacene crystals. Images of dark green crystalline hexacenes (**3-15**)—left and (**3-18**)—right. Despite forming large blocks, hexacene (**3-15**) was found to contain decomposition products.

3.3 Basic Photophysical Properties

UV-Vis and fluorescence spectra of hexacene (**3-18**) are shown in Figure 3-4. It features an absorption band at 720 nm, very close to the predicted value of 713 nm. Two different fluorescence spectra are shown. The red line has an emission maximum at 723 nm, corresponding to the solution spectrum, and shows nearly mirror-image vibronic structure which is very similar to the dioxolane pentacene spectrum in Figure 2-5. The blue line shows the solid-state powdered crystal fluorescence, which appears significantly different from the solution spectrum. This is likely the result of a small Stokes shift of only 3 nm. In the solid state, this would lead to significant reabsorption of the 0-0 vibronic emission band. As reabsorption decreases at longer wavelengths, emission intensity increases despite the smaller Franck-Condon factors involved. Since no quality X-ray crystal data could be obtained and the fluorescence wavelengths are beyond the range of human vision, the crystal emission was key to validating the overall crystal engineering strategy. It demonstrated that at least one of the solid-state fluorescence "tools" developed in chapter 2 was also applicable to the dioxolane hexacene chromophore.

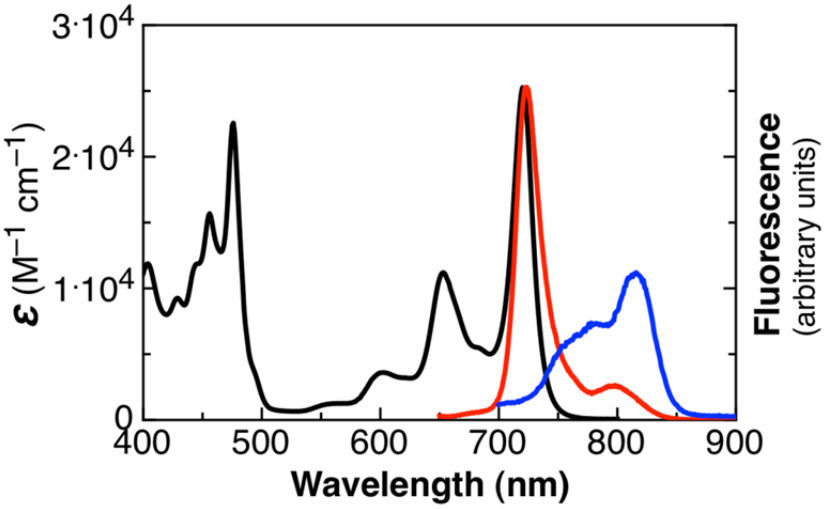

Figure 3-4. UV-Vis molar absorbance and fluorescence spectra of hexacene (**3-18**). Solution spectra (hexanes) feature a long-wavelength absorption maximum at 720 nm (black line, ε = 25,300 M^{-1} cm^{-1}) and an emission maximum at 723 nm (red line). Emission reabsorption leads to significantly different crystalline emission with a maximum at 816 nm (blue line).

Given that pure dioxolane hexacene (**3-18**) was now available, it was appropriate to determine its fluorescence quantum yield. This was measured by the comparative method relative to chlorophyll a in degassed diethyl ether with a reported quantum yield of 32%[99]. The absorbance of each solution was matched at a common excitation wavelength under very dilute conditions, and integrated fluorescence intensities were compared. Results of this experiment were disappointing, revealing a quantum yield of slightly over 1%. Although a lower fluorescence quantum yield was expected for hexacene relative to pentacene[100], it was anticipated to be much higher than 1%. In addition, this result represents the quantum yield in solution, and it may be somewhat lower in a more concentrated state. Several hundred milligrams of hexacene (**3-18**) have been sent to Robert Prud'homme's group for evaluation as a bioimaging dye.

3.4 Dioxolane Heptacenes

In addition to dioxolane hexacenes, analogous heptacenes were also synthesized since preliminary synthesis had already been accomplished. Synthesis began with an aldol condensation between (**3-7a**) or (**3-7b**) and 1,4-cyclohexanedione to produce

heptacenequinones (**3-19a**) and (**3-19b**). These were carried on to produce heptacenes (**3-20**), (**3-21**), and (**3-22**) in the standard manner using the appropriate lithiated alkyne followed by deoxygenation with $SnCl_2$ and HCl as outlined in Figure 3-6.

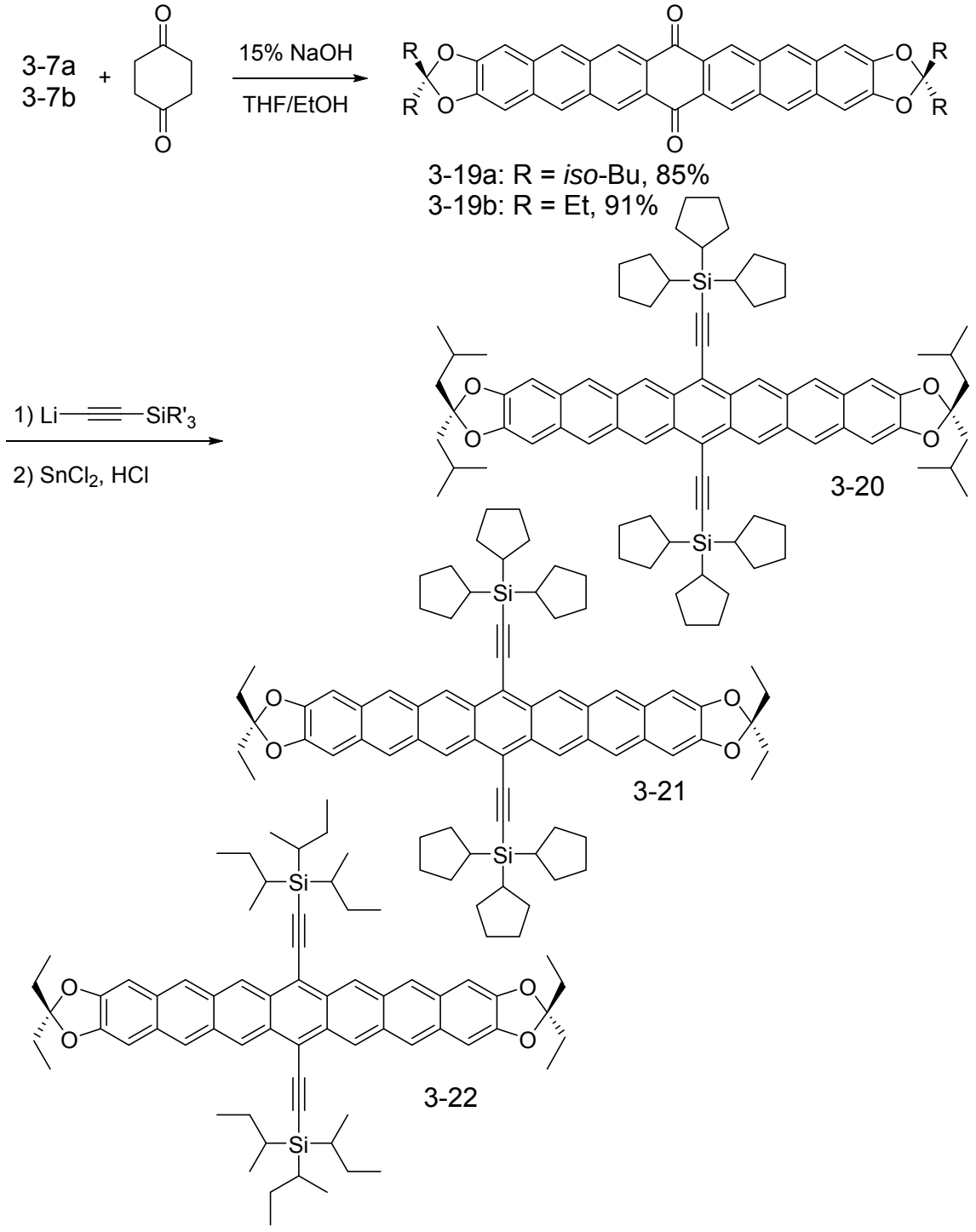

Scheme 3-6. Synthesis of dioxolane heptacenes.

Heptacenequinones (**3-19a**) and (**3-19b**) were soluble enough to grow crystals and were of sufficient quality for X-ray diffraction analysis to produce refined models, confirming their structures. Thermal ellipsoid plots and crystal images are shown in Figure 3-5. Although not of particular importance, there was a striking solubility difference between these two quinones over a wide range of solvents. This was brought to light by the inability to obtain an adequate ^{13}C NMR spectrum for isobutyl derivative (**3-19a**) due to poor solubility. Contrary to expectations, it was found that ethyl derivative (**3-19b**) was significantly more soluble despite having smaller "solubilizing" dioxolane substituents.

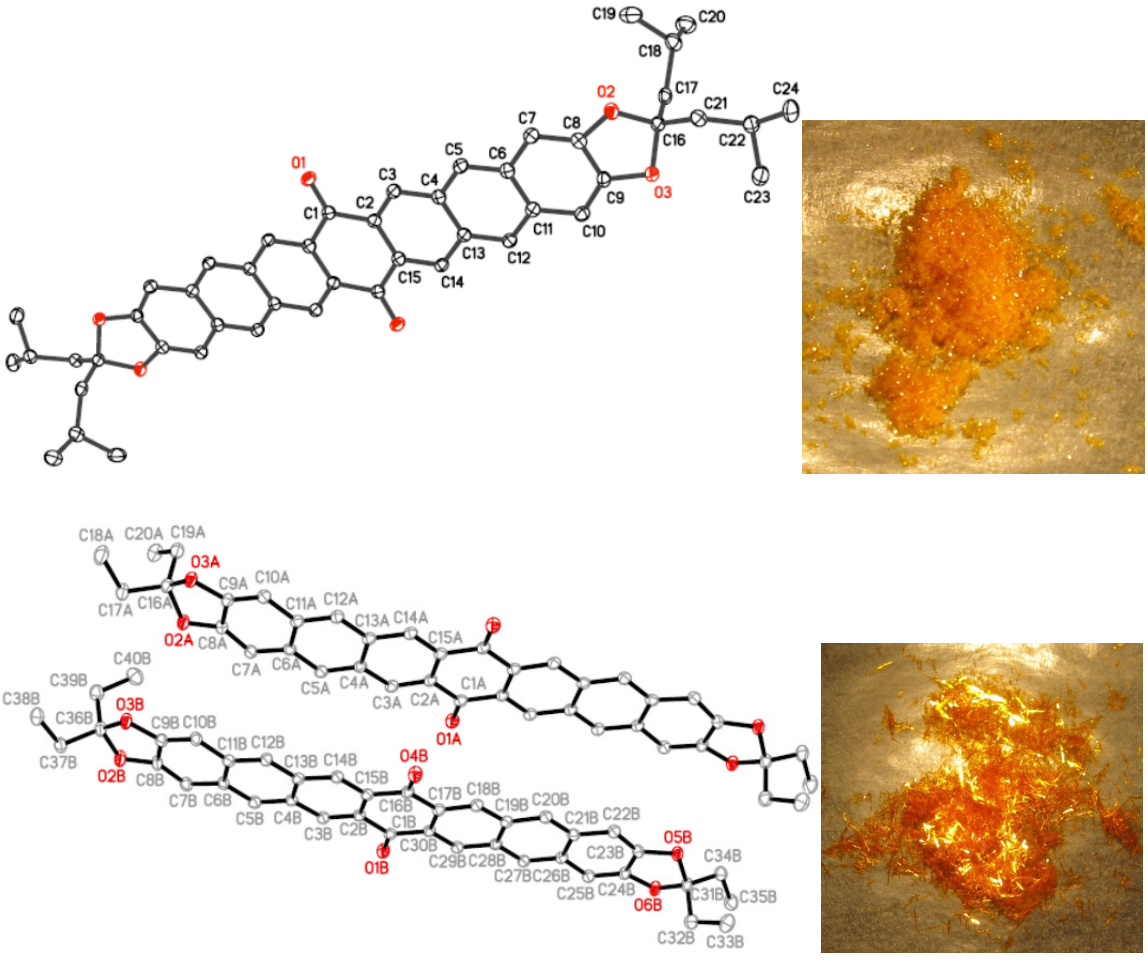

Figure 3-5. Thermal ellipsoid plots and images of heptacenequinones (**3-19a**) and (**3-19b**).

Numerous attempts at isolating these dioxolane-functionalized heptacenes were unsuccessful since they were all found to decompose very quickly. UV-Vis-NIR spectroscopy was the only meaningful characterization obtained from these three species, and a representative example is given in Figure 3-6. The heptacenediols were isolated by silica gel chromatography, and small samples were placed in a cuvette. After dissolving in THF, UV-Vis-NIR spectroscopy revealed the presence of the expected anthracene chromophores, with absorption around 380 nm. After adding $SnCl_2$/HCl, the heptacenes were generated *in situ* and their spectra recorded. Spectra showed the characteristic absorption similar to other silylethynyl-functionalized acenes reported in the literature[68a, 101].

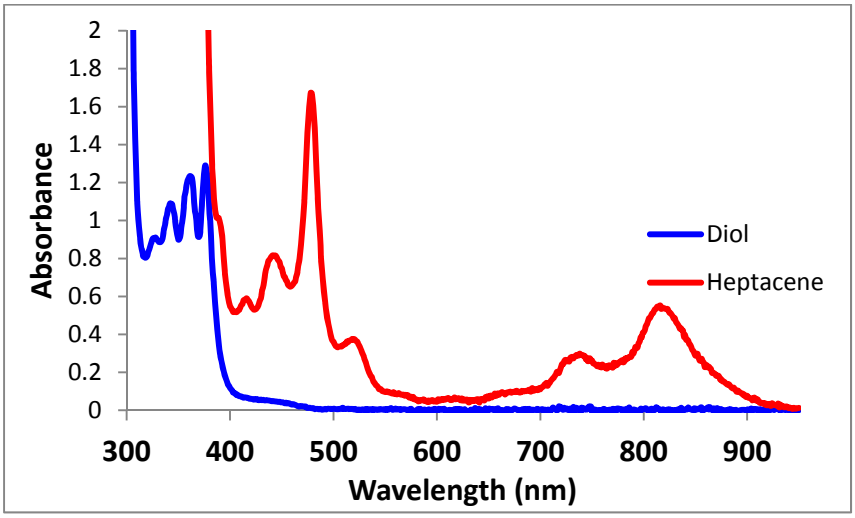

Figure 3-6. Representative UV-Vis-NIR of dioxolane heptacenes. Initially the isolated heptacenediol was scanned, giving the blue trace. Then, 1 drop of 10% HCl saturated with $SnCl_2$ was added, mixed, and quickly rescanned, giving the *in situ* spectrum of heptacene **(3-21)** shown in red.

3.5 Experimental

Dibromodiisobutylnaphthalodioxole (**3-2a**)

In a 250 mL round-bottom flask was combined 6,7-dibromo-2,3-dihydroxynaphthalene **1** (20.0 g, 62.9 mmol), 2,6-dimethyl-4-heptanone (13.3 mL, 75.5 mmol, 1.2 eq), p-TsOH hydrate (0.85 g), and 95 mL toluene. A Dean-Stark trap and reflux condenser were attached and the reaction was refluxed for 8 days. The mixture was poured in a

separatory funnel and washed with aqueous KOH solution. The resulting emulsion was filtered. The aqueous layer was washed once with toluene and the organic layers were combined, dried with $MgSO_4$, filtered, and solvent was removed with rotary evaporation. The material was then eluted through a silica gel plug with 4 hexanes : 1 dichloromethane and concentrated to afford the product, 27.81 g, 74% yield. ^{1}H NMR (400 MHz, $CDCl_3$) δ 7.88 (s, 2H), 6.88 (s, 2H), 1.88 (m, 2H), 1.87 (d, J = 2.4 Hz, 4H), 0.97 (d, J = 6.4 Hz, 12H). ^{13}C NMR (100 MHz, $CDCl_3$) δ 149.7, 131.0, 130.6, 122.9, 119.6, 102.1, 46.8, 24.2, 23.7. MS (EI 70 eV) *m/z* 442 (M^+, 25%), 385 (M^+ - 57, 100%).

Dibromodiethylnaphthalodioxole (**3-2b**)

In a 250 mL round-bottom flask was combined 6,7-dibromo-2,3-dihydroxynaphthalene **1** (20 g, 62.9 mmol), 3-pentanone (10 mL, 94.4 mmol, 1.5 eq), p-TsOH hydrate (1.05 g), and 95 mL toluene. A Dean-Stark trap and reflux condenser were attached and the reaction was refluxed for 2 days. The mixture was poured in a separatory funnel and washed with aqueous KOH solution. The resulting emulsion was filtered. The aqueous layer was washed once with toluene and the organic layers were combined, dried with $MgSO_4$, filtered, and solvent was removed with rotary evaporation. The material was then eluted through a silica gel plug with dichloromethane and concentrated to afford the product, 24.28 g, 96% yield. ^{1}H NMR (400 MHz, $CDCl_3$) δ 7.87 (s, 2H), 6.87 (s, 2H), 1.98 (q, J = 7.4 Hz, 4H), 1.00 (t, J = 7.4 Hz, 6H) . ^{13}C NMR (100 MHz, $CDCl_3$) δ 150.0, 130.9, 130.5, 122.8, 119.6, 101.9, 30.9, 7.2. MS (EI 70 eV) *m/z* 386 (M^+, 30%), 357 (M^+ - 29, 100%).

Dicyanodiisobutylnaphthalodioxole (**3-3a**)

In a 100 mL round-bottom flask was combined **3-2a** (6.75 g, 15.3 mmol) in 46 mL DMF and degassed with N_2 for 20 minutes. To this was added CuCN (5.47g, 61.1 mmol) and the mixture was heated at 140°C overnight. The reaction was then poured into ~200 mL stirring cold water, filtered, and rinsed with water. Organic material was extracted from the filter cake by stirring it in ~200 mL Et_2O and filtering. This was repeated once more.

Excess water was separated from the organic layer before it was dried with $MgSO_4$, filtered, and solvent was removed with rotary evaporation. The material was then eluted through a silica gel plug with 3 hexanes : 1 dichloromethane and concentrated to afford the product, 2.83 g, 55% yield. ^{1}H NMR (400 MHz, $CDCl_3$) δ 8.05 (s, 2H), 7.10 (s, 2H), 1.91 (d, J = 6.8 Hz, 4H), 1.87 (m, 2H), 0.96 (d, J = 6.8 Hz, 12H). ^{13}C NMR (100 MHz, $CDCl_3$) δ 152.4, 133.8, 131.7, 124.9, 116.6, 108.4, 103.8, 46.8, 24.1, 23.6. MS (EI 70 eV) *m/z* 334 (M^+, 20%), 277 (M^+ - 57, 100%).

Dicyanodiethylnaphthalodioxole (**3-3b**)

To a sealed tube was added 65 mL of DMF, **3-2b** (5.00 g, 13.0 mmol), and $Zn(CN)_2$ (6.08 g, 51.8 mmol, 4.00 eq.) which was then purged with nitrogen for 15 minutes. $Pd(PPh_3)_4$ (0.75 g, 0.65 mmol, 0.050 eq.) was then added and the mixture was heated to 110°C and stirred overnight. The resulting dark green-blue solution was filtered and rinsed with a small amount of acetone. This solution was then stirred rapidly while approx. 400 mL of water was added to precipitate the product. The solids were collected by filtration and rinsed with water before being dissolved in dichloromethane. The solution was poured in a separatory funnel to remove residual water, dried with $MgSO_4$, filtered, and solvent was removed with rotary evaporation. The solids were recrystallized from approx. 220 mL 95% ethanol to afford 3.14 g of product. Recrystallizing the mother liquor a second time yielded an additional 0.11 g for a total of 3.25 g, 90% yield. ^{1}H NMR (400 MHz, $CDCl_3$) δ 8.05 (s, 2H), 7.10 (s, 2H), 2.03 (q, J = 7.4 Hz, 4H), 1.00 (t, J = 7.4 Hz, 6H). ^{13}C NMR (100 MHz, $CDCl_3$) δ 152.8, 133.8, 131.6, 124.9, 116.6, 108.4, 103.6, 31.0, 7.0. MS (EI 70 eV) *m/z* 278 (M^+, 15%), 249 (M^+ - 29, 100%). Mp 231-233°C.

Diisobutylnaphthalodioxole dimethanol (**3-6a**)

Hydrolysis: In a 250 mL round-bottom flask was added **3-3a** (10.7 g, 32.1 mmol), KOH (12.6 g, 224 mmol, 7.00 eq.), 130 mL water, and 30 mL EtOH. The solution was refluxed overnight, after which all material had dissolved. The solution was cooled in an ice bath and slowly acidified with 12M HCl (~14-15 mL). A sticky glob of product precipitated

which was filtered. The filtrate was then saturated with NaCl and extracted once with THF. The THF layer was then poured through the sticky glob on the filter, leaving only a small amount of insoluble material behind. The filtrate was dried with $MgSO_4$, filtered, and solvent was removed with rotary evaporation in a tared 250 mL round-bottom flask. This flask was then placed in a vacuum oven for ~ 3-4 hours at 100°C to give 11.48 g (~30.83 mmol) of product. ^{1}H and ^{13}C NMR indicated a mixture of mostly anhydride **3-5a** and some remaining dicarboxylic acid **3-4a** (with only a trace of water) which was not purified further. Anhydride **3-5a**: ^{1}H NMR (400 MHz, $CDCl_3$) δ 8.25 (s, 2H), 7.25 (s, 2H), 1.92 (d, J = 5.2 Hz, 4H), 1.88 (m, 2H), 0.98 (d, J = 6.4 Hz, 12H). ^{13}C NMR (100 MHz, $CDCl_3$) δ 163.7, 152.3, 134.7, 125.7, 124.9, 124.8, 105.4, 46.8, 24.1, 23.7. MS (EI 70 eV) *m/z* 354 (M^+, 15%), 297 (M^+ - 57, 100%).

Reduction: The above dry mixture was dissolved in 60 mL dry THF and cooled in an ice bath before carefully adding a $LiAlH_4$ solution (77 mL 1M in THF, 77 mmol, 2.5 eq.) dropwise. The reaction was refluxed overnight before being cooled in an ice bath and diluted slowly with 50 mL THF. It was quenched with 2.92 mL water, 2.92 mL 15% NaOH, 8.76 mL water, and stirred an additional 15 minutes before it was filtered and rinsed with ethyl acetate. The aluminum salts were then boiled in ethyl acetate for 3-5 minutes and filtered. This was repeated 2 more times and the filtrates were combined, dried with $MgSO_4$, filtered, and solvent was removed with rotary evaporation. The material was dissolved in dichloromethane and eluted through a silica gel plug with dichloromethane followed by dichloromethane /diethyl ether (2:1), collecting a pure and impure fraction. The plug was repeated on the impure fraction to give more pure material, 8.73 g in total, 79% yield. ^{1}H NMR (400 MHz, $CDCl_3$) δ 7.54 (s, 2H), 6.98 (s, 2H), 4.74 (d, J = 2.4 Hz, 4H), 3.59 (s, 2H), 1.89 (m, 2H), 1.86 (d, J = 3.2 Hz, 4H), 0.96 (d, J = 6.4 Hz, 12H). ^{13}C NMR (100 MHz, $CDCl_3$) δ 149.1, 135.3, 130.2, 128.0, 122.1, 103.1, 64.6, 46.9, 24.2, 23.7. MS (EI 70 eV) *m/z* 344 (M^+, 20%), 287 (M^+ - 57, 100%).

Diethylnaphthalodioxole dimethanol (**3-6b**)

Hydrolysis: In a 100 mL round-bottom flask was combined **3-3b** (4.52 g, 16.2 mmol), KOH (5.47 g, 97.4 mmol, 6.00 eq.), water (65 mL), and EtOH (14 mL). The mixture was refluxed overnight and all of the solids had dissolved. The solution was then cooled in an ice bath and acidified very carefully with 7.6 mL 12M HCl whereupon the product precipitated into a sticky glob. The material was filtered. The filtrate was then saturated with NaCl and extracted once with THF. The organic layer and solids were then combined, dried with $MgSO_4$, filtered, and solvent was removed with rotary evaporation. The material was then dried in a vacuum oven at 120°C for several hours to yield 5.14 g product, approximately quantitative yield. ^{1}H and ^{13}C NMR indicated a mixture of anhydride **3-5b** and dicarboxylic acid **3-4b** which was used in the next step without further purification.

Reduction: To the above dry mixture of anhydride and dicarboxylic acid (5.14 g, ~16.2 mmol) was added 30 mL dry THF and cooled in an ice bath. Once dissolved, 1M $LiAlH_4$ in THF (40.5 mmol, 40.5 mL, 2.50 eq.) was carefully added and refluxed overnight. TLC indicated the reaction was complete and the mixture was cooled in an ice bath before carefully adding dropwise 1.54 mL water, 1.54 mL 15% aq. NaOH, and 4.62 mL water. The resulting aluminum salt mixture was stirred 15 more minutes, filtered, and rinsed with ethyl acetate. The aluminum salts were then boiled in ethyl acetate for ~5 minutes and filtered. This was repeated 2 more times and the filtrates were combined, dried with $MgSO_4$, filtered, and solvent was removed with rotary evaporation. The material was dissolved in dichloromethane and eluted through a silica gel plug with a dichloromethane/diethyl ether gradient to yield 3.38 g, 72% yield. ^{1}H NMR (400 MHz, $CDCl_3$) δ 7.53 (s, 2H), 6.97 (s, 2H), 4.73 (s, J = 2.4 Hz, 4H), 3.48 (s, 2H), 1.98 (q, J = 7.3 Hz, 4H), 1.00 (t, J = 7.3 Hz, 6H). ^{13}C NMR (100 MHz, $CDCl_3$) δ 149.5, 135.2, 130.2, 128.0, 122.1, 102.9, 64.6, 30.8, 7.2. MS (EI 70 eV) *m/z* 288 (M^+, 25%), 259 (M^+ - 29, 100%).

Diisobutylnaphthalodioxole dialdehyde (**3-7a**)

In a dry 100 mL round-bottom flask with a large stir magnet was added 20 mL methylene chloride and 1.51 mL oxalyl chloride (17.6 mmol, 3.00 eq.). The reaction was cooled to -78°C under N_2 and a mixture of 2.50 mL DMSO in 5 mL dichloromethane was added dropwise. It was stirred an additional 5 minutes before a mixture of dimethanol **3-6a** (2.00 g, 5.81 mmol, 1.00 eq.) in 15 dichloromethane was added dropwise and stirred 20 minutes. An additional 20 mL dichloromethane was then added dropwise to the thick solution and stirred an additional 40 minutes. Triethylamine (13 mL, 93 mmol, 16 eq.) was then added dropwise and the mixture was slowly warmed to room temperature and washed with 50 mL ice water. The aqueous layer was extracted 3x with dichloromethane and the combined organic layers were dried once with NaCl brine. The solution was dried with $MgSO_4$, filtered, and solvent was removed with rotary evaporation. The material was eluted through a silica gel plug with dichloromethane to give 1.79 g, 90% yield. ^{1}H NMR (400 MHz, $CDCl_3$) δ 10.59 (s, 2H), 8.22 (s, 2H), 7.20 (s, 2H), 1.87 (d, J = 4.8 Hz, 4H), 1.86 (m, 2H), 0.97 (d, J = 6.4 Hz, 12H). ^{13}C NMR (100 MHz, $CDCl_3$) δ 192.8, 151.9, 132.8, 132.6, 131.6, 124.2, 104.9, 46.9, 24.1, 23.7. MS (EI 70 eV) *m/z* 340 (M^+, 50%), 283 (M^+ - 57, 100%).

Diethylnaphthalodioxole dialdehyde (**3-7b**)

In a dry 250 mL round-bottom flask equipped with a large stirring magnet was added 40 mL dichloromethane and oxalyl chloride (3.02 mL, 35.2 mmol, 3.00 eq.) and cooled under nitrogen to -78°C. DMSO (5.0 mL, 70 mmol, 6.0 eq.) was dissolved in 10 mL dichloromethane and added dropwise. The mixture was stirred an additional 5 minutes before adding dropwise over ~15 min dimethanol **3-6b** (3.38 g, 11.7 mmol, 1.00 eq.) dissolved in 30 mL dichloromethane + 5 mL DMSO. The solution was stirred for 20 minutes before adding an additional 40 mL methylene chloride slowly over ~3 minutes and stirring an additional 30 minutes. Triethylamine (26.0 mL, 15.9 eq.) was added and the solution was allowed to warm to room temperature. The mixture was washed with 70 mL ice water and the aqueous layer extracted 3x with dichloromethane. The

combined organic layers were dried with $MgSO_4$, filtered, and solvent was removed with rotary evaporation. The material was eluted through a silica gel plug with dichloromethane to yield 2.82 g, 85%. ^{1}H NMR (400 MHz, $CDCl_3$) δ 10.58 (s, 2H), 8.21 (s, 2H), 7.20 (s, 2H), 2.02 (q, J = 7.4 Hz, 4H), 1.01 (t, J = 7.4 Hz, 6H). ^{13}C NMR (100 MHz, $CDCl_3$) δ 192.8, 152.3, 132.8, 132.6, 131.5, 124.1, 104.6, 31.0, 7.1. MS (EI 70 eV) *m/z* 284 (M^+, 25%), 255 (M^+ - 29, 20%), 227 (M^+ - 57, 100%).

Diisobutylanthradioxole endoxide (**3-8a**)

In a dry 500 mL round-bottom flask was added **3-2a** (15.16g, 34.28 mmol), 110 mL dry Et_2O, 90 mL dry THF, and 25.0 mL furan (343 mmol, 10.0 eq.). The solution was cooled to -78°C and 2.5M *n*-BuLi in hexanes (15.8 mL, 39.4 mmol, 1.15 eq.) was added dropwise. After 35 minutes, excess dry ice was removed from the bath and the reaction was allowed to stir overnight. Brine was added to quench the reaction and then drained. Enough water was added to dissolve the salts and this layer was extracted once with Et_2O. The combined organic layers were dried with $MgSO_4$, filtered, and solvent was removed with rotary evaporation giving 11.82 g crude solids. The solids were recrystallized with a 1,2-dichloroethane/heptane mixture (~1:1, ~10 mL) giving 5.70 g of fine, off-white needles. (Recrystallization from hexanes also works well. When filtering, rinse with ice-cold hexanes.) The mother liquor was concentrated and recrystallized again from 5 mL heptane to give 1.43 g. A third recrystallization gave only an additional 0.15 g, for a total of 7.28 g, 61%. ^{1}H NMR (400 MHz, $CDCl_3$) δ 7.43 (s, 2H), 6.96 (dd, J = 1.2 Hz, J = 0.8 Hz, 2H), 6.93 (s, 2H), 5.76 (s, 2H) 1.87 (m, 2H), 1.85 (d, J = 6.8 Hz, 4H), 0.96 (d, J = 9.2 Hz, 6H), 0.94 (d, J = 9.2 Hz, 6H). ^{13}C NMR (100 MHz, $CDCl_3$) δ 148.7, 143.2, 142.1, 128.2, 122.0, 118.4, 104.3, 82.16, 47.0, 46.9, 24.3, 24.2, 23.7, 23.6. MS (EI 70 eV) *m/z* 350 (M^+, 90%), 293 (M^+ - 57, 20%), 226 (M^+ - 124, 100%). Mp 117-118°C.

Diethylanthradioxole endoxide (**3-8b**)

In a dry 500 mL round-bottom flask under N_2 was added **3-2b** (17.28 g, 44.76 mmol), 145 mL dry Et_2O, 125 mL dry THF, and 32.55 mL furan (447.6 mmol, 10.00 eq.) and

cooled to -78°C. *n*-Butyllithium (21.5 mL 2.5M, 53.7 mmol, 1.20 eq.) was added by dropwise addition and the solution was stirred for 40 minutes before being slowly warmed to room temperature. The reaction was then quenched with ~50 mL NaCl brine and poured in a separatory funnel. The organic layer was separated. Water was added to the aqueous layer to dissolve the salts which was then extracted once with Et_2O. The combined organic layers were dried with $MgSO_4$, filtered, and solvent was removed with rotary evaporation to give thick brown syrup. 1,2-Dichloroethane (~5 mL) was added and heated. A small batch of crystals formed upon cooling which was collected by filtration. The mother liquor was rotovaped down and left alone, resulting in another batch of crystals. This was repeated once more, giving a total of 7.34 g, 56% yield. ^{1}H NMR (400 MHz, $CDCl_3$) δ 7.43 (s, 2H), 6.96 (s, 2H), 6.94 (s, 2H), 5.75 (s, 2H) 1.96 (m, 4H), 0.99 (m, 6H). ^{13}C NMR (100 MHz, $CDCl_3$) δ 149.1, 143.3, 142.1, 128.2, 121.9, 118.3, 104.1, 82.2, 30.9, 30.8, 7.2, 7.1. MS (EI 70 eV) *m/z* 294 (M^+, 45%), 265 (M^+ - 29, 65%), 237 (M^+ - 57, 100%). Mp 150 - 152°C.

Diisobutylanthradioxole phenol (**3-9a**)

Endoxide **3-8a** (7.28 g, 20.8 mmol) was dissolved in 200 mL 1,2-dichloroethane and $Cu(OTf)_2$ (.370 g, 1.02 mmol, 0.05 eq.) was added. The reaction was stirred rapidly and the flask became warm to the touch within 1 minute. TLC showed the reaction was complete after ~5 minutes. The solution was washed with water and extracted twice with dichloromethane. The combined organic layers were dried with $MgSO_4$, filtered, and solvent was removed with rotary evaporation. The material was eluted through a silica gel plug with dichloromethane followed by a dichloromethane /Et_2O mixture (2:1) to give 5.72 g, 79% yield. ^{1}H NMR (400 MHz, $CDCl_3$) δ 8.48 (s, 1H), 8.12 (s, 1H), 7.50 (d, J = 8.4 Hz, 1H), 7.21 (dd, J = 8.4 Hz, J = 7.2 Hz, 1H), 7.15 (s, 1H), 7.09 (s, 1H), 6.70 (d, J = 7.2 Hz, 1H), 5.31 (br, 1H), 1.92 (m, 2H), 1.90 (d, J = 3.6 Hz, 4H), 0.99 (d, J = 6.0 Hz, 12H). ^{13}C NMR (100 MHz, $CDCl_3$) δ 151.2, 149.4, 149.1, 132.1, 130.4, 129.5, 124.5, 124.4, 122.8, 122.0, 120.7, 118.8, 106.2, 102.2, 101.5, 47.0, 24.2, 23.7. MS (EI 70 eV) *m/z* 350 (M^+, 35%), 293 (M^+ - 57, 15%), 226 (M^+ - 124, 100%).

Diethylanthradioxole phenol (**3-9b**)

In a 250 round-bottom flask was added endoxide **3-8b** (7.34 g, 24.9 mmol) and 240 mL 1,2-dichloroethane. While stirring rapidly, $Cu(OTf)_2$ (0.440 g, 1.25 mmol, 0.05 eq.) was added and stirred for 5 minutes during which time the flask became noticeably warm to the touch. The reaction was then washed with 100 mL water and the aqueous layer extracted once with methylene chloride. The combined organic layers were dried with $MgSO_4$, filtered, and solvent was removed with rotary evaporation. The material was eluted through a silica gel plug with dichloromethane to yield 3.77 g, 51%. ^{1}H NMR (400 MHz, $CDCl_3$) δ 8.54 (s, 1H), 8.15 (s, 1H), 7.52 (d, J = 8.4 Hz, 1H), 7.23 (dd, J = 8.4 Hz, J = 7.2 Hz, 1H), 7.19 (s, 1H), 7.13 (s, 1H), 6.70 (d, J = 7.2 Hz, 1H), 5.79 (br, 1H), 2.04 (q, J = 7.4, 4H), 1.06 (t, J = 7.4 Hz, 6H). ^{13}C NMR (100 MHz, $CDCl_3$) δ 151.3, 149.7, 149.4, 132.0, 130.2, 129.4, 124.5, 124.4, 122.8, 121.9, 120.5, 118.9, 106.2, 102.0, 101.3, 30.9, 7.2. MS (EI 70 eV) *m/z* 294 (M^+, 75%), 265 (M^+ - 29, 50%), 226 (M^+ - 68, 100%).

Diisobutyldioxolane-1,4-anthraquinone (**3-10a**)

Phenol **3-9a** (5.72g, 16.3 mmol, 1 eq.) was dissolved in 100 mL DMF, cooled to 0°C, and 60 mL water was added with stirring. A solution of [bis(trifluoroacetoxy)iodo]benzene (14.05 g, 32.60 mmol, 2.000 eq.) in 50 mL DMF was added slowly. Ethyl acetate (~250 mL) was slowly added to the black solution and left to stir for 2 hours. An additional 150 mL of ethyl acetate was added and the solution was washed 3x with ice water, dried with NaCl brine, $MgSO_4$, filtered, and solvent was removed with rotary evaporation. The material was eluted through a silica gel plug starting with 1:1 dichloromethane /hexanes and gradually increasing the ratio to 3:1 to give 2.43 g of yellow solid, 41% yield. *It was subsequently determined this reaction can be done in THF with only a small amount of water. This avoids the messy workup involved with DMF and requires much less solvent. This also increased the yield to roughly 60%.* ^{1}H NMR (400 MHz, $CDCl_3$) δ 8.35 (s, 2H), 7.19 (s, 2H), 6.98 (s, 2H), 1.88 (m, 6H), 0.97 (d, J = 6.4 Hz, 12H). ^{13}C NMR (100 MHz, $CDCl_3$) δ 185.2, 151.6, 139.9, 133.1, 127.23, 127.17, 123.9, 105.2, 46.8, 24.1, 23.7. MS (EI 70 eV) *m/z* 364 (M^+, 15%), 307 (M^+ - 57, 100%).

Diethyldioxolane-1,4-anthraquinone (**3-10b**)

To a 500 mL round-bottom flask was added phenol **3-9b** (3.77 g, 12.8 mmol) and 80 mL DMF. While stirring, 30 mL of water was slowly added and the mixture was cooled in an ice bath. A solution of [bis(trifluoroacetoxy)iodo]benzene (11.57 g, 26.9 mmol, 2.1 eq.) in 41 mL DMF was then slowly added. Ethyl acetate (~300 mL) was slowly added to the resulting black solution to ensure complete solubility and the reaction was stirred for 90 minutes. The mixture was diluted with 100 mL ethyl acetate and washed once with ice water. This first aqueous wash was quite yellow and was extracted once with additional ice and ethyl acetate. The organic layers were combined, washed an additional 2x with ice water and 1x with NaCl brine. The solution was then dried with $MgSO_4$, filtered, and solvent was removed with rotary evaporation. The material was eluted through a silica gel plug with a hexanes/ dichloromethane gradient to yield 1.95 g, 49%. *It was subsequently determined this reaction can be done in THF with only a small amount of water. This avoids the messy workup involved with DMF. The yield was nearly the same.* ^{1}H NMR (400 MHz, $CDCl_3$) δ 8.29 (s, 2H), 7.16 (s, 2H), 6.94 (s, 2H), 2.00 (q, J = 7.4 Hz, 4H), 1.00 (t, J = 7.4 Hz, 6H). ^{13}C NMR (100 MHz, $CDCl_3$) δ 185.1, 151.9, 139.8, 133.0, 127.12, 127.09, 123.8, 105.0, 30.9, 7.1. MS (EI 70 eV) *m/z* 308 (M^+, 15%), 279 (M^+ - 29, 100%).

Diisobutyldioxolane-1,4-anthracenehydroquinone (**3-11a**)

A mixture of anthraquinone **3-10a** (2.43 g, 6.67 mmol), 40 mL dioxane, and 40 mL water were purged with N_2 for 30 minutes. Sodium hydrosulfite (4.41 g, 25.3 mmol, 3.80 eq.) was then added and the solution was stirred overnight. The reaction was then extracted 3x with degassed Et_2O and the combined organic layers washed 3x with degassed water. It was then dried with $MgSO_4$, filtered, and solvent was removed with rotary evaporation to give 2.35 g, 96%. ^{1}H NMR (400 MHz, $CDCl_3$) δ 8.33 (s, 2H), 7.17 (s, 2H), 3.09 (s, 4H), 1.88 (m, 6H), 0.97 (d, J = 6.8 Hz, 12H). ^{13}C NMR (100 MHz, $CDCl_3$) δ 196.4, 151.6, 133.6, 130.0, 126.8, 123.8, 104.8, 46.8, 37.9, 24.1, 23.7. MS (EI 70 eV) *m/z* 366 (M^+, 15%), 309 (M^+ - 57, 100%).

Diethyldioxolane-1,4-anthracenehydroquinone (**3-11b**)

To a 250 mL round-bottom flask was added anthraquinone **3-10b** (1.95g, 6.32 mmol), 80 mL dioxane, and 80 mL water. The mixture was stirred rapidly and degassed with nitrogen for 15 min before adding sodium hydrosulfite (4.18g, 3.80 eq.) and stirred overnight. The mixture was then extracted 3x with degassed Et_2O. The combined organic layers were then washed 3x with degassed water, dried with $MgSO_4$, filtered, and solvent was removed with rotary evaporation followed by high vacuum to give the product. *As dioxane is difficult to completely remove, the yield (>100% by mass) was assumed quantitative and used in the next step with some residual dioxane present.* ^{1}H NMR (400 MHz, $CDCl_3$) δ 8.30 (s, 2H), 7.16 (s, 2H), 3.08 (s, 4H), 2.00 (q, J = 7.4 Hz, 4H), 0.99 (t, J = 7.4 Hz, 6H). ^{13}C NMR (100 MHz, $CDCl_3$) δ 196.4, 151.9, 133.5, 130.0, 126.7, 123.7, 104.5, 37.8, 30.9, 7.1. MS (EI 70 eV) *m/z* 310 (M^+, 20%), 281 (M^+ - 29, 100%).

Isobutyldioxolane hexacenequinone (**3-12a**)

Hydroquinone **3-11a** (0.979 g, 2.67 mmol) and dialdehyde **3-7a** (0.910 g, 2.67 mmol) were dissolved in a degassed solution of 3.9 mL THF and 3.9 mL EtOH. With rapid stirring, 0.4 mL 15% aq. NaOH solution was added (as fast as possible). Precipitates formed almost immediately and the thick slurry was diluted with 10 mL MeOH, stirred 1 minute, and diluted with an additional 30 mL MeOH. After stirring for ~5 minutes, the solution was filtered and rinsed with MeOH followed by ~10 mL acetone to give 1.13 g of yellow-orange powder, 63% yield. ^{1}H NMR (400 MHz, $CDCl_3$) δ 9.00 (s, 2H), 8.70 (s, 2H), 8.42 (s, 2H), 7.258 (s, 2H), 7.18 (s, 2H), 1.92 (m, 12H), 0.99 (d, J = 6.4 Hz, 24H). ^{13}C NMR (100 MHz, $CDCl_3$) δ 183.4, 151.6, 150.7, 133.7, 132.6, 131.3, 130.5, 129.9, 129.4, 127.9, 127.8, 123.7, 123.1, 105.0, 102.2, 47.0, 46.9, 24.21, 24.18, 23.72, 23.69. MS (LDI) *m/z* 670.3 (M^+). Mp 234-236°C (234°C by DSC). Anal. calcd. for $C_{44}H_{46}O_6$: C, 78.78 ; H, 6.91. Found: C, 78.61; H, 6.88.

Ethyldioxolane hexacenequinone (**3-12b**)

To a 250 mL round-bottom flask was added 9.5 mL THF + 9.5 mL EtOH and degassed for 10 minutes with nitrogen. To this was added hydroquinone **3-11b** (~1.96 g, 6.32 mmol*) and dialdehyde **3-7b** (1.79 g, 6.32 mmol) and heated to dissolve everything. When dissolved, 1 mL of 15% aq. NaOH was added (as fast as possible) and precipitates formed within ~5 seconds. This was then diluted with ~15 mL MeOH and stirred for 5 minutes before diluting with MeOH up to 250 mL. It was then stirred an additional 1 min before filtering, rinsing with MeOH followed by a small amount of Et_2O to yield yellow powder, 2.99 g, 85%. ^{1}H NMR (400 MHz, $CDCl_3$) δ 8.95 (s, 2H), 8.66 (s, 2H), 8.37 (s, 2H), 7.24 (s, 2H), 7.16 (s, 2H), 2.04 (q, J = 7.4 Hz, 8H), 1.04 (t, J = 7.4 Hz, 12H). ^{13}C NMR (100 MHz, $CDCl_3$) δ 183.3, 151.9, 151.0, 133.6, 132.5, 131.3, 130.4, 129.9, 129.3, 127.9, 127.7, 123.7, 123.0, 104.8, 101.9, 31.1, 31.0, 7.2. MS (LDI) *m/z* 558.2 (M^+). Mp 327-328°C (327°C by DSC). Anal. calcd. for $C_{36}H_{30}O_6$: C, 77.40; H, 5.41. Found: C, 77.65; H, 5.52.

TIBS ethyldioxolane hexacene (**3-13**)

To a dry 100 mL round-bottom flask was added triisobutylsilylacetylene (0.602 g, 2.68 mmol, 5.00 eq.) and 10 mL hexanes. The solution was cooled to 0°C before slowly adding *n*-BuLi (2.4 mmol, 0.96 mL 2.5 M in hexanes, 4.5 eq.) and stirred 1 hour before adding 35 mL hexanes and hexacenequinone **3-12b** (300 mg, 0.537 mmol, 1 eq.) The reaction was stirred for 10 minutes before adding 5 mL THF and stirring overnight at room temperature. The next day, the reaction was quenched with ~1 mL aqueous NH_4Cl and 20 mL THF was added. The solution was degassed with nitrogen for ~15 minutes and 3 g $SnCl_2$ dihydrate was added along with just enough 10% aq. HCl to dissolve the salts. The mixture was stirred rapidly in the dark for 15 minutes. It was then washed with water 4x and concentrated by rotary evaporation. The mixture was eluted through a silica gel plug with hexanes to separate excess alkyne followed by 6 hexanes : 1 dichloromethane to elute the product. Solvent was removed by rotary evaporation to give 340 mg. This was recrystallized from ~4 mL acetone give 238 mg of green,

microcrystalline masses that were fairly impure by NMR. This compound could not be isolated in pure from. MS (LDI) *m/z* 972.6 (M^-).

TIBS isobutyldioxolane hexacene (**3-14**)

To a dry 100 mL round-bottom flask was added triisobutylsilylacetylene (0.334 g, 1.49 mmol, 5.00 eq.) and 6 mL hexanes. The solution was cooled to 0°C before slowly adding *n*-BuLi (1.3 mmol, 0.54 mL 2.5 M in hexanes, 4.5 eq.) and stirred 1 hour before adding 19 mL hexanes and hexacenequinone **3-12a** (200 mg, 0.298 mmol, 1 eq.) The reaction was stirred for 1 hour before adding 1 mL THF and stirring overnight at room temperature. The next day, the reaction was poured on a dry silica gel plug and excess alkyne was eluted with hexanes. The diol was then eluted with dichloromethane and solvent removed by rotary evaporation. This was dissolved in ~10 mL MeOH with 15-20 mL acetone and degassed with N_2 for 5 minutes before adding 130 mg $SnCl_2$ dihydrate and 0.5 mL 10% aq. HCl. The mixture was stirred rapidly in the dark for 10 minutes and then filtered. TLC showed this material was much less pure than TCPS derivative (**3-16**) at this stage. This was purified on silica gel first with degassed hexanes, then a degassed mixture of 9 hexanes : 1 dichloromethane. Solvent was removed by rotary evaporation and it was recrystallized from MeOH/acetone to give 21.2 mg of light green crystalline clumps. Again, NMR showed the crystals were fairly impure, and no other characterization was attempted.

TCPS ethyldioxolane hexacene (**3-15**)

To a dry 100 mL round-bottom flask was added tricyclopentylsilylacetylene (0.698 g, 2.68 mmol, 5.00 eq.) and 10 mL hexanes. The solution was cooled to 0°C before slowly adding *n*-BuLi (2.41 mmol, 0.96 mL 2.5 M in hexanes, 4.5 eq.) and stirred 1 hour before adding 35 mL hexanes and hexacenequinone **3-12b** (300 mg, 0.537 mmol, 1.00 eq.) The reaction was stirred for 10 minutes before adding 5 mL THF and stirring overnight at room temperature. The next day, the reaction was quenched with ~1 mL aqueous NH_4Cl and 20 mL THF was added. The solution was degassed with nitrogen for ~15 minutes and 3 g $SnCl_2$ dihydrate was added along with just enough 10% aq. HCl to dissolve the

salts. The mixture was stirred rapidly in the dark for 15 minutes. It was then washed with water 4x and concentrated by rotary evaporation. The mixture was eluted through a silica gel plug with hexanes to separate excess alkyne followed by 5 hexanes : 1 dichloromethane to elute the product. Solvent was removed by rotary evaporation to give 390 mg. This was recrystallized from ~40 mL hexanes with ~5 mL DCE to give dark green blocks (3 mm dimensions), 238 mg (42% yield). Despite their size, NMR showed the crystals were somewhat impure. Attempts at recrystallization only resulted in more significant decomposition. ^{1}H NMR (400 MHz, $CDCl_3$) δ 9.38 (s, 2H), 8.91 (s, 2H), 8.31 (s, 2H), 7.06 (s, 2H), 7.03 (s, 2H), 2.07 (m, 20H), 1.81 (m, 24H), 1.66(m, 12H), 1.36 (m, 6H), 1.07 (t, J = 7.1 Hz, 6H), 1.05 (t, J = 7.1 Hz, 6H). MS (LDI) *m/z* 1044.6 (M^-).

TCPS isobutyldioxolane hexacene (**3-16**)

In a dry 100 mL round-bottom flask was added tricyclopentylsilylacetylene (1.55 g, 5.96 mmol, 5.00 eq.) and 16 mL hexanes. The solution was cooled to 0°C before slowly adding *n*-BuLi (5.36 mmol, 2.14 mL 2.5 M in hexanes, 4.50 eq.) and stirred 1 hour before adding 20 mL hexanes, 7 mL THF, and hexacenequinone **3-12a** (800 mg, 1.19 mmol, 1 eq.) The reaction was stirred 1 more hour at 0°C before 17 mL more THF was added and the solution stirred overnight at room temperature. The reaction was then quenched with ~1 mL saturated NH_4Cl, diluted with ~10 mL THF, and degassed with N_2 for 10 minutes before adding 7 g $SnCl_2 \bullet 2\ H_2O$ with ~10 mL 10% HCl and stirred 15 minutes in the dark. The aqueous layer was removed and the organic layer was concentrated by rotary evaporation. The dark green organic residue was dissolved in degassed hexanes and poured on a silica gel plug. It was eluted first with degassed hexanes to remove excess alkyne and then with degassed 9 hexanes : 1 dichloromethane to elute the green hexacene. Solvent was removed under reduced pressure to give 880 mg. This was then recrystallized from 12 mL degassed hexanes to give 380 mg, 28% yield. ^{1}H NMR (400 MHz, $CDCl_3$) δ 9.37 (s, 2H), 8.89 (s, 2H), 8.29 (s, 2H), 7.04 (s, 2H), 7.00 (s, 2H), 2.07 (m, 12H), 1.92 (m, 12H), 1.80(m, 24H), 1.64 (m, 12H), 1.35 (m, 6H), 1.01 (d, J = 6.0 Hz, 12H), 1.00 (d, J = 6.0 Hz, 12H). ^{13}C NMR (100 MHz, $CDCl_3$) δ 149.8, 149.5, 131.3, 131.0, 130.5,

130.3, 129.9, 125.3, 124.4, 124.0, 122.2, 122.1, 117.0, 107.0, 104.5, 101.3, 101.0, 47.11, 47.06, 29.7, 27.4, 24.27, 24.25, 23.7. MS (LDI) *m/z* 1156.7 (M^+). Mp (decomposition at 236°C by DSC). Anal. calcd. for $C_{78}H_{100}O_4Si_2$: C, 80.92; H, 8.71. Found: C, 80.88; H, 8.63.

TSBS ethyldioxolane hexacene (**3-17**)

To a dry 100 mL round-bottom flask was added tri*sec*-butylsilylacetylene (0.904 g, 4.03 mmol, 4.50 eq.) and 16 mL hexanes. The solution was cooled to 0°C before slowly adding *n*-BuLi (3.63 mmol, 1.45 mL 2.5 M in hexanes, 4.05 eq.) and stirred 1 hour before adding 60 mL hexanes and hexacenequinone **3-12b** (500 mg, 0.895 mmol, 1.00 eq.) The reaction was stirred for 2 hours before adding 8 mL THF and stirring overnight at room temperature. Solvent was then removed by rotary evaporation and the material dissolved in hexanes. The mixture was eluted through a silica gel plug with hexanes to separate excess alkyne followed by dichloromethane to elute the diol mixture. Solvent was removed from the diol mixture and it was dissolved in 10 mL MeOH and 10 mL acetone. This solution was degassed with N_2 for 10 minutes before adding 1 g $SnCl_2 \bullet 2 H_2O$ with ~1 mL 10% HCl and stirred 10 minutes in the dark. A dark solid mass of product had formed. Most of the solvent was removed by rotary evaporation and the remaining yellow solution decanted off. The solid mass was rinsed with MeOH and decanted again. Remaining solvent was removed under high vacuum and the solids were dissolved in hexanes. A crude separation on a silica gel plug with 9 hexanes : 1 dichloromethane gave 290 mg of green solids. This was dissolved in hexanes and eluted through a small silica gel column with hexanes, ramping up to 93% hexanes / 7% methylene chloride. Solvent was removed by rotary evaporation to give the product, 170 mg of green solids, 20% yield. All attempts at growing crystals of this material resulted in significant or complete decomposition. ^{1}H NMR (400 MHz, $CDCl_3$) δ 9.46 (s, 2H), 9.00 (s, 2H), 8.37 (s, 2H), 7.11 (s, 2H), 7.09 (s, 2H), 2.08 (m, 14H), 1.62 (m, 6H), 1.41 (d, J = 7.2 Hz, 18H), 1.24 (m, 24H), 1.10 (t, J = 7.3 Hz, 6H), 1.08 (t, J = 7.3 Hz, 6H). ^{13}C NMR (100 MHz, $CDCl_3$) δ 150.2, 149.9, 131.3, 131.0, 130.6, 130.3, 130.0, 125.3, 124.4, 124.0, 122.2, 121.9, 117.0,

107.5, 105.6, 101.1, 100.7, 31.1, 26.00, 25.95, 19.6, 15.03, 14.98, 14.2, 7.2. MS (LDI) *m/z* 972.6 (M^-).

TSBS isobutyldioxolane hexacene (**3-18**)

In a dry 250 mL round-bottom flask was added tri*sec*-butylsilylacetylene (1.34 g, 5.96 mmol, 5.00 eq.) and 25 mL hexanes. The solution was cooled to 0°C before slowly adding *n*-BuLi (5.36 mmol, 2.14 mL 2.5 M in hexanes, 4.50 eq.) and stirred 1 hour before adding 75 mL hexanes, 10 mL THF, and hexacenequinone **3-12a** (800 mg, 1.19 mmol, 1.00 eq.) The reaction was stirred overnight at room temperature. It was then quenched with ~1 mL saturated NH_4Cl, diluted with ~10 mL THF, and degassed with N_2 for 10 minutes before adding 7 g $SnCl_2 \bullet 2\ H_2O$ with ~10 mL 10% HCl and stirred 15 minutes in the dark. The solution was washed with water 3x, dried with $MgSO_4$, and concentrated by rotary evaporation. The dark green organic residue was dissolved in degassed hexanes and poured on a silica gel plug. It was eluted first with degassed hexanes to remove excess alkyne and then with degassed 9 hexanes : 1 dichloromethane to elute the green hexacene. Solvent was removed under reduced pressure to give 800 mg. This was then recrystallized from degassed acetone to give 595 mg, 46% yield. ^{1}H NMR (400 MHz, $CDCl_3$) δ 9.40 (s, 2H), 8.93 (s, 2H), 8.31 (s, 2H), 7.05 (s, 2H), 7.02 (s, 2H), 2.04 (m, 6H), 1.93 (m, 12H), 1.56 (m, 6H), 1.35 (d, J = 7.2 Hz, 18H), 1.20 (m, 24H), 1.02 (q, J = 6.0 Hz, 12H), 1.00 (d, J = 6.0 Hz, 12H). ^{13}C NMR (100 MHz, $CDCl_3$) δ 149.8, 149.5, 131.3, 131.0, 130.5, 130.3, 130.0, 125.3, 124.4, 124.0, 122.2, 122.1, 117.0, 107.4, 105.6, 101.3, 101.0, 47.10, 47.06, 26.0, 25.9, 24.27, 24.25, 23.7, 19.6, 15.02, 14.98, 14.1. MS (LDI) *m/z* 1084.7 (M^+). Mp (decomposition at 180°C, DSC). Anal. calcd. for $C_{72}H_{100}O_4Si_2$: C, 79.65; H, 9.28. Found: C, 79.94; H, 8.94. Fluorescence quantum yield 1% relative to chlorophyll a in diethyl ether.

Isobutyldioxolane heptacenequinone (**3-19a**)

Dialdehyde **3-7a** (427 mg, 1.25 mmol, 2 eq.) and 1,4-cyclohexanedione (70.3 mg, 0.627 mmol, 1 eq.) were dissolved in a mixture of 2 mL EtOH and 3 mL THF. With rapid stirring,

0.4 mL 15% aq. NaOH solution was added (as fast as possible). Precipitates formed almost immediately and the thick slurry was diluted with 5 mL MeOH, stirred 1 minute, and diluted with an additional 20 mL MeOH. After stirring for ~5 minutes, the solution was filtered and rinsed with MeOH followed by ~10 mL acetone to give 452 mg yellow-orange powder, 85% yield. ^{1}H NMR (400 MHz, $CDCl_3$) δ 9.07 (s, 4H), 8.44 (s, 4H), 7.20 (s, 4H), 1.92 (m, 12H), 1.00 (d, J = 6.8 Hz, 24H). This compound was not soluble enough for a perfect ^{13}C NMR. Only the weak carbonyl peak (δ 183.3) was questionable, but compares well with **3-19b**. All other peaks were well above the noise. ^{13}C NMR (100 MHz, $CDCl_3$) δ 183.3, 150.7, 132.6, 131.4, 130.7, 129.7, 127.8, 123.1, 102.1, 47.0, 24.2, 23.7. MS (LDI) *m/z* 720.3 (M^+), 721.3 ($M+H^+$). Mp (354°C by DSC). Anal. calcd. for $C_{48}H_{48}O_6$: C, 79.97 ; H, 6.71. Found: C, 79.87; H, 6.68.

Ethyldioxolane heptacenequinone (**3-19b**)

To a 100 mL round-bottom flask was added dialdehyde **3-7b** (1.03 g, 3.62 mmol, 2 eq.), 1,4-cyclohexanedione (0.203 g, 1.81 mmol, 1eq.), 6 mL THF and 3 mL EtOH. The mixture was heated to dissolve everything and 0.3 mL of 15% aq. NaOH was added (as fast as possible) with rapid stirring and precipitates formed within ~5 seconds. The reaction was diluted with 20 mL MeOH and stirred an additional 3 minutes before filtering, rinsing with MeOH followed by a small amount of Et_2O to yield orange powder, 1.00 g, 91%. ^{1}H NMR (400 MHz, $CDCl_3$) δ 9.02 (s, 4H), 8.40 (s, 4H), 7.17 (s, 4H), 2.05 (q, J = 7.4 Hz, 8H), 1.05 (t, J = 7.4 Hz, 24H). ^{13}C NMR (100 MHz, $CDCl_3$) δ 183.2, 151.1, 132.6, 131.3, 130.6, 129.7, 127.7,123.0, 101.9, 31.1, 7.2. MS (LDI) *m/z* 608.2 (M^+). Mp (400°C by DSC). Anal. calcd. for $C_{40}H_{32}O_6$: C, 78.93; H, 5.30. Found: C, 78.97; H, 5.18.

TCPS isobutyldioxolane heptacene (**3-20**)

To a dry 50 mL round-bottom flask was added tricyclopentylsilylacetylene (0.361 g, 1.39 mmol, 5 eq.) and 6.0 mL hexanes. The solution was cooled to 0°C before slowly adding *n*-BuLi (1.25 mmol, 0.500 mL 2.5 M in hexanes) and stirred 1 hour before adding 10 mL hexanes and heptacenequinone **3-19a** (200 mg, 0.277 mmol, 1 eq.) The reaction was

stirred for 30 minutes before adding 5 mL THF and stirring overnight at room temperature. Some solids remained the next day and an additional 6 mL THF was added and stirred overnight again. The next day, solvent was removed by rotary evaporation and the material dissolved in hexanes. The mixture was eluted through a silica gel plug with hexanes to separate excess alkyne followed by dichloromethane to elute the diol mixture. Solvent was removed by rotary evaporation to give 330 mg of diol mixture. A small portion of this yellow solid was transferred to a UV-Vis cuvette and dissolved in THF. As expected, the UV-Vis-NIR scan revealed the presence of an anthracene chromophore. The addition of 1-2 drops of 10% HCl saturated with $SnCl_2$ resulted in an immediate color change to a light brown solution. A quick UV-Vis-NIR scan revealed the appearance of a characteristic heptacene chromophore. All attempts at isolating this heptacene have been unsuccessful. UV-Vis-NIR (THF): 415, 441, 477 (sh), 510, 734, 806.

TCPS ethyldioxolane heptacene (**3-21**)

To a dry 50 mL round-bottom flask was added tricyclopentylsilylacetylene (0.427 g, 1.64 mmol, 5.00 eq.) and 7 mL hexanes. The solution was cooled to 0°C before slowly adding *n*-BuLi (1.48 mmol, 0.590 mL 2.5 M in hexanes) and stirred 1 hour before adding 18 mL hexanes and heptacenequinone **3-19b** (200 mg, 0.329 mmol, 1 eq.) The reaction was stirred for 10 minutes before adding 5 mL THF and stirring overnight at room temperature. The next day, solvent was removed by rotary evaporation and the material dissolved in hexanes. The mixture was eluted through a silica gel plug with hexanes to separate excess alkyne followed by dichloromethane to elute the diol mixture. Solvent was removed by rotary evaporation to give 192 mg of diol mixture. UV-Vis-NIR spectra were recorded as described for compound **3-20**. All attempts at isolating this heptacene have been unsuccessful. UV-Vis-NIR (THF): 416, 442, 478 (sh), 663, 738, 816.

TSBS ethyldioxolane heptacene (**3-22**)

To a dry 50 mL round-bottom flask was added trisec-butylsilylacetylene (0.368 g, 1.64 mmol, 5.00 eq.) and 7 mL hexanes. The solution was cooled to 0°C before slowly adding

n-BuLi (1.48 mmol, 0.590 mL 2.5 M in hexanes) and stirred 1 hour before adding 18 mL hexanes and heptacenequinone **3-19b** (200 mg, 0.329 mmol, 1 eq.) The reaction was stirred for 10 minutes before adding 5 mL THF and stirring overnight at room temperature. The next day, solvent was removed by rotary evaporation and the material dissolved in hexanes. The mixture was eluted through a silica gel plug with hexanes to separate excess alkyne followed by methylene chloride to elute the diol mixture. Solvent was removed by rotary evaporation to give 158 mg of diol mixture. UV-Vis-NIR spectra were recorded as described for compound **3-20**. All attempts at isolating this heptacene have been unsuccessful. UV-Vis-NIR (THF): 415, 443, 479 (sh), 663, 738, 814.

Chapter 4. Fine-Tuning of Crystal Packing

4.1 Diethynylpentacenes

Slight modifications made to a molecular structure can cause substantial changes in the crystal packing motif. The silylethyne-functionalization strategy gives some degree of control over the solid-state arrangement, often giving face-to-face π-stacked arrangements for acenes. Predicting a more precise 1-D or 2-D π-stacking motif is much more difficult because of the short-axis slip[65a]. As a result, trial and error is still necessary to obtain the desired packing motif. As mentioned in chapter 1, the crystal packing of silylethyne-functionalized acenes was shown to dramatically affect the electronic properties and lead to different potential applications. The 2-D π-stacking motif was found to give materials with higher mobilities, useful for transistors. TIPS- and TIBS-2,3-dicyanopentacene are two compounds which exhibit 2-D π-stacking, but have yet to be tested in transistors[70a, 73a]. Crystal structures of these two compounds are shown in Figure 4-1 and reveal an additional feature in the crystal packing. Molecules within a layer pack with the acene moieties arranged head-to-tail with respect to the nitrile substituents, likely a result of polarity induced by these highly electron-withdrawing substituents. Acene moieties in neighboring layers arrange themselves in the relative opposite direction to minimize this electrostatic repulsion. Based on these two structures, it was reasoned that similarly shaped molecules with polarizing substituents might also result in this same type of 2-D π-stacking with head-to-tail arrangements.

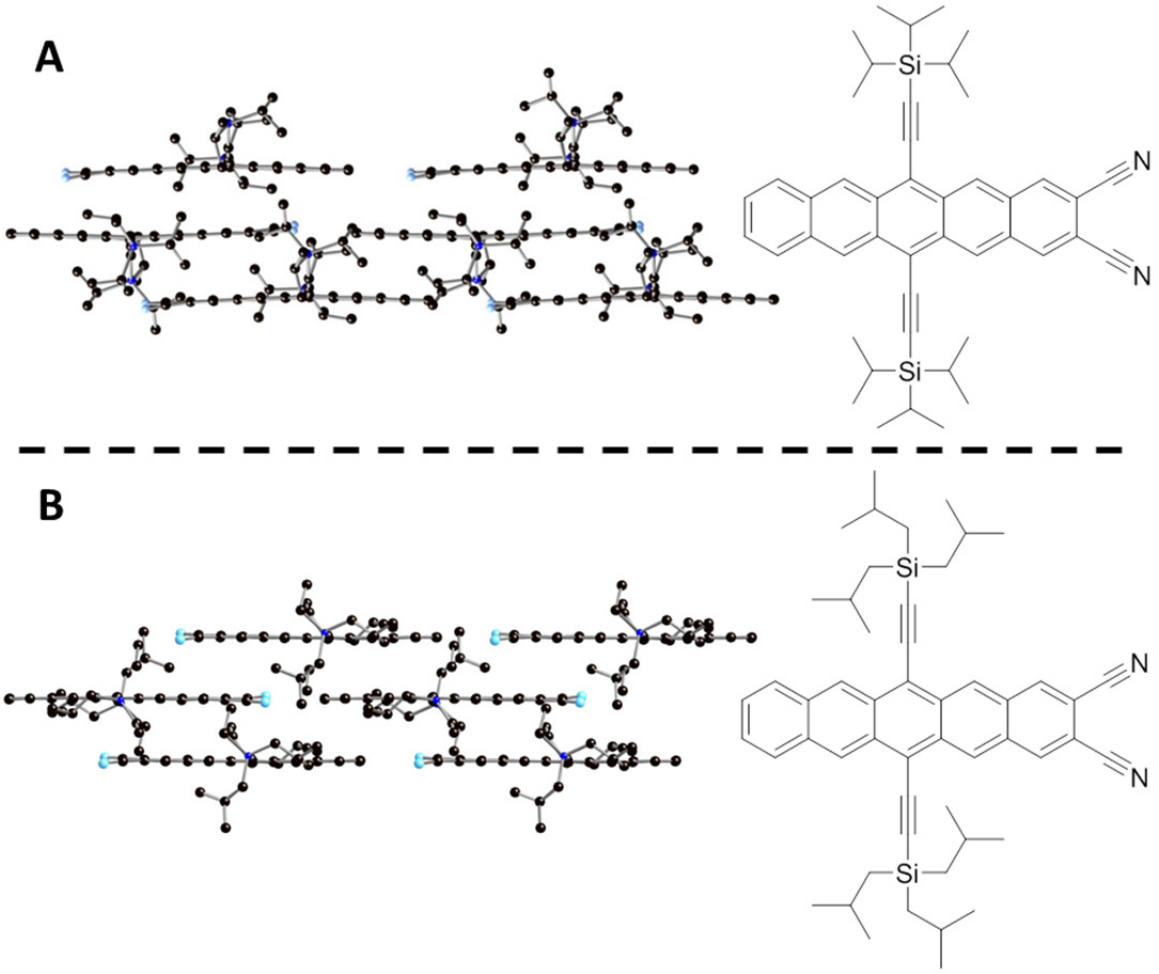

Figure 4-1. 2-D crystal packing of TIPS-2,3-dicyanopentacene (A) and TIBS-2,3-dicyanopentacene (B). The crystal structure of (B) could not be fully refined.

The nitrile substituents present in these two derivatives are very similar in size and shape to terminal alkynes, differing essentially by only a small hydrogen atom with respect to sterics. While not as electron-withdrawing as a nitrile substituent, it was thought alkynes may still induce enough polarity to observe a similar effect. Importantly, previous unpublished work from this group demonstrated that pentacene with four terminal alkynes had sufficient stability for characterization by X-ray crystallography. Therefore, this substitution was a reasonable target, and a series of four pentacenes were synthesized with alkynes replacing nitriles. Synthesis of this series of pentacenes was very straightforward and began by adding various lithiated trialkylsilylacetylenes to 2,3-diiodopentacenequinone, followed by deoxygenation with

$SnCl_2$ and HCl to give diiodopentacenes[73a]. These underwent Sonogashira coupling with trimethylsilylacetylene and selective alkyne deprotection with methoxide to give the final 2,3-diethynylpentacenes shown in Scheme 4-1. Deprotection was only problematic for pentacene (**4-4**) because of similar steric silicon protection between trimethylsilyl and triisobutylsilyl groups. This lower deprotection selectivity resulted in a reduced yield.

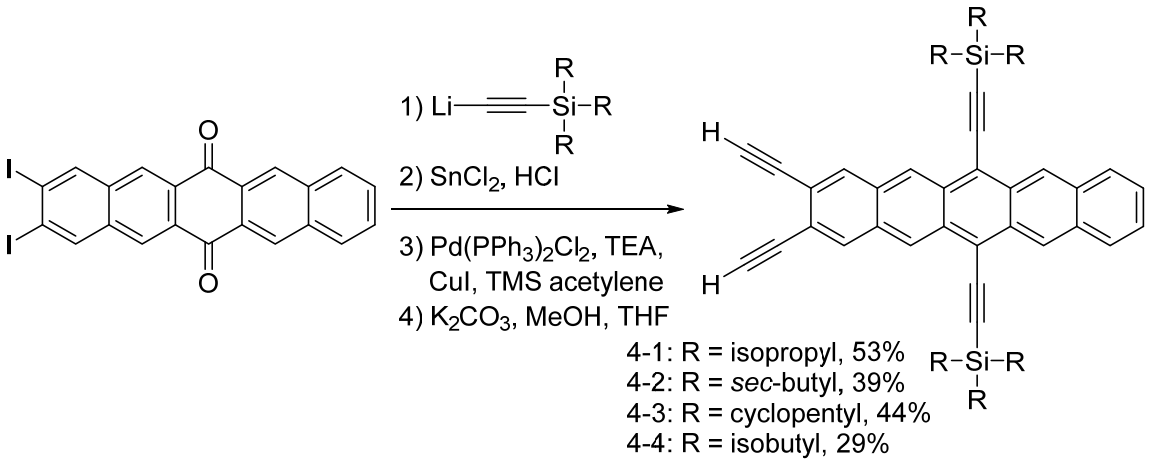

Scheme 4-1. Synthesis of diethynylpentacenes with four different trialkylsilylethynyl substituents.

Crystals of all four derivatives were easily grown from solution, and three of them produced refined models from X-ray crystallography. The TSBS derivative (**4-2**) did not refine, allowing for only the general packing arrangement to be determined. Unfortunately, none of these materials gave the desired 2-D π-stacking motif. TIPS derivative (**4-1**) crystallized as fine, dark blue needles as shown in Figure 4-2. X-ray analysis revealed a 1-D π-stacking motif with intermolecular stacking distances as close as 3.35 Å. This packing arrangement was surprising considering this derivative is a close analog of TIPS-2,3-dicyanopentacene.

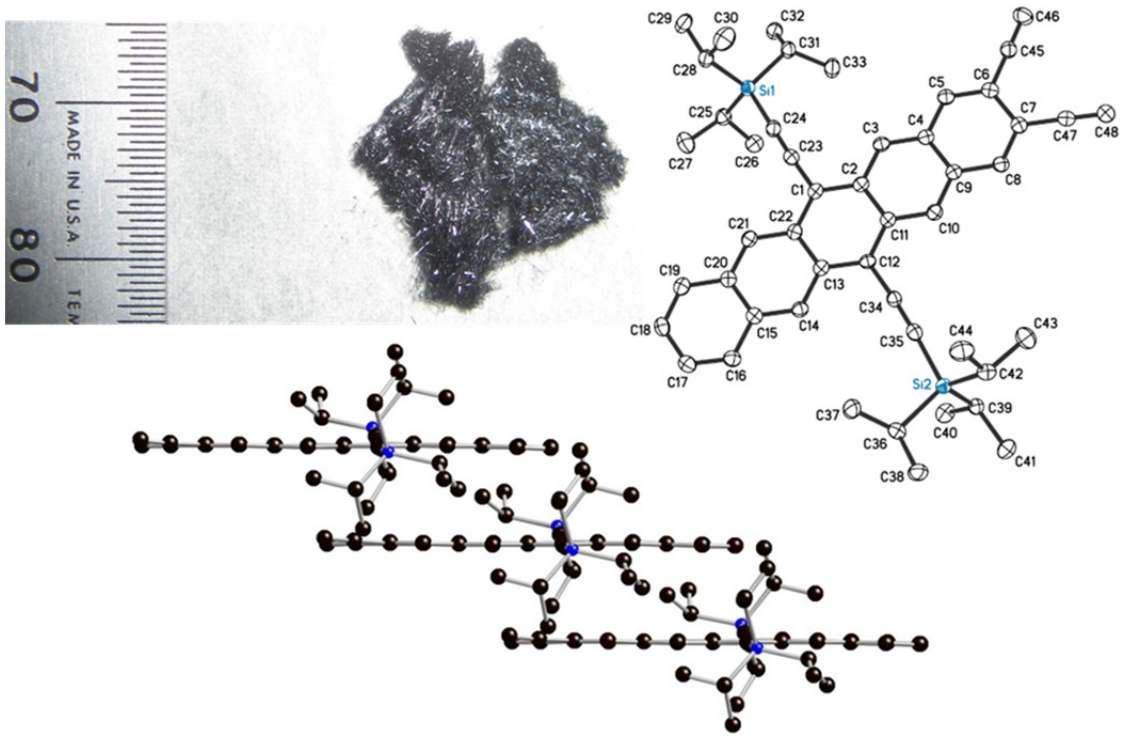

Figure 4-2. Crystal image (mm scale), thermal ellipsoid plot, and packing diagram of TIPS-2,3-diethynylpentacene (**4-1**).

TSBS derivative (**4-2**) crystallized in bulk as tiny blue flakes/needles, and larger crystals for X-ray analysis were grown by solvent diffusion. The crystals diffracted well enough to give the overall crystal packing, but refinement was impeded by twinning in addition to the unresolved chiral centers of the *sec*-butyl groups. The crystal packing diagrams in Figure 4-3 show this derivative has two 1-D stacks which merge at an angle. This arrangement is driven by two intermolecular alkyne C-H···π interactions between neighboring coplanar molecules[102]. Overall, this packing is best considered as 1-D π-stacking since long-range electronic coupling exists in only one direction. Since this model did not refine, it is inappropriate to list close intermolecular π-stacking distances.

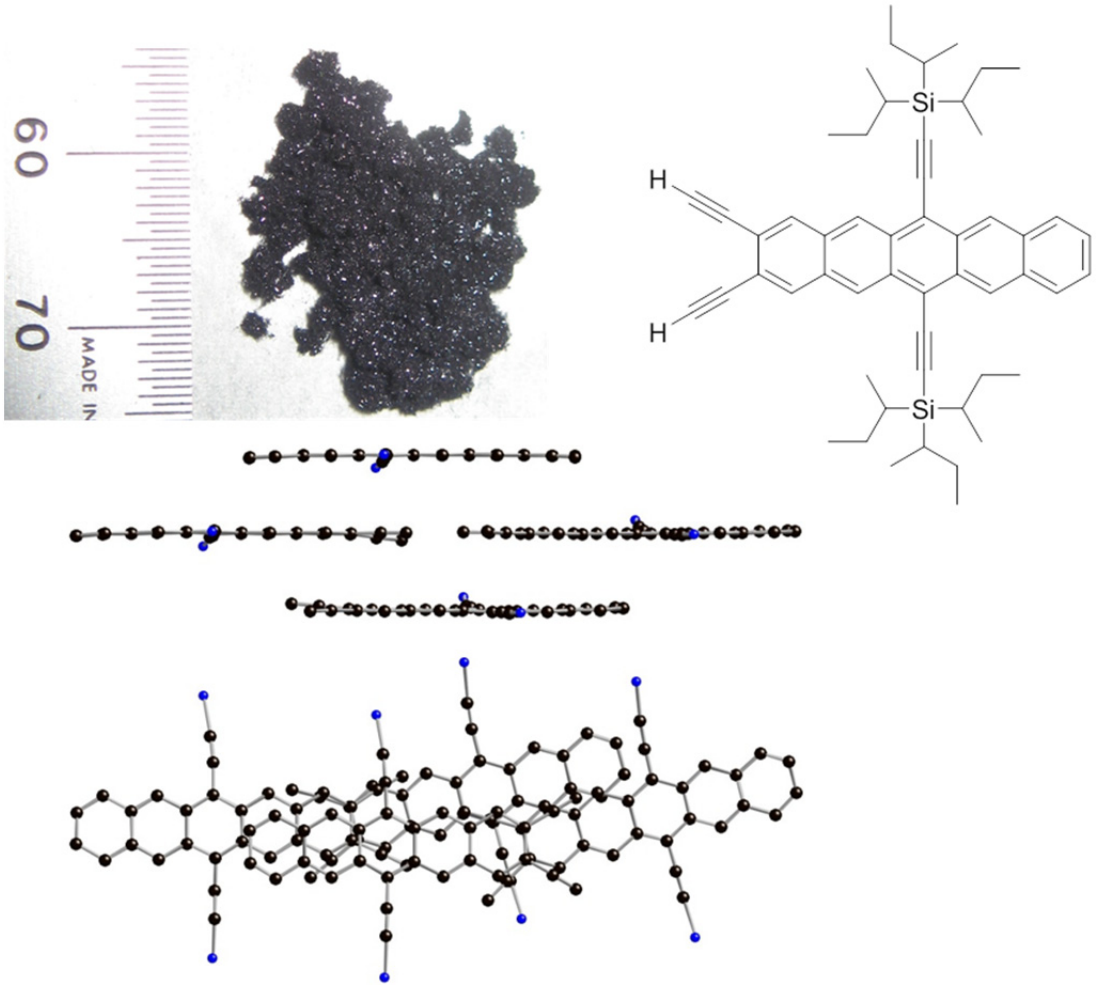

Figure 4-3. Crystal image (mm scale), molecular structure, and packing diagram of TSBS-2,3-diethynylpentacene (**4-2**). Alkyl groups were removed for clarity.

TCPS derivative (**4-3**) crystallized as small, dark blue laths which were large enough for single-crystal X-ray analysis. The thermal ellipsoid plot in Figure 4-4 shows disorder among the trialkylsilyl groups and emphasizes this derivative forms stacked pairs. Similar to TSBS derivative (**4-2**), alkyne C-H···π interactions account for the planarity of neighboring molecules. The packing diagram highlights two intermolecular distances. The closest intermolecular π-stacking distance *within* a molecular pair is 3.45 Å, denoted by the red arrow. *Between* neighboring pairs, this closest distance is a weak alkyne-aryl overlap at 3.55 Å. Because of this rather long distance, overall electronic coupling was expected to be poor, making for a bad transistor material.

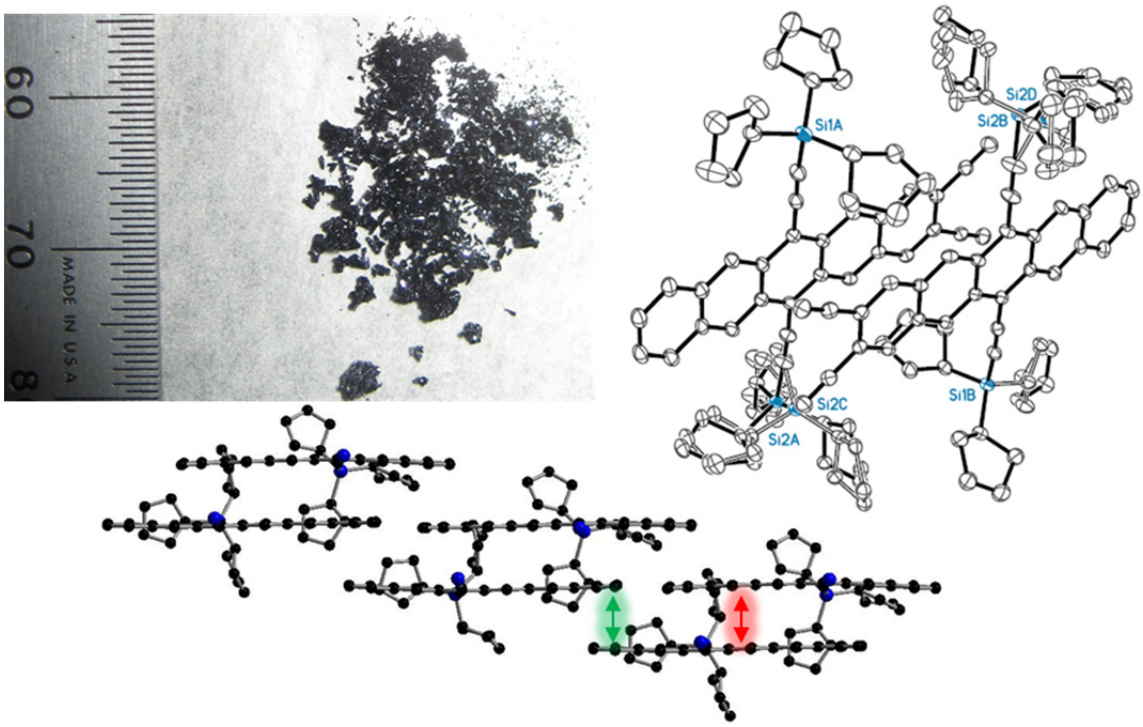

Figure 4-4. Crystal image (mm scale), thermal ellipsoid plot, and packing diagram of TCPS-2,3-diethynylpentacene (**4-3**). The red arrow denotes distance *within* a molecular pair, and the green arrow denotes distance *between* molecular pairs. Front-most alkyl groups were removed for clarity.

Finally, TIBS derivative (**4-4**) crystallized as dark blue blocks, some of which were on the order of about 3 mm. X-ray analysis gave a large amount of diffuse scatter in the data set which complicated refinement, and the ordering of the crystal was surprisingly complex. This is reflected in the thermal ellipsoid plot shown in Figure 4-5. The crystal packing diagram represents only local domain ordering between stacking faults rather than long-range, whole crystal ordering. In one domain, alkynes are oriented in the same direction, whereas the neighboring domain has alkynes pointed in the opposite direction. This inter-domain disorder results in the apparent end-over-end flipping as depicted in the thermal ellipsoid plot. The crystal packing diagram shows this material has 1-D π-stacking with intermolecular distances as close as 3.48 Å. Again, this is surprising since this derivative is a close analog of TIBS-2,3-dicyanopentacene which has 2-D π-stacking.

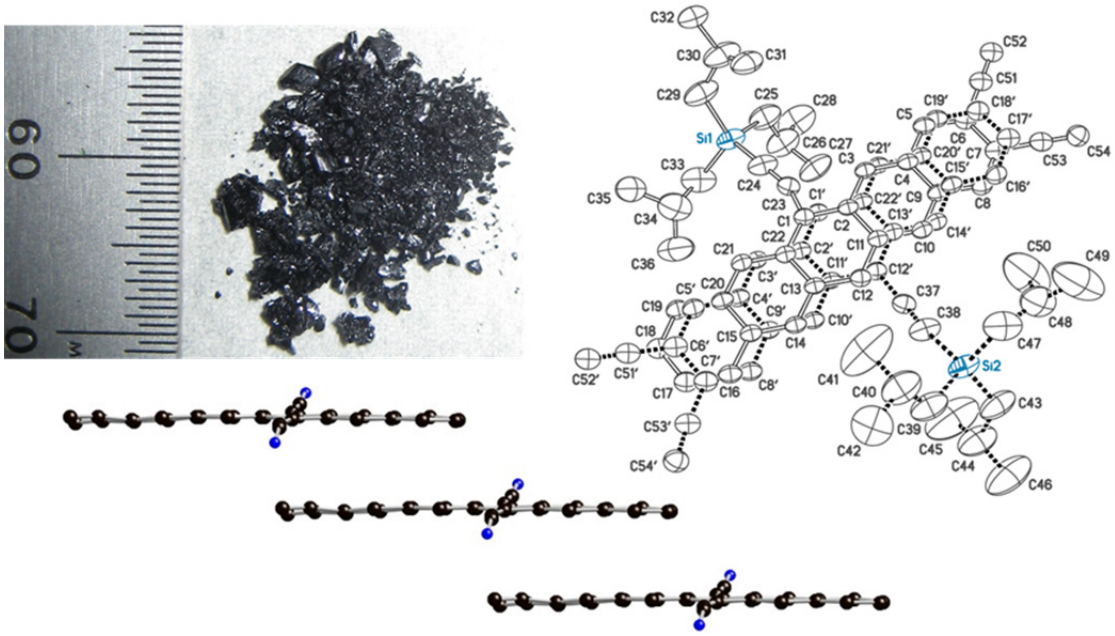

Figure 4-5. Crystal image (mm scale), thermal ellipsoid plot, and packing diagram of TIBS-2,3-diethynylpentacene (**4-4**).

Based on these newly synthesized molecules, it is clear that diethynylpentacenes have very different crystal structures than the two model dicyanopentacenes despite being similar in size. Again, we see that making slight modifications to a molecular structure results in substantial changes to the crystal packing motif. In these molecules, the alkyne C-H···π interactions (weak hydrogen bonds) are clearly observed in TSBS (**4-2**) and TCPS (**4-3**) derivatives, and are at least a factor in the crystal structure of TIPS (**4-1**). This work demonstrated that terminal alkynes simply do not induce the required polarity for head-to-tail arrangements observed in the model dicyanopentacenes. The aromatic dinitrile···electropositive benzene hydrogen interaction demonstrated in Figure 4-1 is another recognized weak hydrogen bond, a type of supramolecular synthon. The replacement of this interaction with alkyne C-H···π interactions allowed the diethynyl systems to form very different π-stacked arrangements.

Electrochemistry of TSBS-2,3-diethynylpentacene (**4-2**) shown in Figure 4-6 revealed one reversible oxidation and two reversible reductions in the electrochemical window. HOMO and LUMO values of -5.27 eV and -3.44 eV, respectively, were calculated from this data relative to the Fc/Fc^{+} internal standard[103].

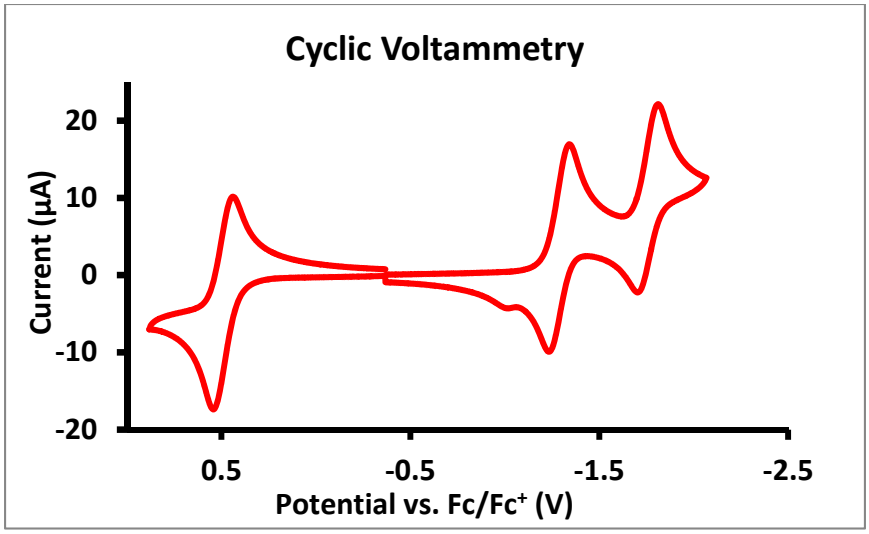

Figure 4-6. Cyclic voltammetry of TSBS-2,3-diethynylpentacene (**4-2**), collected in two successive runs.

Recrystallized samples of all four diethynylpentacenes were sent to Oana Jurchescu's group at Wake Forest University for transistor fabrication, and devices are still being optimized. The basic device architecture of a bottom-contact field-effect transistor is shown in Figure 4-7. When a voltage is applied between the source (S) and gate electrodes, an electric field induces charge carriers in a semiconductor which is situated in a channel between the source (S) and drain (D) electrodes. Once a certain threshold voltage is reached, charge will flow between the source and drain electrodes, and a resulting current can be measured. The amount of current depends on the magnitude of the electric field, and hence, the applied voltage[104].

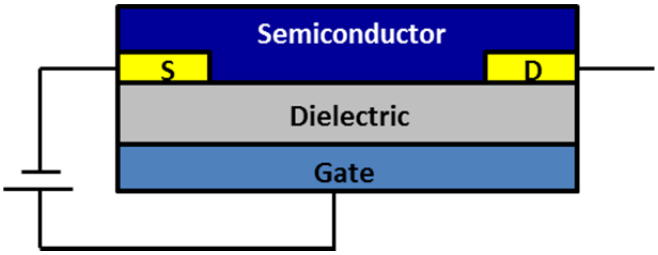

Figure 4-7. General schematic of a bottom-contact field-effect transistor.

Results thus far were obtained from devices with pentacenes drop-cast over an HMDS-treated Si/SiO_2 substrate with gold source and drain electrodes. Micrographs of these devices and accompanying hole mobility (μ) values are shown in Figure 4-8. Overall, initial devices were not impressive, with mobilities ranging from 10^{-6} to 10^{-3} cm^2/Vs; however, poor performance was generally expected from these materials since none of them exhibited the 2-D π-stacking motif. Similar crystal habits are observed in the films as existed in bulk samples. TIPS derivative (**4-1**) formed thin needles on the surface, just as it formed thin needles in the bulk state. TSBS derivative (**4-2**) yielded the smallest crystals in the bulk, and clearly forms the smallest needles as a film. Additionally, the crystalline film of this derivative extends well beyond the edges of the gold electrodes, whereas the other three derivatives seem somewhat more confined to covering only the electrode area. TCPS derivative (**4-3**) formed thicker laths in the bulk form, and thicker structures are observed in the film. TIBS derivative (**4-4**) formed by far the thickest crystals in the bulk samples, and this is also evident in the case of the film. More optimization is currently underway, and preliminary reports indicate improved performance by switching to a BCB dielectric layer.

A crystal structure-transistor performance relationship is somewhat difficult with the available data, but some sense can be made of it. Crystal data for TSBS derivative (**4-2**) was rather poor and only allows the gross packing motif to be determined. Of the remaining three derivatives, TIPS pentacene (**4-1**) performed the best. The closest intermolecular contact distance of 3.35 Å in this derivative is a full 0.1 Å closer than the other two derivatives, and it likely accounts for the better performance observed. TCPS derivative (**4-3**) performed better than TIBS derivative (**4-4**) in spite of the larger

intermolecular π-stacking distances. This may be an effect of small domain sizes and numerous stacking faults mentioned earlier in TIBS derivative (**4-4**). These faults could interrupt charge transport across the channel and lead to very poor hole mobilities.

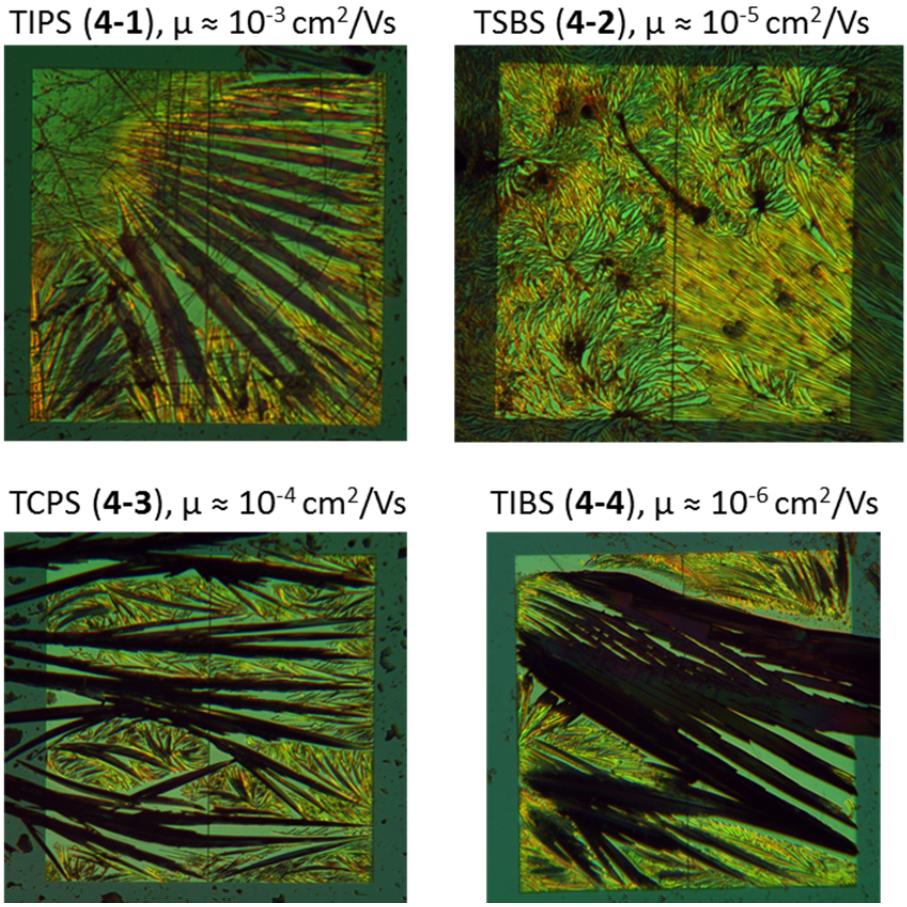

Figure 4-8. Transistors fabricated with the four diethynylpentacenes, courtesy of Yaochuan Mei and Prof. Oana Jurchescu of Wake Forest University.

4.2 Octafluoropentacenes

Octafluoropentacenes are a class of electron-deficient acenes developed several years ago[70a]. TIPS octafluoropentacene was the only derivative reported, and it exhibited the 2-D π-stacking motif. A simple transistor study was included in which this material gave an unoptimized hole mobility of 0.045 cm^2/Vs. The Bao group subsequently studied this same material as an *n*-type semiconductor and achieved an electron mobility of 0.409 cm^2/Vs[105].

In the interest of developing other derivatives, TSBS octafluoropentacene (**4-5**) was synthesized as shown in Scheme 4-2. Lithiated TSBS acetylene was added to octafluoropentacenequinone, followed by deoxygenation with $SnCl_2$/HCl. Similar to diiodopentacenes, heating was required for deoxygenation to proceed.

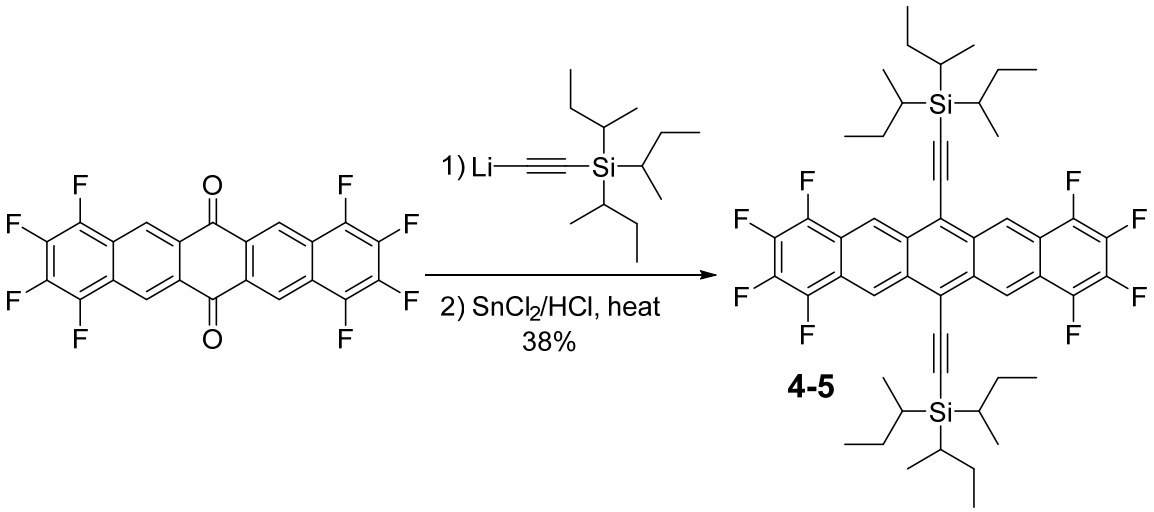

Scheme 4-2. Synthesis of TSBS octafluoropentacene (**4-5**) from octafluoropentacenequinone.

Crystals of this material were found suitable for X-ray analysis and gave a refined model. A comparison of the two octafluoropentacene crystal structures is shown in Figures 4-9 and 4-10. Both of these compounds crystallize with a 2-D π-stacking motif, but there are notable differences. Closest stacking distances between the central acene and four surrounding acene moieties of TIPS octafluoropentacene in increasing order are 3.22, 3.27, 3.33, and 3.38 Å. Corresponding values for TSBS octafluoropentacene (**4-5**) are 3.32, 3.36, 3.41, and 3.42 Å, slightly greater than the TIPS derivative. As highlighted in red, the TIPS derivative has a greater degree of π-stacking. A particularly small overlap is highlighted in the TSBS derivative. In comparing the two derivatives, it is evident that the larger steric interaction between TSBS substituents forces the molecules to slip along the acene long axis (Figure 4-9) as well as the acene short axis (Figure 4-10). The combination of these two directional slips results in the particularly small intermolecular overlap observed, *nearly* forcing a 1-D π-stacking motif.

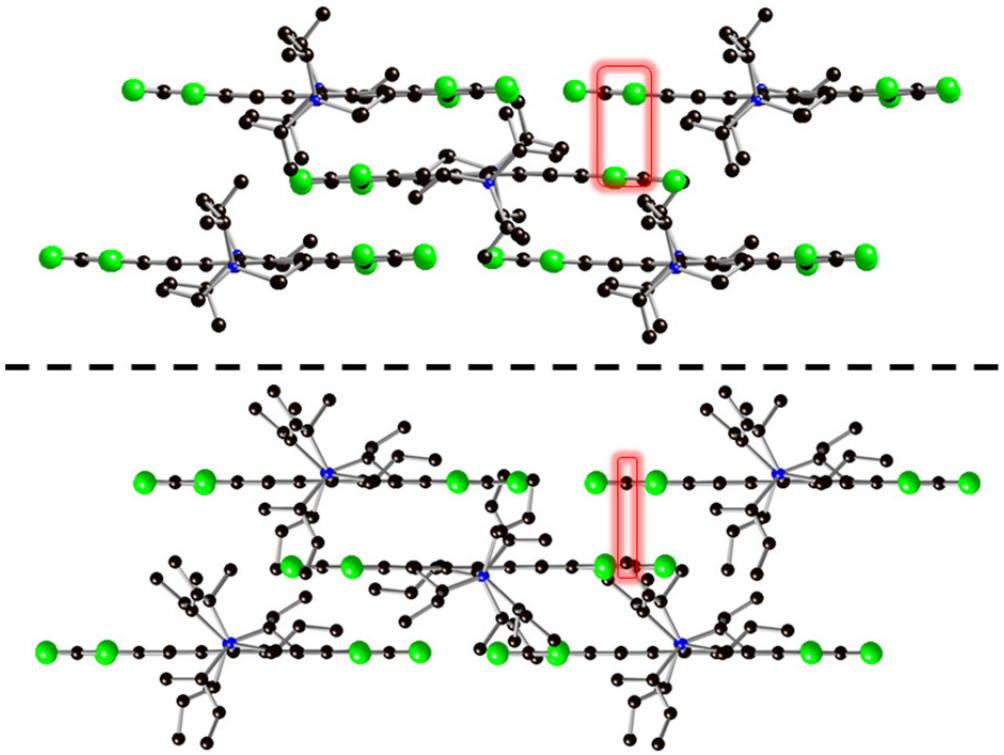

Figure 4-9. Side views of TIPS octafluoropentacene, top, and TSBS octafluoropentacene (**4-5**), bottom. The most notable differences are highlighted in red.

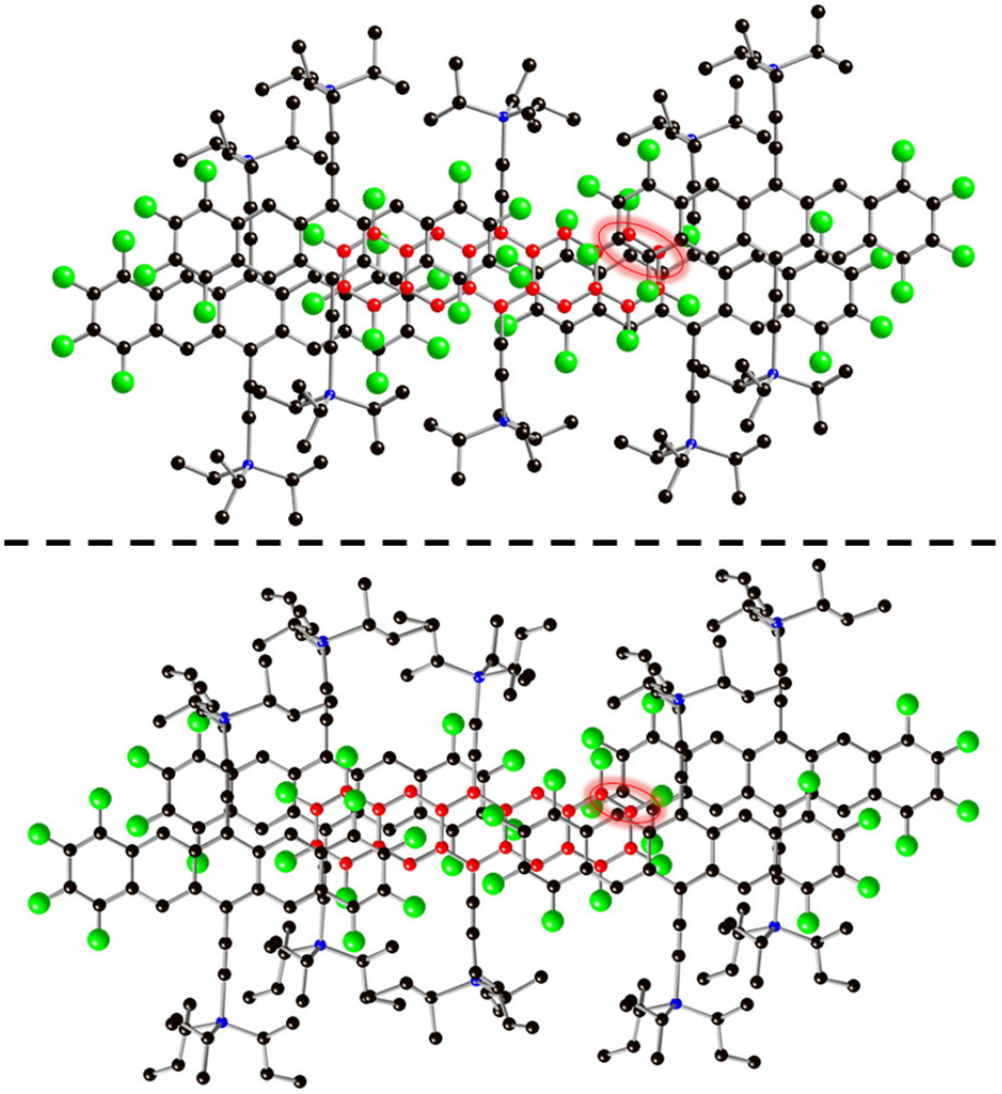

Figure 4-10. Top views of TIPS octafluoropentacene, top, and TSBS octafluoropentacene (**4-5**), bottom. The central pentacene backbone is colored in red for clarity. The π-stacking is particularly small in the bottom structure compared to the top structure.

4.3 Pentacenequinone Acceptors

The 1-D π-stacking motif was mentioned in chapter 1 to be more useful for applications such as solar cells. Since the work presented in chapters 2 and 3 dealt with dioxolane-functionalized acenes, one focus of my research was extending this functionality to solar cell acceptor materials. This project initially focused on soluble dioxolane-functionalized pentacenequinones since only a few quinones have been reported in solar cells[106].

Since pentacenequinones are generally insoluble, solubilizing groups were necessary to allow for solution-processed organic solar cells. Unlike the acenes in chapters 2 and 3, orthogonal dioxolane substituents could not be used in this case because close chromophore packing is needed. A soluble pentacenequinone was devised and synthesized as outlined in Scheme 4-3. Bis(bromomethyl)benzodioxole (**4-6**) was synthesized according to the literature[107] and reduced with sodium borohydride and a phase-transfer catalyst[108] to give dimethylbenzodioxole (**4-7**). Aromatic and benzylic brominations then led to benzodioxole derivative (**4-9**). Direct aromatic bromination of (**4-6**) to form (**4-9**) was attempted, but this resulted in a quite low yield and messy workup which necessitated the alternative route given here. From this, a Cava reaction produced quinone (**4-10**) in surprisingly good yield. The remaining bromine functionalization handles were then used in a Stille coupling to add solubilizing trialkylsilylethynyl substituents and give quinone (**4-11**).

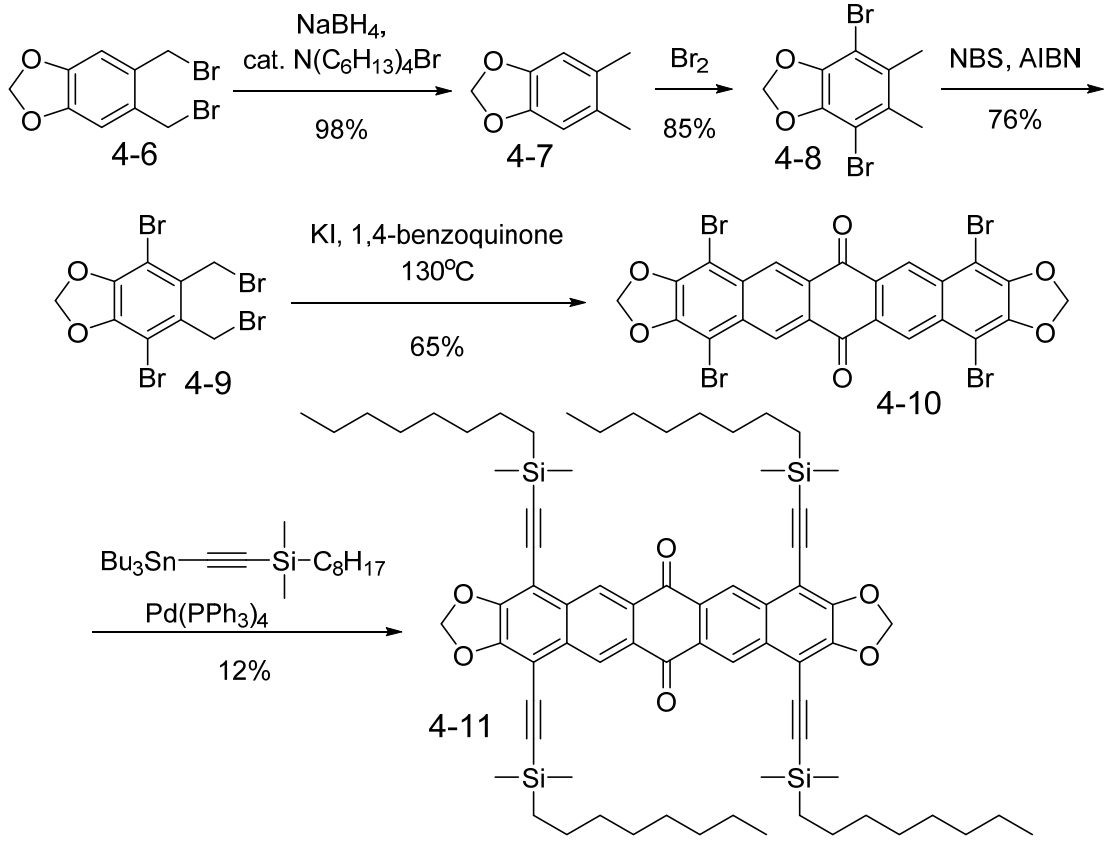

Scheme 4-3. Synthesis of soluble dioxolane-functionalized pentacenequinone.

Crystals of yellow quinone (**4-11**) initially formed as fine, fibrous needles which were much too small for single-crystal X-ray crystallography. Solvent diffusion growth led to higher quality crystals which were large enough for analysis, giving the structure shown in Figure 4-11. It shows some disorder of the long octyl chains and exhibits 1-D π-stacking with a 3.30 Å layer spacing. Since this material had adequate solubility, it was also characterized by electrochemistry. As shown in Figure 4-12, differential pulse voltammetry revealed a reduction potential of -1.56 V relative to the ferrocene/ferrocenium couple, corresponding to a LUMO energy level of -3.24 eV. This value was disappointing, but it was later found to be in approximate agreement with LUMO energies of pentacenequinone (-3.29 eV), tetrafluoropentacenequinone (-3.41 eV), and octafluoropentacenequinone (-3.51 eV)[109].

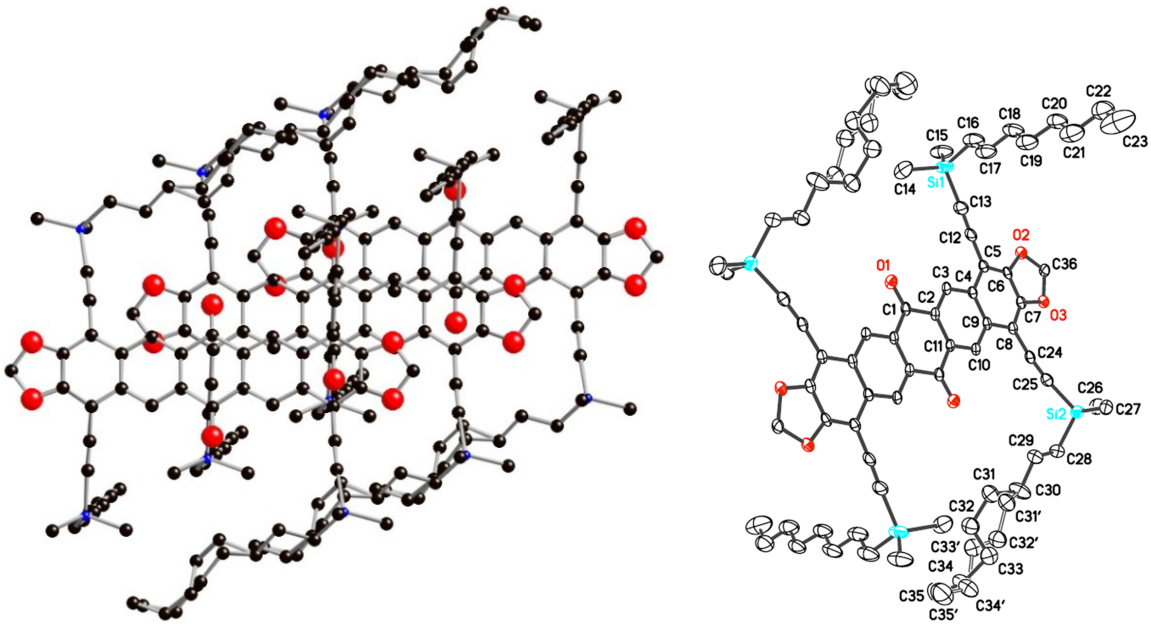

Figure 4-11. Crystal packing and thermal ellipsoid plot of pentacenequinone (**4-11**).

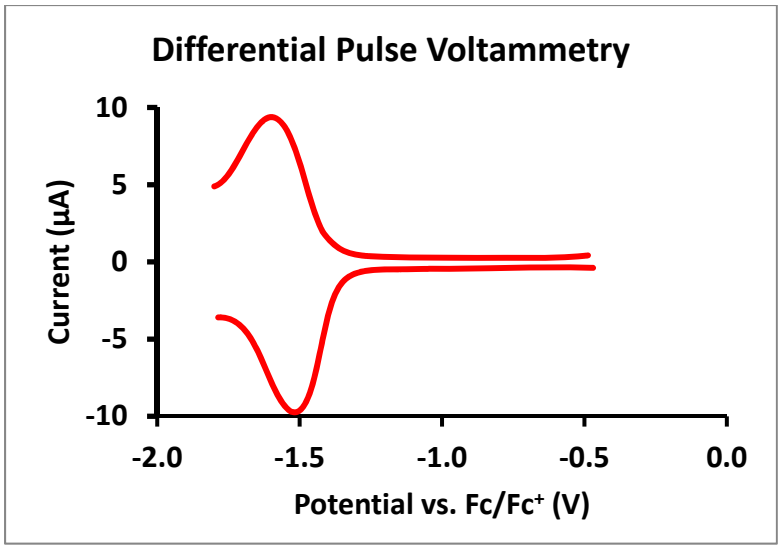

Figure 4-12. Differential pulse voltammetry of pentacenequinone (**4-11**).

In an effort to further reduce the LUMO energy level, an attempt was made at converting tetrabromoquinone (**4-10**) into a pentacene and replacing the bromines with electron-withdrawing nitriles. Since dioxolane pentacenes have reduced solubility and nitriles tend to reduce solubility further, it was thought an extremely solubilizing trialkylsilylethynyl substituent would be necessary. TSBS tends to be one of the best choices for increasing solubility, and a similar alkyne was synthesized for this purpose, as shown in Scheme 4-4. 2-Chloropentane was lithiated and treated with trichlorosilane to give tri-2-pentylsilane (**4-12**). This was then brominated and reacted with lithiated TMS acetylene which yielded (**4-13**). Selective deprotection of the smaller TMS group with base then gave the final acetylene (**4-14**).

As shown in Scheme 4-5, this was then added to quinone (**4-10**) to give pentacene (**4-15**). Solubility of this compound was surprisingly low in a wide range of solvents. For example, boiling 1,4-dioxane was found to solubilize the material the best, and 600 mg of crude crystals recrystallized from ~250 mL of this solvent gave 550 mg of small, flaky crystals upon cooling to room temperature. Attempts at converting this material to the desired tetracyano analog were unsuccessful, possibly the result of poor solubility of pentacene (**4-15**). It is likely the tetracyanopentacene would have even worse solubility, limiting its utility in device fabrication to thermal vapor deposition

under vacuum. Although the fluorescence quantum yield of tetrabromopentacene (**4-15**) was not measured, images in Figure 4-12 show it is quite fluorescent. This is unusual considering the heavy atom effect of four bromine atoms is expected to lead to fluorescence quenching.

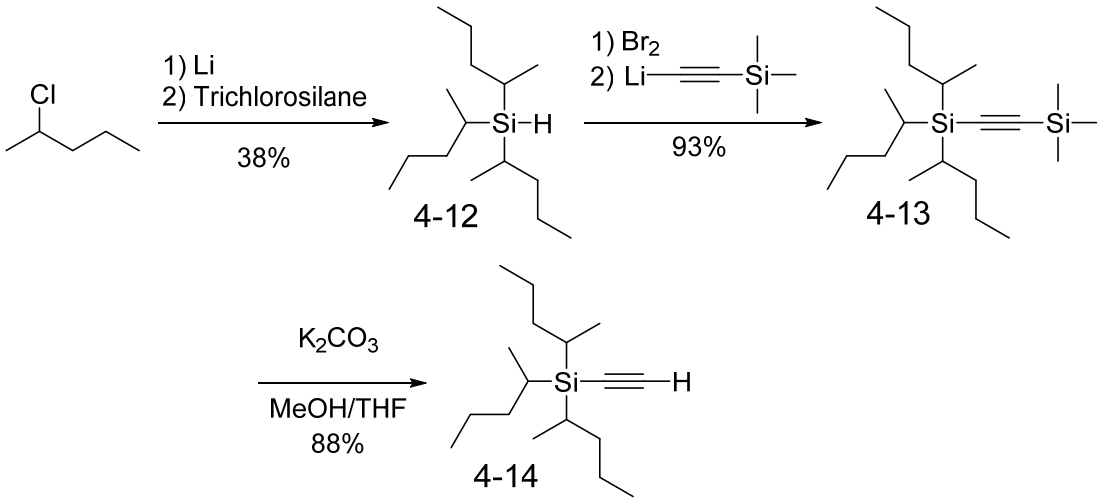

Scheme 4-4. Synthesis of tri-2-pentylsilylacetylene (**4-14**).

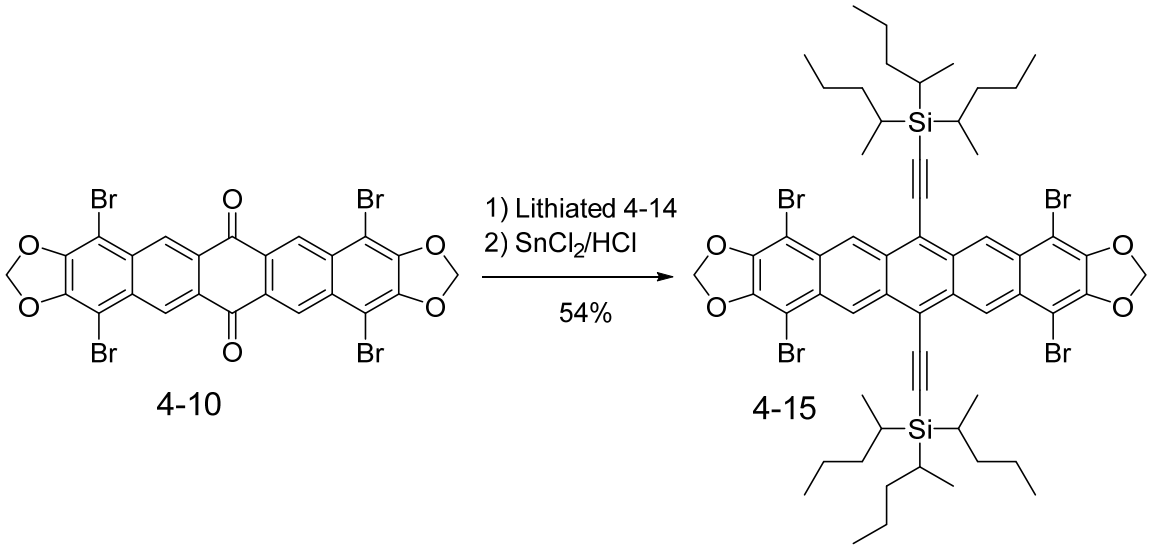

Scheme 4-5. Synthesis of tetrabromopentacene (**4-15**).

Crystals of tetrabromopentacene (**4-15**) were quite small, but proved to be of high quality and gave the refined crystal structure shown in Figure 4-13. It has 1-D π-stacking as close as 3.42 Å and was shown to be the expected mixture of isomers due to the six unresolved chiral centers. Another curious feature is a very small short-axis slip,

the cause of which is unclear. Enhanced halogen···halogen interactions are known to exist in crystal structures, but the distance measured in this case is 3.85 Å, outside the bromine van der Waals radaii sum of 3.72 Å[110]. Any bromine···bromine interaction here is slight to nonexistent. This feature might be the result of close packing, a space-filling effect, and simply induced by the size of the bromine atoms. A sample of this material was tested in transistors, but performed *very* poorly.

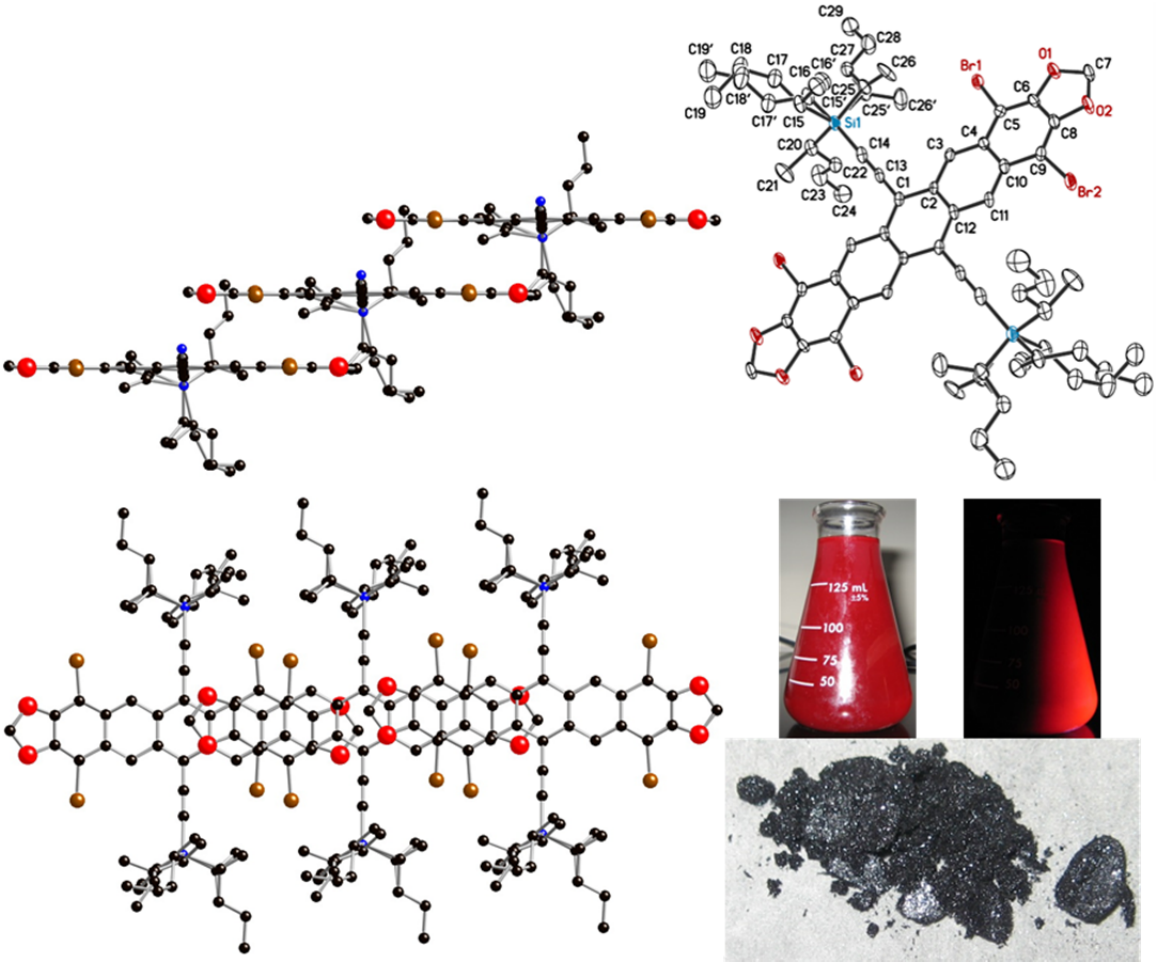

Figure 4-13. Crystal structure, thermal ellipsoid plot, solution, and crystals of tetrabromopentacene (**4-15**). This pentacene exhibits 1-D π-stacking with an unusually small short-axis slip. Front-most alkyl groups were removed for clarity in the side view (top). A saturated solution of the bottom right crystals in 1,4-dioxane shows bright red fluorescence under ambient lighting as well as under a UV lamp, characteristic of the dioxolane pentacene chromophore.

4.4 Crystal Packing & HOMO Energy Levels

The final study in this chapter focused on the influence of crystal packing and π-stacking on HOMO energy levels. Electrochemistry is a method for measuring the oxidation and reduction potentials of various analytes dissolved in solution, and these electrochemical potentials can be converted to HOMO and LUMO energy levels using an internal standard such as the ferrocene/ferrocenium redox couple with a HOMO of -4.8 eV[103, 111]. The HOMO energy level is measured by oxidizing a molecule, i.e., removing an electron from its HOMO and creating a solvated radical cation. It is a widely used, inexpensive technique which quickly estimates energy levels. Strictly speaking, these measured values apply to isolated molecules in solution rather than the aggregate structures which exist in crystals, making them somewhat less applicable to solid-state devices. Ultraviolet photoelectron spectroscopy (UPS) is a useful method for determining the HOMO energy level in films. UPS is a technique in which ultraviolet radiation ionizes a film of molecules, ejecting electrons from which the threshold ionization potential of surface molecules can be measured. Measurements are often done under vacuum, but can also be done in air, and it has been found that results obtained by UPS are sensitive to sample surface conditions[112]. In the case of a crystalline organic semiconductor, the HOMO energy level is expected to change substantially if π-stacking is present. The largest differences between UPS and electrochemical HOMO energy level measurements would therefore be expected in semiconductor films with the highest degree of crystallinity and π-stacking.

To demonstrate this, a series of silylethynyl-functionalized pentacenes was chosen which exhibited different crystal packing. The molecular structures are shown in Figure 4-14 along with electrochemistry. These pentacenes all have essentially identical electronic properties as isolated molecules in solution. This is evident by differential pulse voltammetry giving calculated HOMO values ranging from -5.12 to -5.20 eV. This is expected because no intermolecular coupling occurs in dilute solutions where these values are measured.

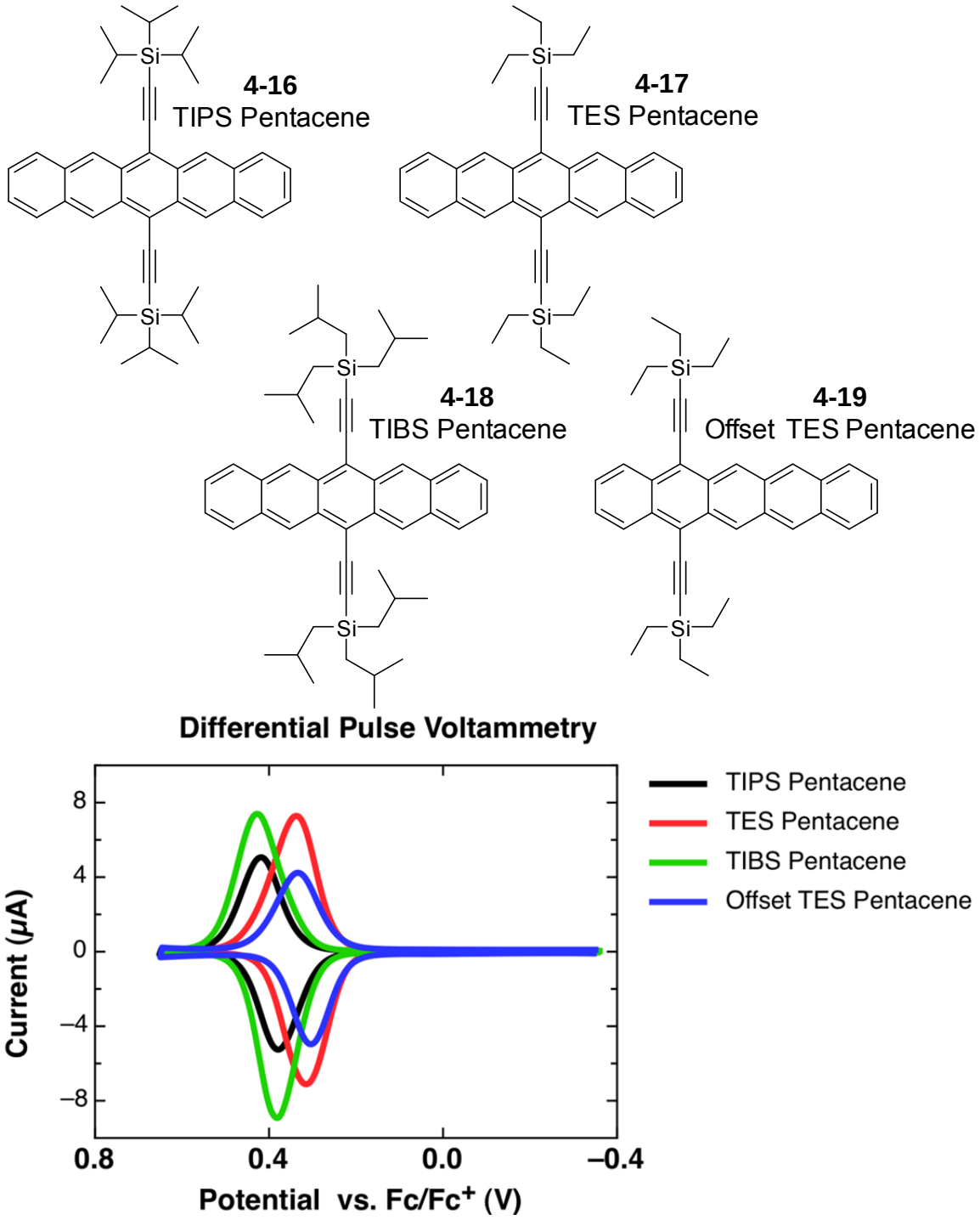

Figure 4-14. Molecular structures and differential pulse voltammetry of pentacene derivatives with different crystal packing. As expected, all of these derivatives have nearly the same oxidation potential.

Crystalline films of these four pentacenes were made by drop-casting onto glass substrates in order to measure their HOMO values by UPS. Since solar cells are often constructed under ambient conditions and exposure to high vacuum can change surface conditions, UPS measurements for this study were taken in air[113]. TIPS pentacene (**4-16**) formed fairly uniform, crystalline films with ease, but thicker films were needed in order to achieve significant crystalline coverage of the substrate for pentacenes (**4-17**), (**4-18**), and (**4-19**). UV-Vis spectra of these films are shown in Figure 4-15. In contrast to electrochemical HOMO values obtained in solution, those measured in the solid state by UPS varied considerably as shown in Table 4-1.

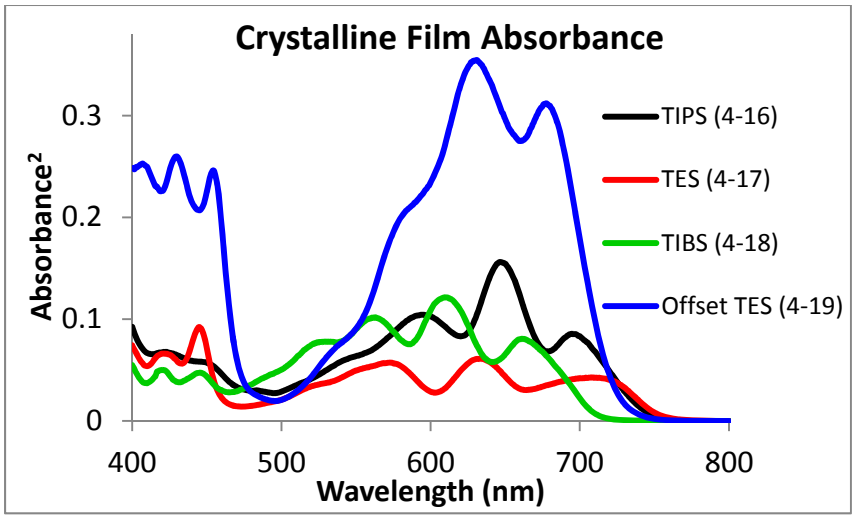

Figure 4-15. Absorbances of several pentacene derivatives as crystalline films.

Pentacene	$HOMO_{e\text{-}chem}$ (eV)	$HOMO_{UPS}$ (eV)	Crystal Abs. Onset (nm)
TIPS (**4-16**)	-5.20	-5.90	743
TES (**4-17**)	-5.13	-5.85	753
TIBS (**4-18**)	-5.20	-5.65	712
Offset TES (**4-19**)	-5.12	-5.70	722

Table 4-1. Trialkylsilylethynyl pentacene derivative data. Solution and crystalline HOMO values for pentacenes studied in addition to estimated crystalline absorption onsets from Figure 4-19.

Electrochemical HOMO energies varied by only 0.08 eV whereas those measured by UPS varied by 0.25 eV. Given the experimental error of about 0.05 eV for UPS, this difference is significant. The larger differences seen in the UPS HOMO energy values can

be explained through analysis of the crystal structures of each compound which are shown in Figure 4-16. TIPS pentacene (**4-16**) crystallizes in a 2-D π-stack and TES pentacene forms a 1-D π-stack. These two derivatives had the lowest (most negative) UPS HOMO energy values of -5.90 and -5.85 eV. This stabilizing π-stacking interaction is supported by the crystalline absorption onsets with shoulders at the longest wavelengths. In contrast, TIBS pentacene (**4-18**) shows no π-stacking in the crystal structure and has the highest (least negative) HOMO energy of -5.65 eV. Finally, offset TES pentacene (**4-19**) exhibits 1-D columnar π-stacking, and this gave a HOMO energy of -5.70 eV by UPS. While only slightly lower than TIBS pentacene (**4-18**) which has no π-stacking, the π-stacking nature is mirrored by the observed stabilization. The degree of orbital overlap between molecules of this derivative also appears smaller than that seen in both TIPS pentacene (**4-16**) and TES pentacene (**4-17**). This data demonstrates crystal packing can have a substantial effect on HOMO energy levels in organic electronic devices.

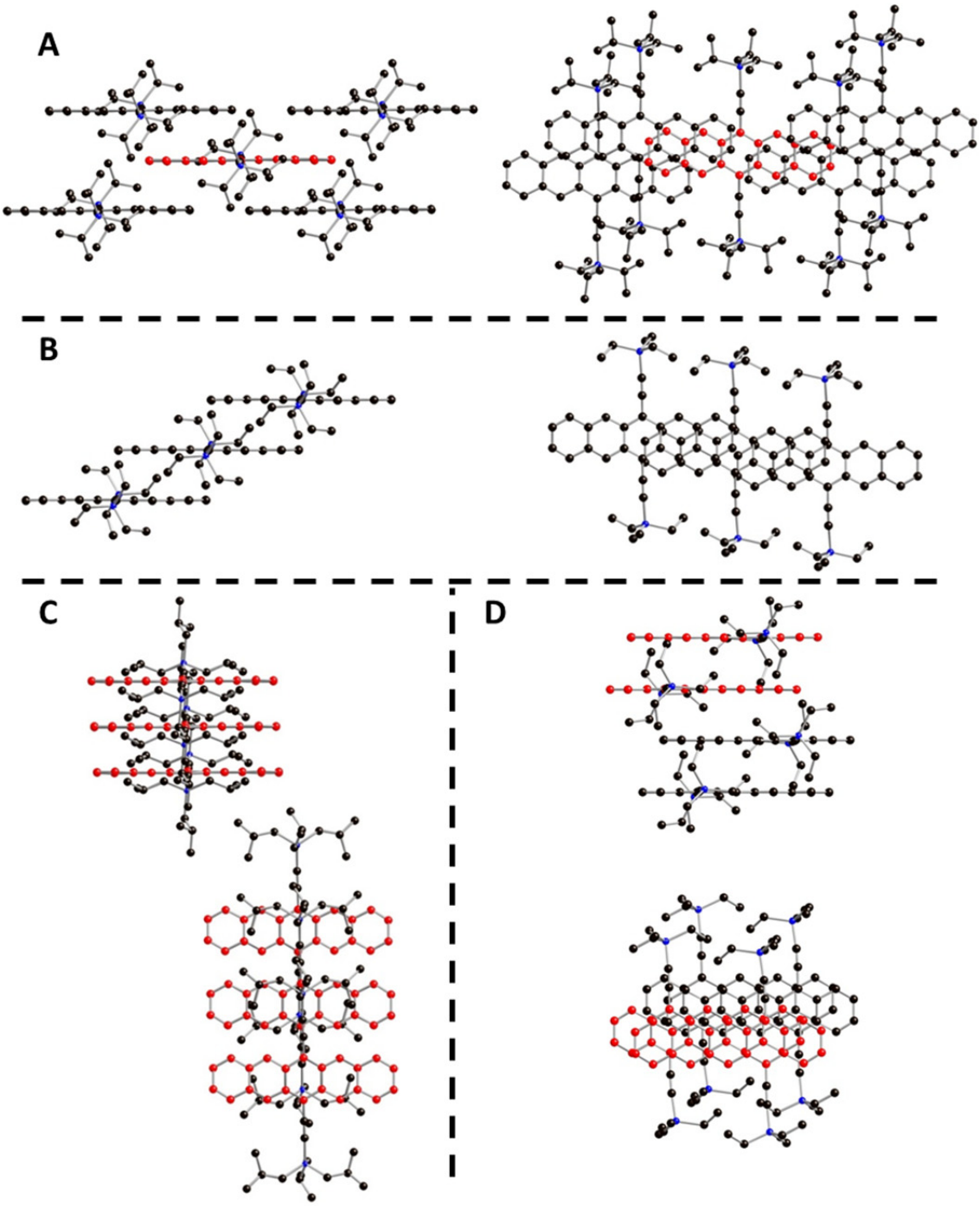

Figure 4-16. Crystal packing of pentacene derivatives in this study. A: TIPS pentacene (**4-16**) crystallizes in a 2-D π-stack. One pentacene backbone is highlighted in red for clarity. B: TES pentacene (**4-17**) crystallizes with 1-D π-stacking interactions. C: TIBS pentacene (**4-18**) shows no overlap in the chromophores which are highlighted in red for clarity. D: Offset TES pentacene (**4-20**) shows 1-D columnar π-stacking in which molecules are arranged in pairs.

4.5 Experimental

TIPS-2,3-diiodopentacene

This compound was synthesized according to the literature[73a] in 87% yield. MS (LDI) *m/z* 890.2 (M^+).

TIPS-2,3-bis[(trimethylsilyl)ethynyl]pentacene

In a 25 mL round-bottom flask was combined 10 mL THF, TIPS-2,3-diiodopentacene (0.69 g, 0.77 mmol) and 1.6 mL triethylamine. The solution was degassed with nitrogen for 10-15 minutes before adding $Pd(PPh_3)_2Cl_2$ (0.036 mmol, 26 mg, 0.047 eq.), CuI (0.073 mmol, 14 mg, 0.094 eq.), and trimethylsilylacetylene (0.210 g, 2.19 mmol, 2.80 eq.). The reaction was heated at 30°C overnight. TLC in hexanes showed the product had nearly the same R_f as the starting material. Investigation with UV-Vis spectroscopy showed the starting diiodo compound had a long-wavelength absorption maximum at 649 nm, whereas the solution had a slight red shift to 652 nm. Appearing complete, the solvent was rotovaped. The material was eluted through a silica gel plug with 9 hexanes : 1 dichloromethane to give 0.74 g (>100% yield). NMR showed a small impurity of a silane product which was carried on without further purification. ^{1}H NMR (400 MHz, $CDCl_3$) δ 9.33 (s, 2H), 9.20 (s, 2H), 8.16 (s, 2H), 7.99 (dd, J = 6.6 Hz, 3.0 Hz, 2H), 7.45 (dd, J = 6.6 Hz, 3.0 Hz, 2H), 1.40 (s, 42H), 0.39 (s, 18H). ^{13}C NMR (100 MHz, $CDCl_3$) δ 134.0, 132.8, 131.3, 131.1, 130.6, 128.9, 126.74, 126.67, 126.5, 121.7, 119.0, 108.0, 104.5, 103.9, 99.3, 19.2, 11.9, 0.4. MS (LDI) *m/z* 830.5 (M^+).

TIPS-2,3-diethynylpentacene (**4-1**)

To the above TIPS-2,3-bis[(trimethylsilyl)ethynyl]pentacene (0.74 g) was added 150 mL MeOH and ~40 mL THF to dissolve everything. The mixture was stirred for 1 hour with 200 mg K_2CO_3 and was shown to be complete by TLC. The reaction was filtered and rotovaped before being eluted through a silica gel plug with 9 hexanes : 1 dichloromethane to give 440 mg of product. This was recrystallized from 15-20 mL hexanes to give 322 mg fine needles, 61% over 2 steps. Larger X-ray quality crystals

were grown from $CHCl_3$/MeOH solvent diffusion in an NMR tube over ~1 week. ^{1}H NMR (400 MHz, $CDCl_3$) δ 9.30 (s, 2H), 9.21 (s, 2H), 8.19 (s, 2H), 7.98 (dd, J = 6.4 Hz, 2.8 Hz, 2H), 7.44 (dd, J = 6.4 Hz, 2.8 Hz, 2H), 3.46 (s, 2H), 1.38 (s, 42H). ^{13}C NMR (100 MHz, $CDCl_3$) δ 134.6, 132.8, 131.3, 131.1, 130.4, 128.9, 127.0, 126.7, 126.6, 120.5, 119.1, 108.1, 104.4, 82.5, 81.6, 19.2, 11.9. MS (LDI) *m/z* 686.4 (M^+). (I also have a complete crystal structure, k13033.)

TSBS-2,3-diiodopentacene

To a flame-dried 100 mL round-bottom flask cooled under N_2 was added TSBS acetylene (1.00 g, 4.46 mmol, 5.00 eq.) and 10 mL hexanes. The solution was cooled in an ice bath and 2.5 M n-BuLi in hexanes (1.61 mL, 4.01 mmol, 4.50 eq.) was added, followed by 3 mL THF. This was stirred for 20 minutes before diluting with 8 mL hexanes and adding 2,3-diiodopentacenequinone (500 mg, 0.893 mmol). This was stirred overnight and all of the material dissolved. The reaction was quenched with 1 mL saturated ammonium chloride solution. THF (~50 mL) was added along with $SnCl_2$ (0.8 g, 4 eq.) and ~5 mL 10% HCl. After stirring for 45 minutes at 60°C, TLC revealed deoxygenation was complete. The aqueous layer was separated and the solution diluted with hexanes. This was washed with water 3x, dried with $MgSO_4$, filtered, and rotovaped. This was purified with a silica gel plug by eluting with hexanes to remove excess alkyne followed by 10 hexanes : 1 dichloromethane to elute the product. Solvent was removed to give 0.73 g of product, 84% yield. ^{1}H NMR (400 MHz, $CDCl_3$) δ 9.26 (s, 2H), 9.10 (s, 2H), 8.56 (s, 2H), 7.96 (dd, J = 6.6 Hz, 3.2 Hz, 2H), 7.43 (dd, J = 6.6 Hz, 3.2 Hz, 2H), 2.00 (m, 6H), 1.53 (m, 6H), 1.32 (d, J = 6.8 Hz, 18H), 1.19 (m, 6H), 1.14 (dt, J = 7.2 Hz, 1.6 Hz, 18H). ^{13}C NMR (100 MHz, $CDCl_3$) δ 139.3, 132.8, 132.0, 131.2, 130.9, 128.9, 126.7, 126.6, 125.9, 119.1, 109.2, 104.5, 104.4, 25.95, 25.91, 19.48, 19.46, 15.00, 14.96, 14.1. MS (LDI) *m/z* 974.3 (M^+).

TSBS-2,3-bis[(trimethylsilyl)ethynyl]pentacene

In a 25 mL round-bottom flask was combined 10 mL THF, TSBS-2,3-diiodopentacene (730 mg, 0.750 mmol) and 1.6 mL triethylamine. The solution was degassed with nitrogen for 10-15 minutes before adding $Pd(PPh_3)_2Cl_2$ (0.038 mmol, 26 mg, 0.050 eq.), CuI (0.075 mmol, 14 mg, 0.10 eq.), and trimethylsilylacetylene (0.22 g, 2.3 mmol, 3.0 eq.). The reaction was heated at 30°C overnight and the solvent rotovaped the next day. The material was eluted through a silica gel plug with 9 hexanes : 1 methylene chloride and concentrated to give 0.68 g of material. NMR showed TMS-butadiyne as a contaminant which was carried on without further purification. ^{1}H NMR (400 MHz, $CDCl_3$) δ 9.33 (s, 2H), 9.21 (s, 2H), 8.18 (s, 2H), 8.01 (dd, J = 6.6 Hz, 3.2 Hz, 2H), 7.47 (dd, J = 6.6 Hz, 3.2 Hz, 2H), 2.05 (m, 6H), 1.59 (m, 6H), 1.38 (d, J = 7.6 Hz, 18H), 1.29 (m, 6H), 1.19 (dt, J = 7.4 Hz, 1.2 Hz, 18H), 0.41 (s, 18H). ^{13}C NMR (100 MHz, $CDCl_3$) δ 134.0, 132.8, 131.3, 131.1, 130.6, 128.9, 126.8, 126.7, 126.5, 121.7, 119.1, 109.0, 104.7, 103.9, 99.2, 25.96, 25.92, 19.5, 15.03, 15.00, 14.1, 0.3. MS (LDI) *m/z* 914.5 (M^-).

TSBS-2,3-diethynylpentacene (**4-2**)

To the above TSBS-2,3-bis[(trimethylsilyl)ethynyl]pentacene (0.68 g) was added 50 mL MeOH and 30 mL THF to dissolve everything (with heating). The mixture was cooled to room temp. and stirred for 1 hour with 300 mg K_2CO_3 and was shown to be complete by TLC. The reaction was filtered and rotovaped before being eluted through a silica gel plug with hexanes followed by 12 hexanes : 1 dichloromethane to give 360 mg of product. This was recrystallized from 5 mL acetone to give 270 mg of tiny blue flakes/needles, 47% yield over two steps. Larger crystals were grown by $CHCl_3$/MeOH solvent diffusion in an NMR tube and were suitable for X-ray analysis, although the structure would not refine. ^{1}H NMR (400 MHz, $CDCl_3$) δ 9.29 (s, 2H), 9.20 (s, 2H), 8.18 (s, 2H), 7.98 (dd, J = 6.6 Hz, 3.2 Hz, 2H), 7.45 (dd, J = 6.6 Hz, 3.2 Hz, 2H), 3.46 (s, 2H), 2.01 (m, 6H), 1.54 (m, 6H), 1.34 (d, J = 7.2 Hz, 18H), 1.20 (m, 6H), 1.15 (t, J = 7.2 Hz, 18H). ^{13}C NMR (100 MHz, $CDCl_3$) δ 134.6, 132.8, 131.3, 131.1, 130.5, 128.9, 127.0, 126.7, 126.6,

120.5, 119.2, 109.2, 104.5, 82.5, 81.6, 25.93, 25.90, 19.5, 15.00, 14.97, 14.1. MS (LDI) *m/z* 770.5 (M^+). (The crystal structure of this compound did not refine well, x13103.)

TCPS-2,3-bis[(trimethylsilyl)ethynyl]pentacene

In a 50 mL round-bottom flask was combined 17 mL THF, TCPS-2,3-diiodopentacene (0.80 g, 0.76 mmol) (synthesized in 93% yield according to the literature[73a])and 1.6 mL triethylamine. The solution was degassed with nitrogen for 10-15 minutes before adding $Pd(PPh_3)_2Cl_2$ (0.038 mmol, 26 mg, 0.050 eq.), CuI (0.075 mmol, 14 mg, 0.10 eq.), and trimethylsilylacetylene (0.22 g, 2.3 mmol, 3.0 eq.). The reaction was heated at 35°C overnight and the solvent rotovaped the next day. The material was eluted through a silica gel plug with 9 hexanes : 1 dichloromethane and concentrated to give 0.53 g of material, 70% yield. ^{1}H NMR (400 MHz, $CDCl_3$) δ 9.26 (s, 2H), 9.13 (s, 2H), 8.12 (s, 2H), 7.96 (dd, J = 6.6 Hz, 3.2 Hz, 2H), 7.44 (dd, J = 6.6 Hz, 3.2 Hz, 2H), 2.07 (m, 12H), 1.79 (m, 24H), 1.65 (m, 12H), 1.36 (m, 6H). ^{13}C NMR (100 MHz, $CDCl_3$) δ 134.0, 132.7, 131.2, 131.0, 130.6, 128.8, 126.7, 126.6, 126.5, 121.6, 119.1, 108.6, 103.9, 103.6, 99.2, 29.6, 27.3, 24.1, 0.3.

TCPS-2,3-diethynylpentacene (**4-3**)

To the above TCPS-2,3-bis[(trimethylsilyl)ethynyl]pentacene (0.53 g) was added 40 mL MeOH and 100 mL THF to dissolve everything (with heating). The mixture was cooled to room temp. and stirred for 1 hour with 300 mg K_2CO_3. The reaction was shown to be complete by TLC (9 hexanes : 1 dichloromethane). The reaction was filtered and rotovaped before being eluted through a silica gel plug with 9 hexanes : 1 dichloromethane to give 350 mg of product. This was recrystallized from ~5 mL 1,2-dichloroethane to give 307 mg of small blue laths, 68% yield. ^{1}H NMR (400 MHz, $CDCl_3$) δ 9.27 (s, 2H), 9.18 (s, 2H), 8.18 (s, 2H), 7.97 (dd, J = 6.6 Hz, 3.2 Hz, 2H), 7.45 (dd, J = 6.6 Hz, 3.2 Hz, 2H), 3.46 (s, 2H), 2.07 (m, 12H), 1.79 (m, 24H), 1.65 (m, 12H), 1.36 (m, 6H). ^{13}C NMR (100 MHz, $CDCl_3$) δ 134.5, 132.8, 131.3, 131.0, 130.5, 128.8, 127.0, 126.7,

126.6, 120.5, 119.2, 108.8, 103.5, 82.5, 81.6, 29.6, 27.3, 24.1. (I also have a complete crystal structure, k13044.)

TIBS-2,3-bis[(trimethylsilyl)ethynyl]pentacene

In a 25 mL round-bottom flask was combined 7 mL THF, TIBS 2,3-diiodopentacene (500 mg, 0.513 mmol) (synthesized in 79% yield according to the literature[73a])and 1.1 mL triethylamine. The solution was degassed with nitrogen for 10-15 minutes before adding $Pd(PPh_3)_2Cl_2$ (0.026 mmol, 18 mg, 0.050 eq.), CuI (0.051 mmol, 9.8 mg, 0.10 eq.), and trimethylsilylacetylene (0.15 g, 1.5 mmol, 3.0 eq.). The reaction was heated at 35°C overnight and the solvent rotovaped the next day. The material was eluted through a silica gel plug with 9 hexanes : 1 methylene chloride and concentrated to give 0.43 g, 92% yield. ^{1}H NMR (400 MHz, $CDCl_3$) δ 9.26 (s, 2H), 9.14 (s, 2H), 8.13 (s, 2H), 7.98 (dd, J = 6.6 Hz, 3.2 Hz, 2H), 7.44 (dd, J = 6.6 Hz, 3.2 Hz, 2H), 2.20 (nonet, J = 6.6 Hz, 6H), 1.20 (d, J = 6.6 Hz, 36H), 0.98 (d, J = 6.6 Hz, 12H), 0.36 (s, 18H). ^{13}C NMR (100 MHz, $CDCl_3$) δ 133.9, 132.7, 131.3, 131.1, 130.6, 128.8, 126.64, 126.57, 126.50, 121.7, 119.0, 110.7, 104.5, 103.9, 99.2, 26.8, 25.7, 25.6, 0.3. MS (LDI) *m/z* 914.5 (M^-).

TIBS-2,3-diethynylpentacene (**4-4**)

To the above TIBS-2,3-bis[(trimethylsilyl)ethynyl]pentacene (0.90 g) was added 150 mL MeOH and ~300 - 350 mL THF to dissolve everything (with heating). The mixture was cooled and stirred with 300 mg K_2CO_3. This reaction was carefully monitored by TLC (hexanes) every 10 minutes and was shown to be complete after 50 minutes. The reaction was filtered and rotovaped before being eluted through a silica gel plug with 12 hexanes : 1 dichloromethane to give 550 mg of product. This was recrystallized from 2.8 mL heptane (105°C) to give 305 mg of large blue blocks, 40% yield. The X-ray crystal structure of this compound was complicated by excessive diffuse scattering, which could not be modeled. This could be caused by stacking faults, domain size problems, and whole-molecule disorder. Nevertheless, a highly constrained and restrained crystal structure was obtained, x13092. ^{1}H NMR (400 MHz, $CDCl_3$) δ 9.28 (s, 2H), 9.19 (s, 2H),

8.20 (s, 2H), 7.99 (dd, J = 6.6 Hz, 3.2 Hz, 2H), 7.46 (dd, J = 6.6 Hz, 3.2 Hz, 2H), 2.21 (nonet, J = 6.6 Hz, 6H), 1.22 (d, J = 6.6 Hz, 36H), 0.99 (d, J = 6.6 Hz, 12H). ^{13}C NMR (100 MHz, $CDCl_3$) δ 134.4, 132.8, 131.3, 131.1, 130.5, 128.8, 126.9, 126.6, 120.6, 119.2, 110.9, 104.4, 82.5, 81.6, 26.8, 25.7, 25.6. MS (LDI) *m/z* 770.5 (M^+).

TSBS octafluoropentacene (**4-5**)

In a dry 50 mL round-bottom flask was combined TSBS acetylene (0.75 g, 3.33 mmol) and 3 mL heptane. The solution was cooled to 0°C and 2.5 M *n*-BuLi solution (1.2 mL, 3.0 mmol) was added dropwise. After stirring for 1 hour, octafluoropentacenequinone (300 mg, 0.665 mmol) and 10 mL heptane were added. The reaction was stirred 2 days and then solvent removed by rotary evaporation. The material was eluted through a silica gel plug with hexanes to separate excess alkyne followed by dichloromethane to elute the diol. Solvent was removed by rotary evaporation. Solids were dissolved in 20 mL MeOH and $SnCl_2 \bullet 2\ H_2O$ (0.72 g, 4.8 eq.) and 15 drops 10% HCl were added. The solution was heated to 50°C and stirred for ~10 minutes. The solution was then cooled in an ice bath and the product was filtered. After drying, the material was eluted through a silica gel plug with hexanes to give 340 mg product. This was recrystallized in ~3 mL hexanes to give 220 mg of blue crystals, 38% yield. ^{1}H NMR (400 MHz, $CDCl_3$) δ 9.53 (s, 4H), 1.98 (m, 6H), 1.52 (m, 6H), 1.31 (d, J = 7.6 Hz, 18H), 1.18 (m, 6H), 1.12 (t, J = 7.2 Hz, 18H). ^{13}C NMR (100 MHz, $CDCl_3$) δ 142.0 (d, J = 270 Hz), 137.7 (d, J = 270 Hz), 130.9, 120.9, 120.2, 120.1 (d, J = 9.7 Hz), 111.6, 103.2, 25.93, 25.89, 19.36, 19.34, 19.32, 14.85, 14.81, 14.80, 14.0. MS (LDI) *m/z* 866.4 (M^-). (I also have a complete crystal structure, x12277.)

dimethylbenzodioxole (**4-7**)

In a 1-L round-bottom flask was combined bis(bromomethyl)benzodioxole (**4-6**) (43.78 g, 142.2 mmol), tetrahexylammonium bromide (6.19 g, 14.2 mmol), and 430 mL dichloromethane. Sodium borohydride (26.3 g, 695 mmol) was dissolved in 69 mL of water and poured into an addition funnel. With the flask cooled in a cool water bath

(~5-10°C), the sodium borohydride solution was added dropwise over ~30 minutes. After addition, the ice bath was removed and the solution stirred another hour. *If bubbling became vigorous, the reaction was cooled again with the water bath and then removed to slowly heat back to room temperature.* The reaction was quenched at 0°C with the careful addition of 10% HCl. This was then filtered and the aqueous layer was extracted once with dichloromethane, dried with $MgSO_4$, filtered, and solvent was removed with rotary evaporation. The material was then vacuum distilled (~100 Torr , 120°C) to give 20.96 g, 98% yield of sickeningly sweet-smelling colorless solid which turns brown over time. ^{1}H NMR (400 MHz, $CDCl_3$) δ 6.64 (s, 2H), 5.88 (s, 2H), 2.18 (s, 6H). ^{13}C NMR (100 MHz, $CDCl_3$) δ 145.6, 129.3, 110.2, 100.7, 19.8. MS (EI 70 eV) *m/z* 150 (M^+, 100%).

dibromodimethylbenzodioxole (**4-8**)

To a stirred solution of dimethylbenzodioxole (20.96 g, 139.6 mmol) in 300 mL dichloromethane was added bromine (21.0 g, 17.3 mL, 335 mmol) in ~5 mL portions every 5 minutes at room temperature. The reaction was stirred for 1 hour after which GC-MS revealed the reaction was complete. Aqueous sodium dithionite was added to remove the excess bromine color. The solution was filtered and the organic layer washed once with sodium bicarbonate. The organic layer was dried with $MgSO_4$, filtered, and solvent was removed with rotary evaporation. The solid was recrystallized in ~450 mL heptane/~10 mL toluene to give 36.70 g, 85% yield. ^{1}H NMR (400 MHz, $CDCl_3$) δ 6.05 (s, 2H), 2.36 (s, 6H). ^{13}C NMR (100 MHz, $CDCl_3$) δ 144.0, 129.9, 103.4, 101.3, 19.9. MS (EI 70 eV) *m/z* 308 (M^+, 100%).

5,6-bis(bromomethyl)-4,7-dibromobenzo[*d*][1,3]dioxole (**4-9**)

To a 2-L round-bottom flask was added dibromodimethylbenzodioxole (36.70 g, 119.2 mmol), NBS (46.7 g, 262 mmol, 2.20 eq.), 900 mL 1,2-dichloroethane, and 540 mg AIBN initiator. The solution was refluxed for 4 hours before adding an additional portion of NBS (6.4 g, 36 mmol, 0.30 eq.) and 120 mg AIBN. The reaction continued refluxing

overnight and the reaction was shown complete by GC-MS. The reaction was washed with sodium dithionite to remove the bromine color, followed by water. The organic layer was dried with $MgSO_4$, filtered, and solvent was removed with rotary evaporation. The solid was recrystallized with ~200 mL DCE to give 40.27 g. The mother liquor was then concentrated and recrystallized a second time to give a negligible 1.88 g more for a total of 42.15 g, 76 % yield. *Since the solubility was low, CCl_4 was added to $CDCl_3$ to obtain NMR spectra.* 1H NMR (400 MHz, $CDCl_3$ + CCl_4) δ 6.16 (s, 2H), 4.78 (s, 4H). ^{13}C NMR (100 MHz, $CDCl_3$ + CCl_4) δ 146.7, 131.1, 103.6, 102.1, 29.2. MS (EI 70 eV) *m/z* 466 (M^+, 10%), 385 (M^+ - 81, 100%), 306 (M^+ - 160, 75%).

tetrabromodioxolane pentacenequinone (**4-10**)

In a 250 mL round-bottom flask with a very large stirring magnet was added 1,4-benzoquinone (11.2 mmol, 1.21 g, 1.00 eq.), 5,6-bis(bromomethyl)-4,7-dibromobenzo[*d*][1,3]dioxole (10.47 g, 22.48 mmol, 2 eq.), and 79 mL *N, N*-dimethylacetamide. The mixture was heated to 90°C and KI (25 g, 150 mmol, 6.7 eq.) was added in small portions to maintain stirring of the thick slurry. The temperature was increased to 130°C and maintained for 2 full days. The reaction was then poured into ~400 mL of stirring water, filtered, and rinsed with water and acetone. The solids were then boiled in acetone for 10 minutes, filtered, and rinsed with dichloromethane. Finally, the solids were boiled in 80 mL DMSO for 15 minutes and carefully filtered in a fume hood while hot. *Since the solution will be ~190°C while filtering, the Büchner funnel and vacuum flask should be taken directly out of a hot oven before use to avoid cracking from thermal shock.* The solids were then rinsed with a small amount of hot DMSO followed by acetone and allowed to dry overnight to give 5.17 g, 65%. MS (LDI) *m/z* 712.7 (M^+ + H).

tetrakis[(dimethyl-n-octyl)silylethynyl]pentacenequinone (**4-11**)

To a dry 25 mL round-bottom flask was added 15 mL hexanes, dimethyl-*n*-octylsilyl acetylene (1.10 g, 5.62 mmol, 8.00 eq.) and *n*-BuLi (2.25 mL, 5.62 mmol, 8.00 eq.) at 0°C. The mixture was stirred for 1 hour before adding 1 mL THF and $SnBu_3Cl$ (1.6 mL, 5.93

mmol) and stirred another 1 hour. The reaction was filtered and concentrated by rotary evaporation. This freshly prepared Stille reagent was then added to a sealed tube with 10 mL dimethylacetamide, tetrabromodioxolane pentacenequinone (500 mg, 0.702 mmol, 1.00 eq.), and degassed for 15 minutes before adding $Pd(PPh_3)_4$ (140 mg, 0.121 mmol). The tube was sealed and heated at 115°C for 13 hours. Solvent was then removed with rotary evaporation. The material was purified on a silica gel plug with hexanes to remove excess Stille reagent, followed by methylene chloride to elute the product, 113 mg. The material was recrystallized in heptane/toluene to afford blocky yellow-orange crystals of $Pd(PPh_3)_2Br_2$. These were filtered and solvent was removed. The solids were then boiled in heptane and the precipitates filtered to yield ~100 mg, 12% yield. Crystals suitable for single-crystal x-ray analysis were grown by solvent diffusion with chloroform/methanol. ^{1}H NMR (400 MHz, $CDCl_3$) δ 9.17 (s, 4H), 6.29 (s, 4H), 1.55 (m, 8H), 1.44 (p, J = 7.1 Hz, 8H), 1.28 (m, 32H), 0.83 (m, 20H), 0.39 (s, 24H). ^{13}C NMR (100 MHz, $CDCl_3$) δ 182.6, 151.9, 133.3, 130.7, 126.7, 107.6, 103.1, 101.7, 95.7, 33.5, 32.2, 29.54, 29.51, 24.1, 22.9, 16.3, 14.3, -1.4. MS (LDI) *m/z* 1172.7 (M^-). (I also have a complete crystal structure, x12374.)

tri(2-pentyl)silane (**4-12**)

To a dry, argon purged 1000 mL flask was added lithium (6.73 g, 970 mmol, 2.00 eq.) and 480 mL anhydrous pentane. (In reality, the solvent should be thoroughly purged with argon **before** the addition of lithium. If repeated this way, higher yields will likely result because less purple Li_3N salts will form.) 2-Chloropropane (59.4 mL, 485 mmol) was slowly added and the solution was refluxed overnight at 43°C with the reflux condenser cooled by a water chiller. The next day, heating was stopped and the purple salts were allowed to settle for several hours. This solution was then transferred with a filtering cannula to another dry 1000 mL round-bottom flask and cooled in an ice bath. Trichlorosilane (121 mmol, 12.2 mL, 0.250 eq.) was added slowly and the solution was stirred for 1 hour. THF (5 mL) was then added and the solution was refluxed for 30 minutes at 45°C. (I would advise using only 0.15 – 0.20 eq. of trichlorosilane initially, and

adding more as necessary.) GC-MS indicated no change in the reaction and it was assumed complete. The reaction was quenched with NH_4Cl followed by water, and the aqueous layer was extracted once with pentane. The organic layers were combined, dried with $MgSO_4$, filtered, and solvent was removed with rotary evaporation. The material was eluted through a silica gel plug with hexanes and distilled under high vacuum to give a clear, colorless oil, 11.14 g, 38% yield. ^{1}H NMR (400 MHz, $CDCl_3$) δ 3.43 (m, J = 2.0 Hz, 1H), 1.50 (m, 6H), 1.28 (m, 6H), 1.02 (m, 12H), 0.90 (t, J = 6.6 Hz, 9H). ^{13}C NMR (100 MHz, $CDCl_3$) δ 36.20, 36.17, 36.04, 35.97, 21.9, 16.2, 16.0, 15.6, 15.5, 14.4. MS (EI, 70 eV) *m/z* 242 (M^+, 2%), 171 (M^+ -71, 100%).

tri(2-pentyl)silyl-trimethylsilyl acetylene (**4-13**)

To a dry 100 mL round-bottom flask was added trimethylsilylacetylene (13.1 mL, 91.9 mmol, 2.00 eq.) in 20 mL THF and cooled to 0°C. A 2.5 M hexanes solution of *n*-BuLi (82.7 mmol, 33.1 mL, 1.90 eq.) was slowly added and the solution was stirred ~1-2 hours. In a 250 mL round-bottom flask was added tri(2-pentyl)silane (11.14 g, 45.93 mmol, 1 eq.) and 150 mL DCE and the solution cooled to 0°C. The solution was titrated with Br_2 (2.35 mL, 45.93 mmol) until a slight bromine color persisted. The solution was then heated to boiling for 10 minutes to evolve HBr and excess Br_2 to give tri(2-pentylsilyl) bromide [MS (EI, 70 eV) *m/z* 320 (M^+, 1%), 249 (M^+ -71, 100%)]. The solution was then cooled and solvent removed by rotary evaporation before placing in an ice bath under nitrogen. The above prepared lithiated trimethylsilylacetylene solution was then slowly added by cannula transfer and the solution was stirred overnight. GC-MS indicated the reaction was complete and the reaction was quenched with NH_4Cl. The aqueous layer was extracted with hexanes and the organic layers were combined, dried with $MgSO_4$, filtered, and solvent was removed with rotary evaporation. The material was eluted through a silica gel plug with hexanes and distilled under high vacuum to give a colorless oil, 14.49 g, 93% yield. ^{1}H NMR (400 MHz, $CDCl_3$) δ 1.54 (m, 6H), 1.23 (m, 6H), 1.02 (d, J = 7.2 Hz, 9H), 0.95 (m, 3H), 0.89 (t, J = 6.4 Hz, 9H), 0.16 (s, 9H). ^{13}C NMR

(100 MHz, $CDCl_3$) δ 116.4, 111.6, 34.8, 21.9, 16.3, 15.0, 14.3, 0.2. MS (EI, 70 eV) *m/z* 338 (M^+, < 1%), 267(M^+ - 71, 100%).

tri(2-pentyl)silyl acetylene (**4-14**)

To a 250 mL round-bottom flask was added tri(2-pentyl)silyl-trimethylsilyl acetylene (14.49 g, 42.78 mmol) and 85 mL MeOH. Enough THF (~15 mL) was added to homogenize the solution followed by K_2CO_3 (3 g, excess). The solution was stirred 1 hour at room temperature and GC-MS showed the reaction was complete. The solid K_2CO_3 was filtered and the solution was extracted 3x with hexanes. The organic layers were combined, dried with $MgSO_4$, filtered, and solvent was removed with rotary evaporation. The material was eluted through a silica gel plug with hexanes and distilled under high vacuum to give a colorless oil, 12.49g, 88%. ^{1}H NMR (400 MHz, $CDCl_3$) δ 2.35 (s, 1H), 1.55 (m, 6H), 1.24 (m, 6H), 1.05 (d, J = 6.4 Hz, 9H), 0.98 (m, 3H), 0.89 (t, J = 6.4 Hz, 9H). ^{13}C NMR (100 MHz, $CDCl_3$) δ 94.7, 87.2, 34.3, 21.6, 16.0, 14.6, 14.0. MS (EI, 70 eV) *m/z* 266 (M^+, 1%), 195 (M^+ - 71, 100%).

bis(tri(2-pentyl)silylethynyl)-tetrabromodioxolane pentacene (T2PS tetrabromodioxolane pentacene) (**4-15**)

In a dry 100 mL round-bottom flask was combined 10 mL THF and tri(2-pentyl)silylacetylene (1.12 g, 4.22 mmol, 5.00 eq.) and cooled to 0°C. *n*-BuLi solution (1.5 mL [2.5M in hexanes], 3.8 mmol, 4.5 eq.) was added dropwise and the solution was stirred 10 minutes. An additional 30 mL THF was added followed by tetrabromodioxolane pentacenequinone (600 mg, 0.842 mmol). The solution was kept at 0°C for at least 1 hour before slowly warming to room temperature overnight. The solvent was then removed with rotary evaporation and the solids were stirred in a small amount of hexanes. This was added to a silica gel plug. Excess alkyne was eluted with hexanes, and the diols were eluted with methylene chloride / acetone. The diol mixture fraction was rotovaped and dissolved in 60 mL acetone + 30 mL THF. To this was added $SnCl_2$ dihydrate (0.57g, 3.0 eq.) with 5-10 mL 10% HCl and stirred for 10 minutes forming

dark blue/black precipitates. This was then filtered and rinsed with acetone to give 600 mg of tiny crystals. This was recrystallized from ~250 mL dioxane to give 550 mg (54% yield) of shiny, small, blue crystals. ^{1}H NMR (400 MHz, $CDCl_3$) δ 9.45 (s, 4H), 6.25 (s, 4H), 1.84 (m, 12H), 1.66 (m, 12H), 1.33 (m, 24H), 0.92 (t, J = 7.2 Hz, 18H). This compound was not soluble enough for ^{13}C NMR. MS (LDI) *m/z* 1210.2 (M^-). (I also have a complete crystal structure, x12602.)

Chapter 5. Acenes & Heteroacenes for Singlet Fission

5.1 Singlet Fission in TCHS Hexacene

To date, acenes are one of only a few classes of organic materials in which singlet fission has been demonstrated. As scientific inquiry continues, it is likely more classes of materials will also exhibit this seemingly rare phenomenon. As outlined in chapter 1, acenes possess the rather restrictive combination of excited singlet and triplet energy levels required for singlet fission. The influence of crystal packing and specific intermolecular coupling on singlet fission remains very unclear. Significantly more work needs to be done in this field of research to identify specific solid-state intermolecular coupling arrangements. The objective of the work in this dissertation, done in collaboration with the group of Marc Baldo at MIT, was to observe singlet fission in additional acenes and heteroacenes whose crystal packing arrangements are known.

Tetracene and pentacene are among the most widely studied acenes for singlet fission. Purity and stability are required of new materials in order to study and observe singlet fission, and this generally precludes the study of larger acenes. The silylethyne-functionalization strategy was reported by the Anthony group for hexacene and heptacene in 2005 and resulted in improved stability relative to unsubstituted hexacene and heptacene[68a]. The functionalized hexacene work was then expanded to give several additional derivatives with variable solution stability and crystal packing motifs[68b]. Among these was tricylclohexylsilylethynyl (TCHS) hexacene (**5-1**) which crystallized with a 1-D π-stacking motif. There is considerable strain in the hexacene backbone due to crystal packing effects. As shown in Figure 5-1, two chromophores sandwich together with an overlap of about three benzene rings and a small short-axis slip. There is a significantly larger short-axis slip between these sandwiches, but still sufficient overlap for overall 1-D π-stacking. As mentioned in chapter 1, the short-axis slip is believed necessary for singlet fission to occur[84].

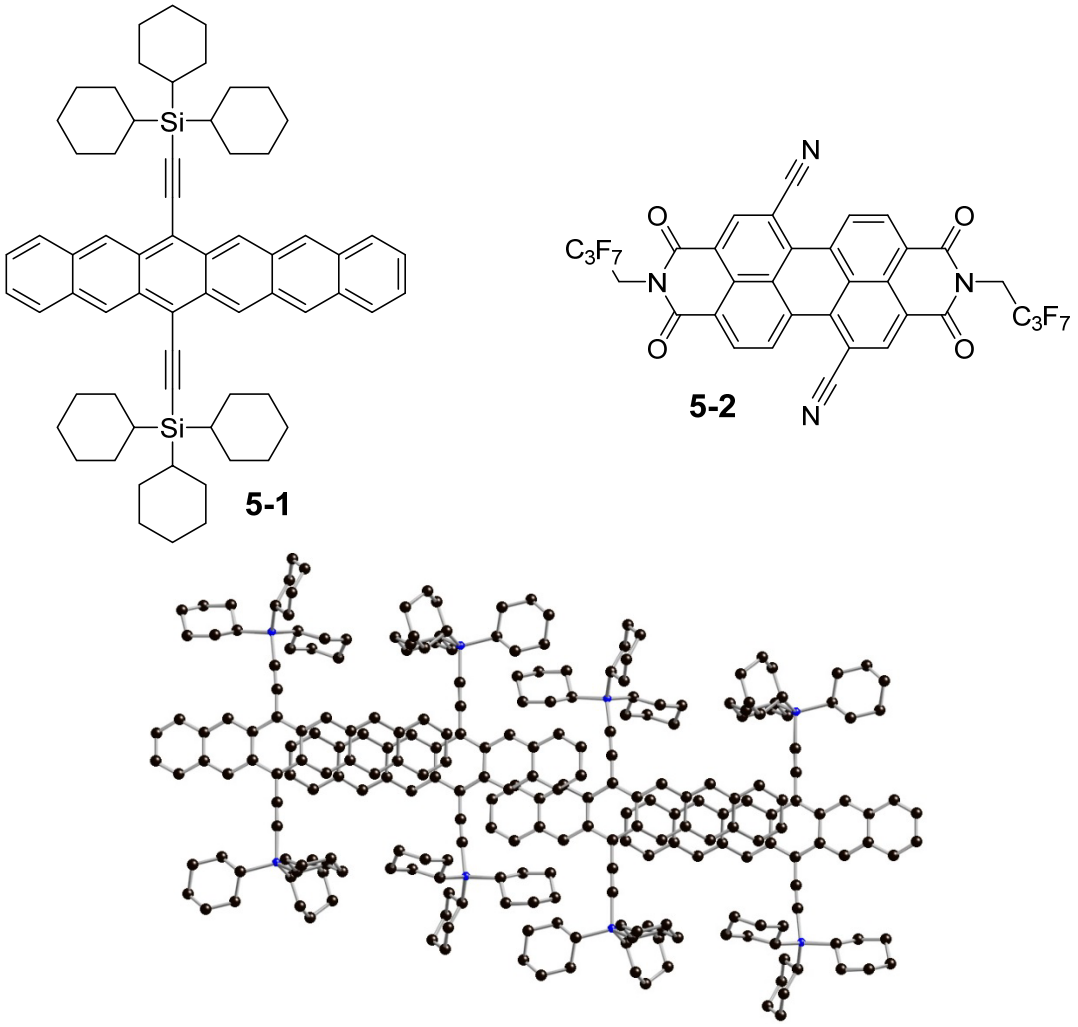

Figure 5-1. Top: Molecular structures of TCHS hexacene (**5-1**) and PDIF-CN_2 (**5-2**) used in a bilayer solar cell. Bottom: Crystal packing of TCHS hexacene (**5-2**) with two different short-axis slips.

Singlet fission in a thin film of TCHS hexacene (**5-1**) was confirmed by transient absorption spectroscopy as shown in Figure 5-2[114]. In this method, a film is irradiated with a short (femtoseconds), intense laser pulse which populates molecular excited states. After a variable delay ranging from mere femtoseconds to picoseconds, a second, low-intensity probe pulse is used to observe the new absorption spectrum. This spectrum is then subtracted from the typical absorption spectrum to produce a difference spectrum showing very small changes due to the presence of excited species. By varying the time delay between excitation and probe pulses, the change in absorption over time can be monitored and allow for the observation of transient

(short-lived) species and eventual decay to the ground state. In the case of this TCHS hexacene (**5-1**) film excited at 750 nm, an initially formed (0.5 ps) excited state singlet (S_1) absorption is observed at 535 nm, as shown in Figure 5-2 (a). After only 30 ps, a new feature dominates with a peak at 570 nm. This spectrum agrees well with the reported hexacene T_1 transient absorption in solution and is also assigned as T_1 absorption[115]. As shown in Figure 5-2 (b), the evolution in time is most clearly seen by plotting only these peak frequencies. It is clear that the initially formed singlet species decays with concomitant increase in the triplet population and demonstrates singlet fission.

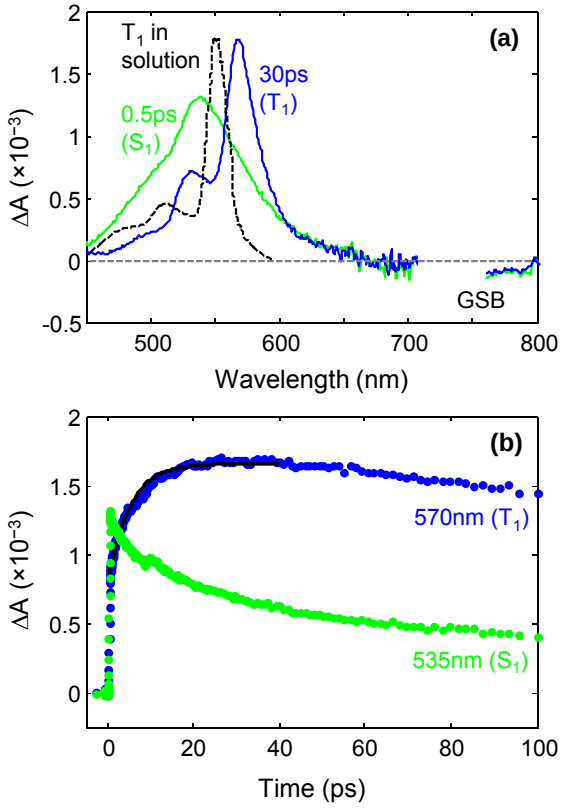

Figure 5-2. Transient absorption data of a TCHS hexacene (**5-1**) film. Graph (a) shows the evolution from 0.5 ps to 30 ps with the S_1 (green) and T_1 (blue) film absorption spectra. The T_1 solution absorption spectrum (black dotted) is also shown for comparison. Graph (b) shows the absorption changes at specific wavelengths over time. As the S_1 (green) absorption decays, the T_1 (blue) absorption increases due to singlet fission. Adapted with permission from John Wiley & Sons, Copyright © 2013[114].

Additional evidence for singlet fission was provided by constructing a bilayer solar cell using spin-coated TCHS hexacene (**5-1**) as a donor with thermally evaporated PDIF-CN_2 (**5-2**) as an acceptor. Given the HOMO energy level of -5.00 eV for hexacene (**5-1**)[68b] and an S_0-T_1 gap of about 0.5 eV, the T_1 energy is about -4.5 eV. The LUMO energy of PDIF-CN_2 (**5-2**) is also about -4.5 eV, low enough to dissociate hexacene triplets and suitable as an acceptor. As shown by the external quantum efficiency in Figure 5-3, this solar cell demonstrated photocurrent from both the donor and acceptor layers. Under selective excitation of hexacene (**5-1**), this cell also exhibited a magnetic field dependence which confirmed singlet fission. This phenomenon was described by Johnson and Merrifield to help account for delayed fluorescence in anthracene crystals[116]. An applied magnetic field changes the rate of singlet fission. As described in chapter 1, the ^{1}(TT) is a pair-state consisting of two coupled triplets with an overall combined spin of a singlet. There are nine possible combinations of two interacting triplets in this initially formed pair-state; however, only those pair-states with overall singlet spin character are allowed. Under no applied magnetic field, only three of these states have singlet character and result in singlet fission. Under low magnetic fields, the Zeeman interaction of the spin Hamiltonian gives singlet character to six of the pair-states, and the rate of singlet fission increases. At very high magnetic fields, the Zeeman interaction dominates the wavefunction and only two pair-states have singlet character[74, 76]. This effect is seen in Figure 5-4 where small changes in photocurrent are observed in the solar cell when TCHS hexacene is selectively illuminated at 660 nm. This effect is seen to a much lesser extent at 530 nm where absorption is dominated by PDIF-CN_2 (**5-2**). Although the quantum efficiency of the cell was very low, this work confirmed the presence of singlet fission in a hexacene derivative for the first time, consistent with smaller members of the acene series.

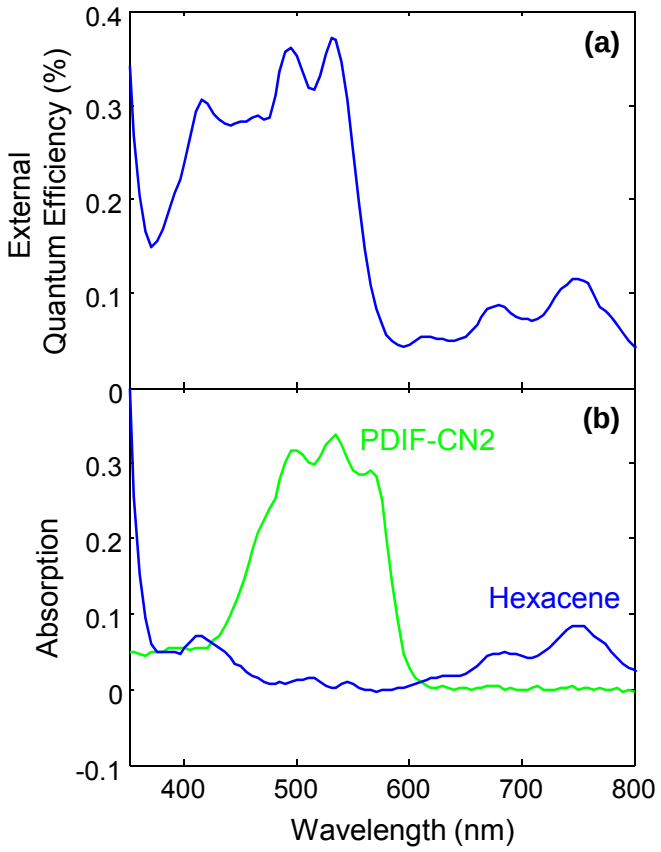

Figure 5-3. External quantum efficiency and absorption spectra of a bilayer solar cell. Both PDIF-CN_2(**5-2**) and TCHS hexacene (**5-1**) contribute to the photocurrent. Adapted with permission from John Wiley and Sons, Copyright © 2013[114].

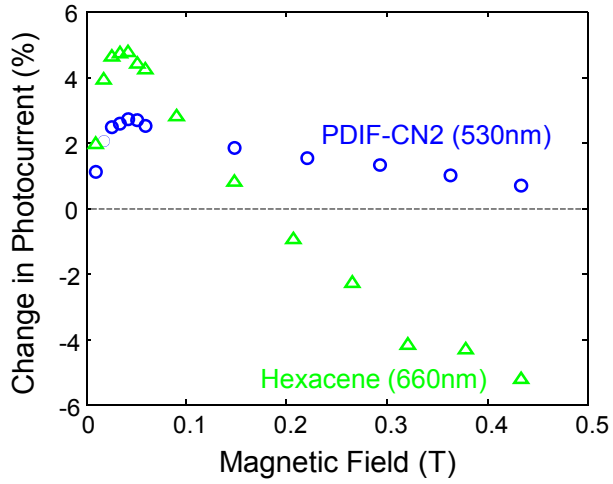

Figure 5-4. Magnetic field dependence of photocurrent in a bilayer solar cell under selective excitation. Adapted with permission from John Wiley & Sons, Copyright © 2013[114].

5.2 Pentadithiophenes

With confirmation of singlet fission in a larger acene, additional materials were sought. Pentadithiophenes are heteroacenes consisting of a pentacene core with fused thiophenes on each end, making them analogous to heptacene. Silylethyne-substituted derivatives of this core were first synthesized by the Anthony group[67a]. Fluorination of the end thiophene rings of anthradithiophene derivatives was found to enhance stability[70b], and this fluorination approach was later applied to tetra- and pentadithiophene derivatives[67b]. The fluorinated pentadithiophene derivative F-TSBS-PDT (**5-4**) crystallized in a 2-D π-stack and demonstrated sufficient stability to test in thin-film transistors.

Given the stability of this chromophore with an appropriate silylethynyl substituent, we decided to develop other derivatives to explore their utility in studying singlet fission. Silylethynyl substituents influence both molecular stability and solubility of acenes, with larger acenes requiring larger, bulkier groups for stability. While bulky groups such as tri-*tert*-butylsilyl, tricyclohexylsilyl, and tricyclopentylsilyl can be used to give added stability through sterics, they usually do not lead to highly soluble materials. As acenes get larger, their solubilities also decrease. This combination of factors necessitates the careful choice of silylethyne substituents which require them to be fairly large and provide steric stability but also provide the necessary solubility. Besides the already-synthesized TSBS derivative, two other alkynes were available which have these properties: triisobutylsilyl and tri-2-pentylsilyl. These two new derivatives were synthesized as a mixture of *syn*- and *anti*-isomers in an analogous manner to F-TSBS-PDT (**5-4**) beginning with quinone (**5-3**) as shown in Scheme 5-1. The yields were very poor, but were done on scales large enough to obtain small quantities of crystals. Whereas the tri-2-pentylsilyl derivative (**5-5**) showed only the slightest degradation after an overnight ^{13}C NMR scan, triisobutylsilyl derivative (**5-6**) decomposed almost completely in this time period.

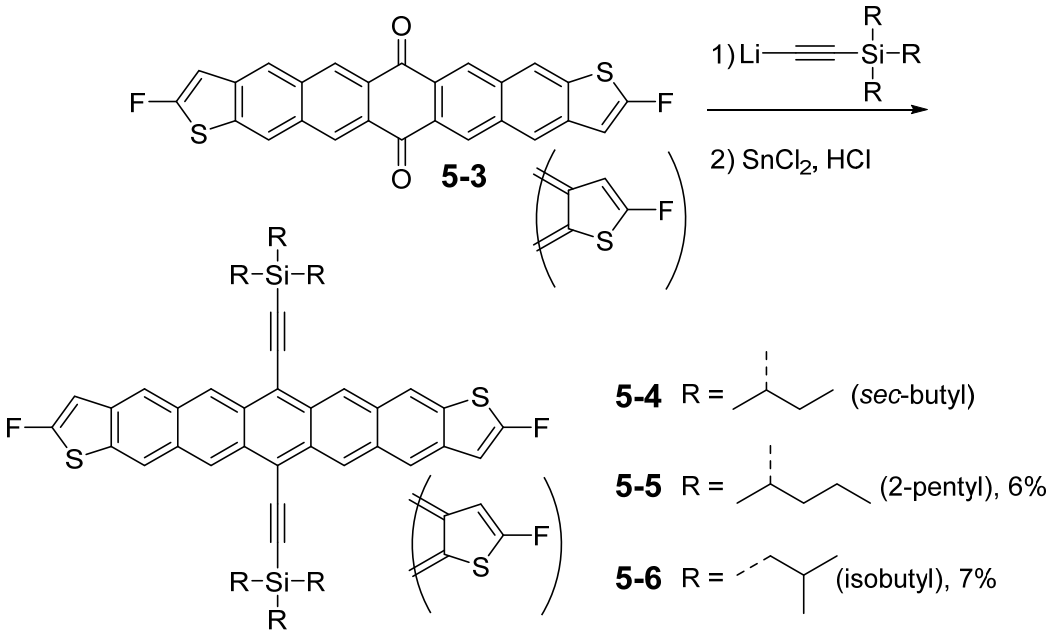

Scheme 5-1. Synthesis of new pentadithiophene derivatives (**5-5**) and (**5-6**) as *syn*- and *anti*-isomers. The *sec*-butyl derivative (**5-4**) was previously synthesized by Dr. Zhong Li.

High-quality crystals of both new derivatives were grown and proved amenable to X-ray crystallography. Tri-2-pentylsilylethynyl derivative (**5-5**) crystallized with 1-D π-stacking with a typical short-axis slip as shown in Figure 5-5. As expected, the crystal structure was disordered with respect to the thiophene rings as a result of the mixture of *syn*- and *anti*-isomers. Additional disorder resulted from the six unresolved chiral 2-pentyl substituents, but a refined model was still obtained as shown in the thermal ellipsoid plot. Intermolecular contacts were as close as 3.40 Å and the structure was very planar. Triisobutylsilylethynyl derivative (**5-6**) is shown in Figure 5-6 and also crystallized in a 1-D π-stack with a slightly smaller short-axis slip relative to derivative (**5-5**). This derivative also shows disorder in the thiophene rings for the same reason as derivative (**5-5**). A very slight out-of-plane bend of a carbon atom in one of the thiophene rings (highlighted in red) leads to a close intermolecular contact of 3.24 Å whereas the remaining contacts are on the order of 3.40 Å or larger.

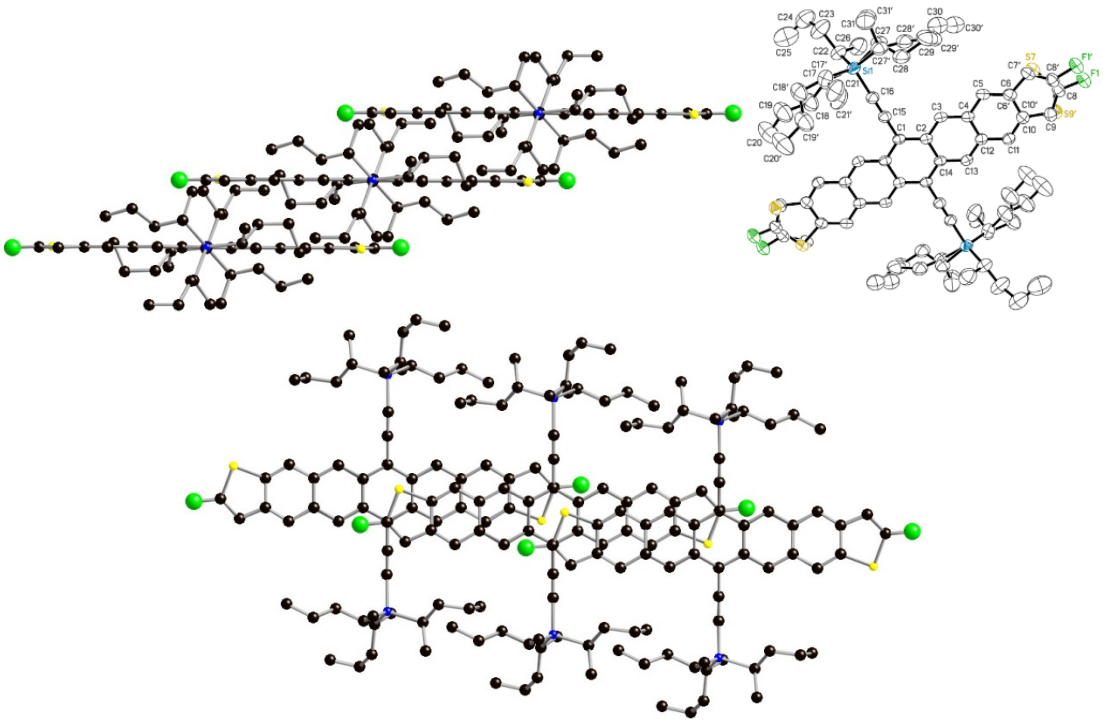

Figure 5-5. Crystal structure of pentadithiophene derivative (**5-5**) exhibiting 1-D π-stacking. Molecular disorder in the packing diagrams has been removed for clarity.

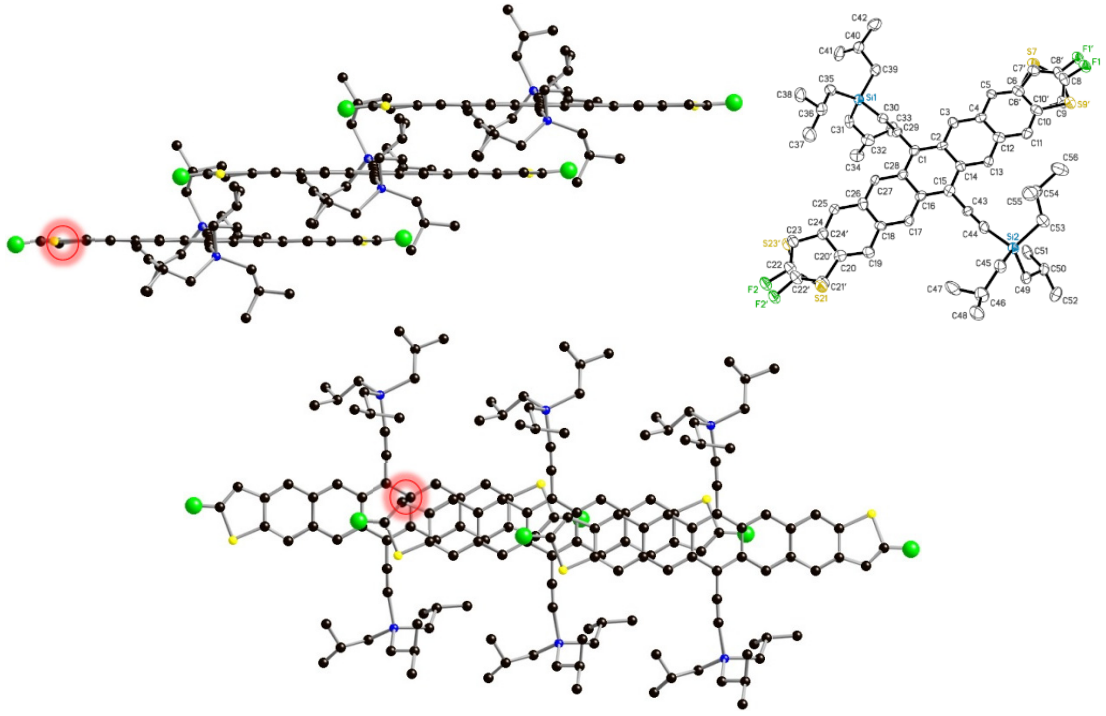

Figure 5-6. Crystal structure of pentadithiophene derivative (**5-6**) exhibiting 1-D π-stacking. Molecular disorder in the packing diagrams has been removed for clarity.

While pentadithiophene (**5-5**) had adequate stability judged by NMR data, derivative (**5-6**) decomposed fairly rapidly. It is clear that the triisobutylsilylethynyl substituents were not sterically demanding enough to inhibit decomposition, likely through an alkyne-acene Diels-Alder dimerization[67a]. This degree of instability likely precludes the study of singlet fission in this material. Similar to the tri-*sec*-butylsilyl substituent, the tri-2-pentylsilyl substituent was more bulky and prevented dimerization. It appears this derivative has the required stability for studying singlet fission. At this point, none of these fluorinated pentadithiophene derivatives have been studied for singlet fission.

5.3 Experimental

T2PS-F_2-pentadithiophene (**5-5**)

To a dry 50 mL round-bottom flask was added 6 mL of hexanes and tri(2-pentyl)silyl acetylene (0.584 g, 2.19 mmol). The solution was cooled to 0°C and a 2.5 M solution of *n*-BuLi in hexanes (0.79 mL, 2.0 mmol) was added dropwise. After 1 hour, difluoropentadithiophenequinone (200 mg, .438 mmol) was added along with 10 mL hexanes and 6 mL of THF. The next day, an additional 6 mL of THF was added and stirred another few hours. The reaction was poured through a thin silica gel plug and flushed with THF. Solvent was removed through rotary evaporation. The mixture was eluted through a silica gel plug with hexanes to remove excess alkyne followed by 1 hexanes : 1 dichloromethane and then pure dichloromethane to elute diol mixture. Solvent was removed by rotary evaporation and solids were dissolved in ~25 mL acetone. $SnCl_2 \bullet 2 H_2O$ (0.14 g) and ~ 0.5 mL 10% HCl were added to make a dark green solution of product. After TLC showed reaction was complete, it was filtered and the solids purified on a silica gel plug with hexanes to give ~40 mg product. This was recrystallized in ~1 mL of hexanes to give 27 mg of product, 6% yield. Larger, X-ray quality crystals were grown by solvent diffusion with $CHCl_3$/MeOH in an NMR tube. ^{1}H NMR (400 MHz, $CDCl_3$) δ 9.38 (s, 2H), 9.33 (s, 2H), 8.24 (s, 2H), 8.18 (s, 2H), 6.72 (s, 1H), 6.71 (s, 1H), 1.90 (m, 6H), 1.74 (m, 6H), 1.58 (m, 6H), 1.44 (m, 6H), 1.36 (s, 24H), 1.01 (t, J = 7.2 Hz, 18H). ^{13}C NMR (100

MHz, $CDCl_3$) δ 167.1, 164.1, 136.65, 136.59, 133.6, 130.7, 130.3, 126.3, 125.5, 121.7, 121.5, 118.2, 109.0, 105.2, 102.6, 102.5, 35.22, 35.20, 35.18, 22.1, 16.93, 16.90, 15.48, 15.46, 14.5. MS (LDI) *m/z* 954.5 (M^-). (I also have a complete crystal structure, x13009.)

TIBS-F_2-pentadithiophene (**5-6**)

To a dry 50 mL round-bottom flask was added 6 mL of THF and TIBS acetylene (0.492 g, 2.19 mmol). The solution was cooled to 0°C and a 2.5 M solution of *n*-BuLi in hexanes (0.79 mL, 2.0 mmol) was added dropwise. After 10 minutes, difluoropentadithiophenequinone (200 mg, .438 mmol) was added along with 6 mL of THF. The next day, the reaction was poured through a thin silica gel plug and flushed with THF. Solvent was removed through rotary evaporation. The mixture was eluted through a silica gel plug with hexanes to remove excess alkyne followed by 1 hexanes : 1 dichloromethane and then pure dichloromethane to elute diol mixture. Solvent was removed by rotary evaporation and solids were dissolved in ~25 mL acetone. $SnCl_2 \bullet 2 H_2O$ (0.17 g) and ~ 0.5 mL 10% HCl were added to make a dark green solution of product. The reaction was heated to 40°C to ensure complete reaction. After TLC showed reaction was complete, it was filtered and the solids purified on a silica gel plug with hexanes to give 62 mg product. This was recrystallized in hexanes to give 25 mg of dark green needles, 7% yield. ^{1}H NMR (400 MHz, $CDCl_3$) δ 9.34 (s, 2H), 9.28 (s, 2H), 8.23 (s, 2H), 8.16 (s, 2H), 6.73 (s, 1H), 6.72 (s, 1H), 2.23 (m, 6H), 1.23 (d, J = 7.0 Hz, 36H), 1.00 (d, J = 7.0 Hz, 12H). This compound was too unstable for an overnight ^{13}C NMR. MS (LDI) *m/z* 870.4 (M^-). (I also have a complete crystal structure, x13034.)

Chapter 6. Conclusions

6.1 Summary of Work

As demonstrated in this dissertation, crystal engineering is a useful process with broad applicability and can give structurally similar molecules significantly different properties in the solid state. Bioimaging with fluorescent dyes generally focuses only on isolated molecules. Although aggregation-induced quenching is a widely known phenomenon in this field, very little other work has been done with respect to crystal engineering strategies to prevent this process. The dioxolane pentacene work in chapter 2 led to three new dioxolane substituents which gave solid-state fluorescent pentacenes. Unfortunately, work aimed at extending the absorption and emission of pentacenes to longer wavelengths was hampered by poor yields and difficult purification. Nevertheless, this work proved necessary since these crystal engineering "tools" were used to isolate a crystalline hexacene with sufficient stability. Although this chromophore was less fluorescent than we hoped, the crystal engineering strategy still proved effective in allowing fluorescence to be demonstrated in the solid state.

Several other smaller projects were also presented in chapters 4 and 5, all of which related to organic electronics with a heavy emphasis on crystal engineering. The diethynyl pentacene work showed that these acenes had π-stacking arrangements very different from the dicyano pentacenes from which they were modeled. This is likely a result of the reduced polarity of diethynyl pentacenes relative to dicyano pentacenes, and the dicyano pentacenes are significantly influenced by weak hydrogen bonding, a supramolecular synthon. TSBS octafluoropentacene gave a nice example of how slightly increasing the size of the trialkylsilyl group causes the crystal packing to change. Work toward dioxolane pentacenequinones as acceptor materials in photovoltaics resulted in a crystalline derivative with good π-stacking interactions, but was disappointing in that the LUMO energy level was unfavorable. Attempts at making a similar, more electron-withdrawing dioxolane pentacene were hampered by very poor solubility of the tetrabromodioxolane pentacene, and the work was necessarily abandoned. The effect

of crystal packing on HOMO energy levels was demonstrated with a series of similar pentacenes. π-Stacked arrangements clearly resulted in altered HOMO energies measured by ultraviolet photoelectron spectroscopy. Finally, crystal engineering may lead to better understanding of singlet fission. This process remains poorly understood with respect to crystal packing. I contributed to the study of TCHS hexacene and developed two new pentadithiophenes, one of which likely possesses the necessary stability for its use in singlet fission studies.

6.2 Future Study

Much more work needs to be done to evaluate dioxolane pentacenes and hexacenes in bioimaging applications. Several publications have already emerged which used the dioxolane pentacenes, but we are still waiting on feedback from Robert Prud'homme for the dioxolane hexacene derivative in deep-tissue imaging applications. It may prove necessary to increase the Stokes shift. Adding even bulkier substituents to the dioxolane heptacenes may result in their successful isolation, although it is unlikely they will be very fluorescent. Diethynyl pentacenes are still being evaluated by Oana Jurchescu's group in field-effect transistors, and I have received some indication that the devices were improved using a BCB dielectric. While the diethynyl pentacenes did not have the desired π-stacking motif, additional work could be done to explore other promising supramolecular synthons to achieve this. Finally, a new pentadithiophene was synthesized for singlet fission studies, but the quantity produced was not enough for device studies. More of this material should be made for evaluation in singlet fission photovoltaics.

REFERENCES

1. Berlman, I. B., *Handbook of Fluorescence Spectra of Aromatic Molecules*. Second Edition ed.; Academic Press: New York, 1971; p 473.
2. Acuña, A. U.; Amat-Guerri, F.; Morcillo, P. n.; Liras, M.; Rodríguez, B. n., Structure and Formation of the Fluorescent Compound of Lignum nephriticum. *Organic Letters* **2009,** *11* (14), 3020-3023.
3. Clarke, E. D., Account of a newly discovered variety of Green Fluor Spar, of very uncommon Beauty, and with remarkable Properties of Colour and Phosphorescence. In *Annals of Philosophy*, Thomson, T., Ed. C. Baldwin: London, 1819; Vol. 14, pp 34-36.
4. Brewster, S. D., On the Colours of Natural Bodies. In *Transactions of the Royal Society of Edinburgh*, Charles Tait, Bell & Bradfute, T. Cadell: London, 1834; Vol. 12, pp 538-545.
5. Herschel, J. F. W., Ἀμόρφωτα, No. I. On a Case of Superficial Colour Presented by a Homogeneous Liquid Internally Colourless. *Philosophical Transactions of the Royal Society of London* **1845,** *135*, 143-145.
6. Stokes, G. G., On the Change of Refrangibility of Light. *Philosophical Transactions of the Royal Society of London* **1852,** *142*, 463-562.
7. Lakowicz, J. R., Introduction to Fluorescence. In *Principles of Fluorescence Spectroscopy*, Springer US: 2006; pp 1-26.
8. Udenfriend, S., Development of the spectrophotofluorometer and its commercialization. *Protein Science* **1995,** *4* (3), 542-551.
9. Kobayashi, H.; Ogawa, M.; Alford, R.; Choyke, P. L.; Urano, Y., New Strategies for Fluorescent Probe Design in Medical Diagnostic Imaging. *Chemical Reviews* **2010,** *110* (5), 2620-2640.
10. Lakowicz, J. R., Fluorophores. In *Principles of Fluorescence Spectroscopy*, Springer US: 2006; pp 63-95.
11. Pansare, V. J.; Hejazi, S.; Faenza, W. J.; Prud'homme, R. K., Review of Long-Wavelength Optical and NIR Imaging Materials: Contrast Agents, Fluorophores, and Multifunctional Nano Carriers. *Chemistry of Materials* **2012,** *24* (5), 812-827.
12. Resch-Genger, U.; Grabolle, M.; Cavaliere-Jaricot, S.; Nitschke, R.; Nann, T., Quantum dots versus organic dyes as fluorescent labels. *Nature methods* **2008,** *5* (9), 763-75.
13. Dabbousi, B. O.; Rodriguez-Viejo, J.; Mikulec, F. V.; Heine, J. R.; Mattoussi, H.; Ober, R.; Jensen, K. F.; Bawendi, M. G., (CdSe)ZnS Core−Shell Quantum Dots: Synthesis and Characterization of a Size Series of Highly Luminescent Nanocrystallites. *The Journal of Physical Chemistry B* **1997,** *101* (46), 9463-9475.
14. Larson, D. R.; Zipfel, W. R.; Williams, R. M.; Clark, S. W.; Bruchez, M. P.; Wise, F. W.; Webb, W. W., Water-Soluble Quantum Dots for Multiphoton Fluorescence Imaging in Vivo. *Science* **2003,** *300* (5624), 1434-1436.
15. Ye, L.; Yong, K.-T.; Liu, L.; Roy, I.; Hu, R.; Zhu, J.; Cai, H.; Law, W.-C.; Liu, J.; Wang, K.; Liu, J.; Liu, Y.; Hu, Y.; Zhang, X.; Swihart, M. T.; Prasad, P. N., A pilot study in non-human primates shows no adverse response to intravenous injection of quantum dots. *Nat Nano* **2012,** *7* (7), 453-458.
16. Zrazhevskiy, P.; Gao, X., Multifunctional quantum dots for personalized medicine. *Nano Today* **2009,** *4* (5), 414-428.
17. Haase, M.; Schäfer, H., Upconverting nanoparticles. *Angewandte Chemie* **2011,** *50* (26), 5808-29.

18. Zhan, Q.; Qian, J.; Liang, H.; Somesfalean, G.; Wang, D.; He, S.; Zhang, Z.; Andersson-Engels, S., Using 915 nm Laser Excited Tm3+/Er3+/Ho3+-Doped NaYbF4 Upconversion Nanoparticles for in Vitro and Deeper in Vivo Bioimaging without Overheating Irradiation. *ACS Nano* **2011,** *5* (5), 3744-3757.
19. Heer, S.; Kömpe, K.; Güdel, H. U.; Haase, M., Highly Efficient Multicolour Upconversion Emission in Transparent Colloids of Lanthanide-Doped NaYF4 Nanocrystals. *Advanced Materials* **2004,** *16* (23-24), 2102-2105.
20. Boyer, J.-C.; van Veggel, F. C. J. M., Absolute quantum yield measurements of colloidal NaYF4: Er3+, Yb3+ upconverting nanoparticles. *Nanoscale* **2010,** *2* (8), 1417-1419.
21. Skoog, D. A.; Holler, F. J.; Nieman, T. A., Molecular Luminescence Spectrometry. In *Principles of Instrumental Analysis*, 5th ed.; Thomson Learning: U.S.A., 1998.
22. Treibs, A.; Kreuzer, F.-H., Difluorboryl-Komplexe von Di- und Tripyrrylmethenen. *Justus Liebigs Annalen der Chemie* **1968,** *718* (1), 208-223.
23. Ulrich, G.; Ziessel, R.; Harriman, A., The Chemistry of Fluorescent Bodipy Dyes: Versatility Unsurpassed. *Angewandte Chemie International Edition* **2008,** *47* (7), 1184-1201.
24. (a) Umezawa, K.; Nakamura, Y.; Makino, H.; Citterio, D.; Suzuki, K., Bright, Color-Tunable Fluorescent Dyes in the Visible−Near-Infrared Region. *Journal of the American Chemical Society* **2008,** *130* (5), 1550-1551; (b) Umezawa, K.; Matsui, A.; Nakamura, Y.; Citterio, D.; Suzuki, K., Bright, Color-Tunable Fluorescent Dyes in the Vis/NIR Region: Establishment of New "Tailor-Made" Multicolor Fluorophores Based on Borondipyrromethene. *Chemistry – A European Journal* **2009,** *15* (5), 1096-1106.
25. (a) Tasior, M.; Murtagh, J.; Frimannsson, D. O.; McDonnell, S. O.; O'Shea, D. F., Water-solubilised BF2-chelated tetraarylazadipyrromethenes. *Organic & Biomolecular Chemistry* **2010,** *8* (3), 522-525; (b) Tasior, M.; O'Shea, D. F., BF2-Chelated Tetraarylazadipyrromethenes as NIR Fluorochromes. *Bioconjugate Chemistry* **2010,** *21* (7), 1130-1133.
26. Nakazumi, H.; Ohta, T.; Etoh, H.; Uno, T.; Colyer, C. L.; Hyodo, Y.; Yagi, S., Near-infrared luminescent bis-squaraine dyes linked by a thiophene or pyrene spacer for noncovalent protein labeling. *Synthetic Metals* **2005,** *153* (1–3), 33-36.
27. Basheer, M. C.; Santhosh, U.; Alex, S.; Thomas, K. G.; Suresh, C. H.; Das, S., Design and synthesis of squaraine based near infrared fluorescent probes. *Tetrahedron* **2007,** *63* (7), 1617-1623.
28. (a) Umezawa, K.; Citterio, D.; Suzuki, K., A Squaraine-based Near-infrared Dye with Bright Fluorescence and Solvatochromic Property. *Chemistry Letters* **2007,** *36* (12), 1424-1425; (b) Umezawa, K.; Citterio, D.; Suzuki, K., Water-soluble NIR Fluorescent Probes Based on Squaraine and Their Application for Protein Labeling. *Analytical Sciences* **2008,** *24* (2), 213-217.
29. Mayerhoffer, U.; Fimmel, B.; Wurthner, F., Bright near-infrared fluorophores based on squaraines by unexpected halogen effects. *Angewandte Chemie* **2012,** *51* (1), 164-7.
30. Sun, Y. Q.; Liu, J.; Lv, X.; Liu, Y.; Zhao, Y.; Guo, W., Rhodamine-inspired far-red to near-infrared dyes and their application as fluorescence probes. *Angewandte Chemie* **2012,** *51* (31), 7634-6.
31. Koide, Y.; Urano, Y.; Hanaoka, K.; Terai, T.; Nagano, T., Evolution of Group 14 Rhodamines as Platforms for Near-Infrared Fluorescence Probes Utilizing Photoinduced Electron Transfer. *ACS Chemical Biology* **2011,** *6* (6), 600-608.
32. Koide, Y.; Urano, Y.; Hanaoka, K.; Piao, W.; Kusakabe, M.; Saito, N.; Terai, T.; Okabe, T.; Nagano, T., Development of NIR Fluorescent Dyes Based on Si–rhodamine for in Vivo Imaging. *Journal of the American Chemical Society* **2012,** *134* (11), 5029-5031.
33. Yuan, L.; Lin, W.; Yang, Y.; Chen, H., A Unique Class of Near-Infrared Functional Fluorescent Dyes with Carboxylic-Acid-Modulated Fluorescence ON/OFF Switching: Rational

Design, Synthesis, Optical Properties, Theoretical Calculations, and Applications for Fluorescence Imaging in Living Animals. *Journal of the American Chemical Society* **2012,** *134* (2), 1200-1211.
34. He, G. S.; Tan, L.-S.; Zheng, Q.; Prasad, P. N., Multiphoton Absorbing Materials: Molecular Designs, Characterizations, and Applications. *Chemical Reviews* **2008,** *108* (4), 1245-1330.
35. Birge, R. R.; Pierce, B. M., Semiclassical time-dependent theory of two-photon spectroscopy. The effect of dephasing in the virtual level on the two-photon excitation spectrum of isotachysterol. *International Journal of Quantum Chemistry* **1986,** *29* (4), 639-656.
36. Pawlicki, M.; Collins, H. A.; Denning, R. G.; Anderson, H. L., Two-Photon Absorption and the Design of Two-Photon Dyes. *Angewandte Chemie International Edition* **2009,** *48* (18), 3244-3266.
37. Kogej, T.; Beljonne, D.; Meyers, F.; Perry, J. W.; Marder, S. R.; Brédas, J. L., Mechanisms for enhancement of two-photon absorption in donor–acceptor conjugated chromophores. *Chemical Physics Letters* **1998,** *298* (1–3), 1-6.
38. Lee, S.; Thomas, K. R. J.; Thayumanavan, S.; Bardeen, C. J., Dependence of the Two-Photon Absorption Cross Section on the Conjugation of the Phenylacetylene Linker in Dipolar Donor−Bridge−Acceptor Chromophores. *The Journal of Physical Chemistry A* **2005,** *109* (43), 9767-9774.
39. Albota, M.; Beljonne, D.; Brédas, J.-L.; Ehrlich, J. E.; Fu, J.-Y.; Heikal, A. A.; Hess, S. E.; Kogej, T.; Levin, M. D.; Marder, S. R.; McCord-Maughon, D.; Perry, J. W.; Röckel, H.; Rumi, M.; Subramaniam, G.; Webb, W. W.; Wu, X.-L.; Xu, C., Design of Organic Molecules with Large Two-Photon Absorption Cross Sections. *Science* **1998,** *281* (5383), 1653-1656.
40. Lee, S. K.; Yang, W. J.; Choi, J. J.; Kim, C. H.; Jeon, S.-J.; Cho, B. R., 2,6-Bis[4-(p-dihexylaminostyryl)styryl]anthracene Derivatives with Large Two-Photon Cross Sections. *Organic Letters* **2004,** *7* (2), 323-326.
41. Huang, P.-H.; Shen, J.-Y.; Pu, S.-C.; Wen, Y.-S.; Lin, J. T.; Chou, P.-T.; Yeh, M.-C. P., Synthesis and characterization of new fluorescent two-photon absorption chromophores. *Journal of Materials Chemistry* **2006,** *16* (9), 850-857.
42. Cho, B. R.; Son, K. H.; Lee, S. H.; Song, Y.-S.; Lee, Y.-K.; Jeon, S.-J.; Choi, J. H.; Lee, H.; Cho, M., Two Photon Absorption Properties of 1,3,5-Tricyano-2,4,6-tris(styryl)benzene Derivatives. *Journal of the American Chemical Society* **2001,** *123* (41), 10039-10045.
43. Ahn, H.-Y.; Yao, S.; Wang, X.; Belfield, K. D., Near-Infrared-Emitting Squaraine Dyes with High 2PA Cross-Sections for Multiphoton Fluorescence Imaging. *ACS Applied Materials & Interfaces* **2012,** *4* (6), 2847-2854.
44. Parker, C. A.; Hatchard, C. G., Sensitized Anti-Stokes Delayed Fluorescence. *Proceedings of the Chemical Society* **1962,** (December), 386-387.
45. (a) Singh-Rachford, T. N.; Castellano, F. N., Photon upconversion based on sensitized triplet–triplet annihilation. *Coordination Chemistry Reviews* **2010,** *254* (21–22), 2560-2573; (b) Zhao, J.; Ji, S.; Guo, H., Triplet-triplet annihilation based upconversion: from triplet sensitizers and triplet acceptors to upconversion quantum yields. *RSC Advances* **2011,** *1* (6), 937-950.
46. Singh-Rachford, T. N.; Castellano, F. N., Nonlinear Photochemistry Squared: Quartic Light Power Dependence Realized in Photon Upconversion. *The Journal of Physical Chemistry A* **2009,** *113* (33), 9266-9269.
47. Singh-Rachford, T. N.; Castellano, F. N., Supra-Nanosecond Dynamics of a Red-to-Blue Photon Upconversion System. *Inorganic Chemistry* **2009,** *48* (6), 2541-2548.
48. Baluschev, S.; Yakutkin, V.; Miteva, T.; Avlasevich, Y.; Chernov, S.; Aleshchenkov, S.; Nelles, G.; Cheprakov, A.; Yasuda, A.; Müllen, K.; Wegner, G., Blue-Green Up-Conversion:

Noncoherent Excitation by NIR Light. *Angewandte Chemie International Edition* **2007,** *46* (40), 7693-7696.
49. Du, P.; Eisenberg, R., Energy upconversion sensitized by a platinum(ii) terpyridyl acetylide complex. *Chemical Science* **2010,** *1* (4), 502-506.
50. Zhao, W.; Castellano, F. N., Upconverted Emission from Pyrene and Di-tert-butylpyrene Using Ir(ppy)3 as Triplet Sensitizer. *The Journal of Physical Chemistry A* **2006,** *110* (40), 11440-11445.
51. (a) Liu, Q.; Yang, T.; Feng, W.; Li, F., Blue-Emissive Upconversion Nanoparticles for Low-Power-Excited Bioimaging in Vivo. *Journal of the American Chemical Society* **2012,** *134* (11), 5390-5397; (b) Liu, Q.; Yin, B.; Yang, T.; Yang, Y.; Shen, Z.; Yao, P.; Li, F., A General Strategy for Biocompatible, High-Effective Upconversion Nanocapsules Based on Triplet-Triplet Annihilation. *Journal of the American Chemical Society* **2013**.
52. Singh-Rachford, T. N.; Nayak, A.; Muro-Small, M. L.; Goeb, S.; Therien, M. J.; Castellano, F. N., Supermolecular-Chromophore-Sensitized Near-Infrared-to-Visible Photon Upconversion. *Journal of the American Chemical Society* **2010,** *132* (40), 14203-14211.
53. Johnson, B. K.; Prud'homme, R. K., Flash NanoPrecipitation of Organic Actives and Block Copolymers using a Confined Impinging Jets Mixer. *Australian Journal of Chemistry* **2003,** *56* (10), 1021-1024.
54. (a) Ungun, B.; Prud'homme, R. K.; Budijon, S. J.; Shan, J.; Lim, S. F.; Ju, Y.; Austin, R., Nanofabricated upconversion nanoparticles for photodynamic therapy. *Opt. Express* **2009,** *17* (1), 80-86; (b) Shan, J.; Budijono, S. J.; Hu, G.; Yao, N.; Kang, Y.; Ju, Y.; Prud'homme, R. K., Pegylated Composite Nanoparticles Containing Upconverting Phosphors and meso-Tetraphenyl porphine (TPP) for Photodynamic Therapy. *Advanced Functional Materials* **2011,** *21* (13), 2488-2495.
55. (a) Kim, S.; Kim, J. H.; Jeon, O.; Kwon, I. C.; Park, K., Engineered polymers for advanced drug delivery. *European journal of pharmaceutics and biopharmaceutics : official journal of Arbeitsgemeinschaft fur Pharmazeutische Verfahrenstechnik e.V* **2009,** *71* (3), 420-30; (b) Hida, K.; Hida, Y.; Shindoh, M., Understanding tumor endothelial cell abnormalities to develop ideal anti-angiogenic therapies. *Cancer science* **2008,** *99* (3), 459-66.
56. Payne, M. M.; Delcamp, J. H.; Parkin, S. R.; Anthony, J. E., Robust, Soluble Pentacene Ethers. *Organic Letters* **2004,** *6* (10), 1609-1612.
57. Wolak, M. A.; Melinger, J. S.; Lane, P. A.; Palilis, L. C.; Landis, C. A.; Delcamp, J.; Anthony, J. E.; Kafafi, Z. H., Photophysical Properties of Dioxolane-Substituted Pentacene Derivatives Dispersed in Tris(quinolin-8-olato)aluminum(III). *The Journal of Physical Chemistry B* **2006,** *110* (15), 7928-7937.
58. Langhals, H.; Potrawa, T.; Nöth, H.; Linti, G., The Influence of Packing Effects on the Solid-State Fluorescence of Diketopyrrolopyrroles. *Angewandte Chemie International Edition in English* **1989,** *28* (4), 478-480.
59. Desiraju, G. R., Supramolecular Synthons in Crystal Engineering—A New Organic Synthesis. *Angewandte Chemie International Edition in English* **1995,** *34* (21), 2311-2327.
60. Desiraju, G. R.; Vittal, J. J.; Ramanan, A., *Crystal Engineering: A Textbook*. World Scientific Publishing Co. Pte. Ltd.: Hackensack, NJ, 2011; p 216.
61. (a) Suh, M. P.; Park, H. J.; Prasad, T. K.; Lim, D.-W., Hydrogen Storage in Metal–Organic Frameworks. *Chemical Reviews* **2012,** *112* (2), 782-835; (b) Getman, R. B.; Bae, Y.-S.; Wilmer, C. E.; Snurr, R. Q., Review and Analysis of Molecular Simulations of Methane, Hydrogen, and Acetylene Storage in Metal–Organic Frameworks. *Chemical Reviews* **2012,** *112* (2), 703-723.
62. Li, J.-R.; Sculley, J.; Zhou, H.-C., Metal–Organic Frameworks for Separations. *Chemical Reviews* **2012,** *112* (2), 869-932.

63. Yoon, M.; Srirambalaji, R.; Kim, K., Homochiral Metal–Organic Frameworks for Asymmetric Heterogeneous Catalysis. *Chemical Reviews* **2012,** *112* (2), 1196-1231.
64. Inokuma, Y.; Yoshioka, S.; Ariyoshi, J.; Arai, T.; Hitora, Y.; Takada, K.; Matsunaga, S.; Rissanen, K.; Fujita, M., X-ray analysis on the nanogram to microgram scale using porous complexes. *Nature* **2013,** *495* (7442), 461-466.
65. (a) Anthony, J. E.; Eaton, D. L.; Parkin, S. R., A Road Map to Stable, Soluble, Easily Crystallized Pentacene Derivatives. *Organic Letters* **2002,** *4* (1), 15-18; (b) Anthony, J. E.; Brooks, J. S.; Eaton, D. L.; Parkin, S. R., Functionalized Pentacene: Improved Electronic Properties from Control of Solid-State Order. *Journal of the American Chemical Society* **2001,** *123* (38), 9482-9483.
66. Watanabe, M.; Chang, Y. J.; Liu, S. W.; Chao, T. H.; Goto, K.; Islam, M. M.; Yuan, C. H.; Tao, Y. T.; Shinmyozu, T.; Chow, T. J., The synthesis, crystal structure and charge-transport properties of hexacene. *Nature chemistry* **2012,** *4* (7), 574-8.
67. (a) Payne, M. M.; Odom, S. A.; Parkin, S. R.; Anthony, J. E., Stable, Crystalline Acenedithiophenes with up to Seven Linearly Fused Rings. *Organic Letters* **2004,** *6* (19), 3325-3328; (b) Goetz, K. P.; Li, Z.; Ward, J. W.; Bougher, C.; Rivnay, J.; Smith, J.; Conrad, B. R.; Parkin, S. R.; Anthopoulos, T. D.; Salleo, A.; Anthony, J. E.; Jurchescu, O. D., Effect of acene length on electronic properties in 5-, 6-, and 7-ringed heteroacenes. *Advanced Materials* **2011,** *23* (32), 3698-703.
68. (a) Payne, M. M.; Parkin, S. R.; Anthony, J. E., Functionalized Higher Acenes: Hexacene and Heptacene. *Journal of the American Chemical Society* **2005,** *127* (22), 8028-8029; (b) Purushothaman, B.; Parkin, S. R.; Anthony, J. E., Synthesis and Stability of Soluble Hexacenes. *Organic Letters* **2010,** *12* (9), 2060-2063.
69. Purushothaman, B.; Bruzek, M.; Parkin, S. R.; Miller, A.-F.; Anthony, J. E., Synthesis and structural characterization of crystalline nonacenes. *Angewandte Chemie* **2011,** *50* (31), 7013-7.
70. (a) Swartz, C. R.; Parkin, S. R.; Bullock, J. E.; Anthony, J. E.; Mayer, A. C.; Malliaras, G. G., Synthesis and Characterization of Electron-Deficient Pentacenes. *Organic Letters* **2005,** *7* (15), 3163-3166; (b) Subramanian, S.; Park, S. K.; Parkin, S. R.; Podzorov, V.; Jackson, T. N.; Anthony, J. E., Chromophore Fluorination Enhances Crystallization and Stability of Soluble Anthradithiophene Semiconductors. *Journal of the American Chemical Society* **2008,** *130* (9), 2706-2707.
71. Payne, M. M.; Parkin, S. R.; Anthony, J. E.; Kuo, C.-C.; Jackson, T. N., Organic Field-Effect Transistors from Solution-Deposited Functionalized Acenes with Mobilities as High as 1 cm2/V·s. *Journal of the American Chemical Society* **2005,** *127* (14), 4986-4987.
72. Lloyd, M. T.; Mayer, A. C.; Subramanian, S.; Mourey, D. A.; Herman, D. J.; Bapat, A. V.; Anthony, J. E.; Malliaras, G. G., Efficient Solution-Processed Photovoltaic Cells Based on an Anthradithiophene/Fullerene Blend. *Journal of the American Chemical Society* **2007,** *129* (29), 9144-9149.
73. (a) Lim, Y.-F.; Shu, Y.; Parkin, S. R.; Anthony, J. E.; Malliaras, G. G., Soluble n-type pentacene derivatives as novel acceptors for organic solar cells. *Journal of Materials Chemistry* **2009,** *19* (19), 3049; (b) Shu, Y.; Lim, Y.-F.; Li, Z.; Purushothaman, B.; Hallani, R.; Kim, J. E.; Parkin, S. R.; Malliaras, G. G.; Anthony, J. E., A survey of electron-deficient pentacenes as acceptors in polymer bulk heterojunction solar cells. *Chemical Science* **2011,** *2* (2), 363.
74. Smith, M. B.; Michl, J., Singlet Fission. *Chemical Reviews* **2010,** *110* (11), 6891-6936.
75. Zimmerman, P. M.; Zhang, Z.; Musgrave, C. B., Singlet fission in pentacene through multi-exciton quantum states. *Nature chemistry* **2010,** *2* (8), 648-652.
76. Pope, M.; Swenberg, C., *Electronic Processes in Organic Crystals*. Oxford University Press: New York, 1982; p 821.

77. (a) Rao, A.; Wilson, M. W. B.; Hodgkiss, J. M.; Albert-Seifried, S.; Bässler, H.; Friend, R. H., Exciton Fission and Charge Generation via Triplet Excitons in Pentacene/C60 Bilayers. *Journal of the American Chemical Society* **2010,** *132* (36), 12698-12703; (b) Roberts, S. T.; McAnally, R. E.; Mastron, J. N.; Webber, D. H.; Whited, M. T.; Brutchey, R. L.; Thompson, M. E.; Bradforth, S. E., Efficient singlet fission discovered in a disordered acene film. *Journal of the American Chemical Society* **2012,** *134* (14), 6388-400.
78. Shockley, W.; Queisser, H. J., Detailed Balance Limit of Efficiency of p-n Junction Solar Cells. *Journal of Applied Physics* **1961,** *32* (3), 510-519.
79. Hanna, M. C.; Nozik, A. J., Solar conversion efficiency of photovoltaic and photoelectrolysis cells with carrier multiplication absorbers. *Journal of Applied Physics* **2006,** *100* (7), 074510-8.
80. Sariciftci, N. S.; Smilowitz, L.; Heeger, A. J.; Wudl, F., Photoinduced Electron Transfer from a Conducting Polymer to Buckminsterfullerene. *Science* **1992,** *258* (5087), 1474-1476.
81. (a) Chan, W. L.; Ligges, M.; Jailaubekov, A.; Kaake, L.; Miaja-Avila, L.; Zhu, X. Y., Observing the multiexciton state in singlet fission and ensuing ultrafast multielectron transfer. *Science* **2011,** *334* (6062), 1541-5; (b) Congreve, D. N.; Lee, J.; Thompson, N. J.; Hontz, E.; Yost, S. R.; Reusswig, P. D.; Bahlke, M. E.; Reineke, S.; Van Voorhis, T.; Baldo, M. A., External Quantum Efficiency Above 100% in a Singlet-Exciton-Fission–Based Organic Photovoltaic Cell. *Science* **2013,** *340* (6130), 334-337.
82. Xiao, Z.; Ye, G.; Liu, Y.; Chen, S.; Peng, Q.; Zuo, Q.; Ding, L., Pushing fullerene absorption into the near-IR region by conjugately fusing oligothiophenes. *Angewandte Chemie* **2012,** *51* (36), 9038-41.
83. Jadhav, P. J.; Mohanty, A.; Sussman, J.; Lee, J.; Baldo, M. A., Singlet exciton fission in nanostructured organic solar cells. *Nano letters* **2011,** *11* (4), 1495-8.
84. Smith, M. B.; Michl, J., Recent Advances in Singlet Fission. *Annual Review of Physical Chemistry* **2013,** *64* (1), 361-386.
85. Ramanan, C.; Smeigh, A. L.; Anthony, J. E.; Marks, T. J.; Wasielewski, M. R., Competition between singlet fission and charge separation in solution-processed blend films of 6,13-bis(triisopropylsilylethynyl)pentacene with sterically-encumbered perylene-3,4:9,10-bis(dicarboximide)s. *Journal of the American Chemical Society* **2012,** *134* (1), 386-97.
86. Johnson, J. C.; Nozik, A. J.; Michl, J., The Role of Chromophore Coupling in Singlet Fission. *Accounts of Chemical Research* **2013**.
87. Anderson, D. R.; Koch, T. H., 2,3-Bis(trimethylsilyloxy)-1,3-butadiene as a useful reactive diene in the Diels-Alder reaction. *The Journal of organic chemistry* **1978,** *43* (13), 2726-2728.
88. Anthony, J. E.; Gierschner, J.; Landis, C. A.; Parkin, S. R.; Sherman, J. B.; Bakus Ii, R. C., A new functionalization strategy for pentacene. *Chemical communications* **2007,** (45), 4746-8.
89. Ried, W.; Anthöfer, F., Einfache Synthese für Pentacen-6,13-chinon. *Angewandte Chemie* **1953,** *65* (23), 601-601.
90. Newman, M. S.; Kanakarajan, K., Synthesis of 8-hydroxy- and 11-hydroxy-7,12-dimethylbenz[a]anthracenes. Tin(II) chloride mediated reductions. *The Journal of organic chemistry* **1980,** *45* (12), 2301-2304.
91. Lehnherr, D.; McDonald, R.; Tykwinski, R. R., Exploring Electronically Polarized Pentacenes. *Organic Letters* **2008,** *10* (19), 4163-4166.
92. Wan, J.; Shi, L.; Benson, B.; Bruzek, M. J.; Anthony, J. E.; Sinko, P. J.; Prudhomme, R. K.; Stone, H. A., Microfluidic generation of droplets with a high loading of nanoparticles. *Langmuir : the ACS journal of surfaces and colloids* **2012,** *28* (37), 13143-8.
93. D'Addio, S. M.; Baldassano, S.; Shi, L.; Cheung, L.; Adamson, D. H.; Bruzek, M.; Anthony, J. E.; Laskin, D. L.; Sinko, P. J.; Prud'homme, R. K., Optimization of cell receptor-specific targeting

through multivalent surface decoration of polymeric nanocarriers. *Journal of Controlled Release* **2013,** *168* (1), 41-49.
94. Cammidge, A. N.; Chambrier, I.; Cook, M. J.; Garland, A. D.; Heeney, M. J.; Welford, K., Octaalkyl- and octaalkoxy-2,3-naphthalocyanines. *Journal of Porphyrins and Phthalocyanines* **1997,** *1* (1), 77-86.
95. Iqbal, Z.; Lyubimtsev, A.; Hanack, M., Synthesis of Phthalonitriles Using a Palladium Catalyst. *Synlett* **2008,** *2008* (EFirst), 2287-2290.
96. Chen, Z.; Swager, T. M., Synthesis and Characterization of Fluorescent Acenequinones as Dyes for Guest−Host Liquid Crystal Displays. *Organic Letters* **2007,** *9* (6), 997-1000.
97. Peng, F.; Fan, B.; Shao, Z.; Pu, X.; Li, P.; Zhang, H., Cu(OTf)2-Catalyzed Isomerization of 7-Oxabicyclic Alkenes: A Practical Route to the Synthesis of 1-Naphthol Derivatives. *Synthesis* **2008,** *2008* (19), 3043-3046.
98. Wu, A.; Duan, Y.; Xu, D.; Penning, T. M.; Harvey, R. G., Regiospecific oxidation of polycyclic aromatic phenols to quinones by hypervalent iodine reagents. *Tetrahedron* **2010,** *66* (12), 2111-2118.
99. Weber, G.; Teale, F. W. J., Determination of the absolute quantum yield of fluorescent solutions. *Transactions of the Faraday Society* **1957,** *53* (0), 646-655.
100. Rauhut, M. M.; Roberts, B. G.; Maulding, D. R.; Bergmark, W.; Coleman, R., Infrared liquid-phase chemiluminescence from reactions of bis(2,4,6-trichlorophenyl) oxalate, hydrogen peroxide, and infrared fluorescent compounds. *The Journal of organic chemistry* **1975,** *40* (3), 330-335.
101. (a) Chun, D.; Cheng, Y.; Wudl, F., The most stable and fully characterized functionalized heptacene. *Angewandte Chemie* **2008,** *47* (44), 8380-5; (b) Kaur, I.; Stein, N. N.; Kopreski, R. P.; Miller, G. P., Exploiting Substituent Effects for the Synthesis of a Photooxidatively Resistant Heptacene Derivative. *Journal of the American Chemical Society* **2009,** *131* (10), 3424-3425; (c) Qu, H.; Chi, C., A Stable Heptacene Derivative Substituted With Electron-Deficient Trifluoromethylphenyl and Triisopropylsilylethynyl Groups. *Organic Letters* **2010,** *12* (15), 3360-3363.
102. Allen, F. H.; Wood, P. A.; Galek, P. T. A., The versatile role of the ethynyl group in crystal packing: an interaction propensity study. *Acta Crystallographica Section B* **2013,** *69* (3), 281-287.
103. Pommerehne, J.; Vestweber, H.; Guss, W.; Mahrt, R. F.; Bässler, H.; Porsch, M.; Daub, J., Efficient two layer LEDs on a polymer blend basis. *Advanced Materials* **1995,** *7* (6), 551-554.
104. Horowitz, G., Organic Field-Effect Transistors. *Advanced Materials* **1998,** *10* (5), 365-377.
105. Tang, M. L.; Oh, J. H.; Reichardt, A. D.; Bao, Z., Chlorination: A General Route toward Electron Transport in Organic Semiconductors. *Journal of the American Chemical Society* **2009,** *131* (10), 3733-3740.
106. Deng, X.; Zheng, L.; Yang, C.; Li, Y.; Yu, G.; Cao, Y., Polymer Photovoltaic Devices Fabricated with Blend MEHPPV and Organic Small Molecules. *The Journal of Physical Chemistry B* **2004,** *108* (11), 3451-3456.
107. Belloni, M.; Manickam, M.; Wang, Z.-H.; Preece, J. A., TOWARD BORONATE ESTER MESOGENIC STRUCTURES. *Molecular Crystals and Liquid Crystals* **2003,** *399* (1), 93-114.
108. Hutchins, R. O.; Kandasamy, D.; Dux, F.; Maryanoff, C. A.; Rotstein, D.; Goldsmith, B.; Burgoyne, W.; Cistone, F.; Dalessandro, J.; Puglis, J., Nucleophilic borohydride: selective reductive displacement of halides, sulfonate esters, tertiary amines, and N,N-disulfonimides with borohydride reagents in polar aprotic solvents. *The Journal of organic chemistry* **1978,** *43* (11), 2259-2267.

109. Liang, Z.; Tang, Q.; Liu, J.; Li, J.; Yan, F.; Miao, Q., N-Type Organic Semiconductors Based on π-Deficient Pentacenequinones: Synthesis, Electronic Structures, Molecular Packing, and Thin Film Transistors. *Chemistry of Materials* **2010,** *22* (23), 6438-6443.
110. Desiraju, G. R.; Parthasarathy, R., The nature of halogen···halogen interactions: are short halogen contacts due to specific attractive forces or due to close packing of nonspherical atoms? *Journal of the American Chemical Society* **1989,** *111* (23), 8725-8726.
111. D'Andrade, B. W.; Datta, S.; Forrest, S. R.; Djurovich, P.; Polikarpov, E.; Thompson, M. E., Relationship between the ionization and oxidation potentials of molecular organic semiconductors. *Organic Electronics* **2005,** *6* (1), 11-20.
112. Park, Y.; Choong, V.; Gao, Y.; Hsieh, B. R.; Tang, C. W., Work function of indium tin oxide transparent conductor measured by photoelectron spectroscopy. *Applied Physics Letters* **1996,** *68* (19), 2699-2701.
113. Davis, R. J.; Lloyd, M. T.; Ferreira, S. R.; Bruzek, M. J.; Watkins, S. E.; Lindell, L.; Sehati, P.; Fahlman, M.; Anthony, J. E.; Hsu, J. W. P., Determination of energy level alignment at interfaces of hybrid and organic solar cells under ambient environment. *Journal of Materials Chemistry* **2011,** *21* (6), 1721.
114. Lee, J.; Bruzek, M. J.; Thompson, N. J.; Sfeir, M. Y.; Anthony, J. E.; Baldo, M. A., Singlet exciton fission in a hexacene derivative. *Advanced Materials* **2013,** *25* (10), 1445-8.
115. Angliker, H.; Rommel, E.; Wirz, J., Electronic spectra of hexacene in solution (ground state. Triplet state. Dication and dianion). *Chemical Physics Letters* **1982,** *87* (2), 208-212.
116. (a) Johnson, R.; Merrifield, R.; Avakian, P.; Flippen, R., Effects of Magnetic Fields on the Mutual Annihilation of Triplet Excitons in Molecular Crystals. *Physical Review Letters* **1967,** *19* (6), 285-287; (b) Johnson, R.; Merrifield, R., Effects of Magnetic Fields on the Mutual Annihilation of Triplet Excitons in Anthracene Crystals. *Physical Review B* **1970,** *1* (2), 896-902.

VITA

Matthew Bruzek

Education

Undergraduate

Southwest Minnesota State University, 2004-2008

Degree: B.S. Chemistry (Minor: Mathematics)

Graduation Date: May 2008

Graduate

University of Kentucky, 2008-2013

Graduation Date: (expected) 2013

Professional Experience

Laboratory technician, Archer Daniels Midland Company, Marshall, MN, May 2008-July 2008

Conferences and Presentations

"Voltammetry of Propazine"—poster presented at the American Chemical Society National Meeting, March 26, 2007, Chicago, IL

"Voltammetry of Propazine"—poster presented (again) at the American Chemical Society National Meeting, April 7, 2008, New Orleans, LA

"Organic solar cells: synthesis and testing of novel, soluble fullerene derivatives"—poster presented at the American Chemical Society National Meeting, April 7, 2008, New Orleans, LA

"Crystal Design for Organic Photovoltaic Acceptors"—oral presentation at the Materials Research Society Fall Meeting, November 28, 2012, Boston, MA

Awards/Honors

University of Kentucky Chemistry Dept. "100% Plus Award", May 2010

University of Kentucky Research Challenge Trust Fund Fellowship, 2011-2013

Publications

Guse, D.; Bruzek, M.; DeVos, P.; Brown, J. “Electrochemical reduction of atrazine: NMR evidence for reduction of the triazine ring” *J. Electroanal. Chem.*, **2009**, *626*, 171.

Bruzek, M.; Henderson, J.; Hull, R.; Becht, S.; Brown, J. “Electrochemical reduction of propazine: NMR evidence for dechlorination and reduction of the triazine ring” *J. Electroanal. Chem.*, **2010**, *642*, 13.

Davis, R.; Lloyd, M.; Ferreira, S.; Bruzek, M,; Watkins, S.; Lindell, L.; Sehati, P.; Fahlman, M.; Anthony, J.; Hsu, J. “Determination of energy level alignment at interfaces of hybrid and organic solar cells under ambient environment” *J. Mater. Chem.*, **2011**, *21*, 1721.

Purushothaman, B.; Bruzek, M.; Parkin, S.; Miller, A.-F.; Anthony, J. “Synthesis and structural characterization of crystalline nonacenes” *Angew. Chem. Int. Ed.*, **2011**, *50*, 7013.

Wan, J.; Shi, L.; Benson, B.; Bruzek, M.; Anthony, J.; Sinko, P.; Prud’homme, R.; Stone, H. “Microfluidic generation of droplets with a high loading of nanoparticles” *Langmuir*, **2012**, *28*, 13143.

Lee, J.; Bruzek, M.; Thompson, N.; Sfeir, M.; Anthony, J.; Baldo, M. “Singlet exciton fission in a hexacene derivative” *Adv. Mater.*, **2013**, *25*, 1445.

D’Addio, S.; Baldassano, S.; Shi, L.; Cheung, L.; Adamson, D.; Bruzek, M.; Anthony, J.; Laskin, D.; Sinko, P.; Prud’homme, R. “Optimization of cell receptor-specific targeting through multivalent surface decoration of polymeric nanocarriers” *J. Control. Release*, **2013**, *168*, 41.

Bruzek, M.; Parkin, S.; Anthony, J. “Synthesis and optical properties of dioxolane-functionalized hexacenes and heptacenes” *Org. Lett. (manuscript submitted)*.

Pansare, V.; Bruzek, M.; Adamson, D.; Anthony, J.; Prud’homme, R. “Composite fluorescent nanoparticles for biomedical imaging applications” *Mol. Imaging Biol. (manuscript submitted)*.